Politecnico di Torino

Scuola di Dottorato

Dottorato in

Ingegneria Elettronica e delle Comunicazioni - XXVI Ciclo

Doctorate Dissertation

Hybrid and Cooperative Positioning Solutions for Wireless Networks

Zhoubing Xiong

Tutore
Prof. Roberto Garello

Coordinatore
Prof. Ivo Montrosset

Istituto Superiore Mario Boella
Dr. Maurizio A. Spirito
Ing. Francesco Sottile

February 2014

Zhoubing Xiong: *Hybrid and Cooperative Positioning Solutions for Wireless Networks,* Tesi di Dottorato in Ingegneria Elettronica e delle Comunicazioni - XXVI Ciclo, Dipartimento di Elettronica e Telecomunicazioni, Politecnico di Torino, Torino, Italia © February 2014

Dedicated to my mother.

ACKNOWLEDGMENTS

First of all, I want to thank my adviser Prof. Roberto Garello for his guidance and support over the past years.

Then I would like to thank all the excellent professionals, whom I had the chance to work with, my colleagues Francesco Sottile, Claudio Pastrone, Dr. Maurizio Spirito. Also I want to express my gratefulness to all of my colleagues at the PerT Lab in Istituto Superiore Mario Boella. Moreover I would like to show my gratitude to Mauricio for invaluable discussion and Etim for the support of the carried experiment.

At last but not the least, I want to thank my friends and my family, in particular my mother for all the unconditional support along these years.

ABSTRACT

In this thesis, some hybrid and cooperative solutions are proposed and analyzed to locate the user in challenged scenarios, with the aim to overcome the limits of positioning systems based on single technology. The proposed approaches add hybrid and cooperative features to some conventional position estimation techniques like Kalman filter and particle filter, and fuse information from different radio frequency technologies. The concept of cooperative positioning is enhanced with hybrid technologies, in order to further increase the positioning accuracy and availability.

In particular, wireless sensor networks and radio frequency identification technology are used together to enhance the collected data with position information. Terrestrial ranging techniques (i.e., ultra-wide band technology) are employed to assist the satellite-based localization in urban canyons and indoors. Moreover, some advanced positioning algorithms, such as energy efficient, cognitive tracking and non-line-of-sight identification, are studied to satisfy the different positioning requirements in harsh indoor environments.

The proposed hybrid and cooperative solutions are tested and verified by first Monte Carlo simulations then real experiments. The obtained results demonstrate that the proposed solutions can increase the robustness (positioning accuracy and availability) of the current localization systems.

PUBLICATIONS

Some results and figures presented in this thesis have been previously published in the following publications:

Journal Paper

- [1] **Z. Xiong**, Z. Song, A. Scalera, E. Ferrera, F. Sottile, P. Brizzi, R. Tomasi, and M.A. Spirito "**Hybrid WSN and RFID indoor positioning and tracking system**," in *EURASIP Journal on Embedded Systems*, 2013:6.

Book Chapter

- [2] F. Sottile, **Z. Xiong**, C. Pastrone "**Analysis of Real-Time Hybrid-Cooperative GNSS-Terrestrial Positioning Algorithms**," to appear in *Advancing Embedded Systems and Real-Time Communications with Emerging Technologies*, IGI Global, 2014.

Conference Papers

- [3] **Z. Xiong**, M. Dai, F. Sottile, M.A. Spirito and R. Garello, "**A Cognitive and Cooperative Tracking Approach in Wireless Networks**," in *Proceedings of IEEE International Conference on Communications (ICC)*, Budapest, Hungary, June 9–13, 2013, pp. 1310–1314.

- [4] **Z. Xiong**, F. Sottile, M.A. Spirito and R. Garello, "**Analysis of Hybrid and Cooperative Positioning Algorithms in Urban Canyon Scenarios**," in *Proceedings of International Conference on Localization and GNSS (ICL-GNSS)*, Turin, Italy, June 25–27, 2013, pp. 1–6.

- [5] **Z. Xiong**, Z. Song, A. Scalera, E. Ferrera, F. Sottile, P. Brizzi, R. Tomasi, and M.A. Spirito, "**Enhancing WSN-based Indoor Positioning and Tracking through RFID Technology**," in *Proceedings of fourth International EURASIP Workshop on RFID Technology*, Turin, Italy, September 27–28, 2012, pp. 107–114.

- [6] **Z. Xiong**, F. Sottile, M.A. CACERES, M.A. Spirito and R. Garello, "**Hybrid WSN-RFID Cooperative Positioning Based on Extended Kalman Filter**," in *Proceedings of IEEE Topical Conference on Antennas and Propagation in Wireless Communications*, Turin, Italy, September 12–17, 2011, pp. 990–993.

- [7] **Z. Xiong**, F. Sottile, M.A. Spirito and R. Garello, "**Hybrid Indoor Positioning Approaches Based on WSN and RFID**," in *Proceedings of 4th IFIP International Conference on New Technologies, Mobility and Security (NTMS)*, Paris, France, February 7–10, 2011, pp. 1–5.

CONTENTS

LIST OF FIGURES

LIST OF TABLES

LIST OF ALGORITHMS

ACRONYMS

A-GPS Assisted-GPS

AWGN Additive White Gaussian Noise

BP Belief Propagation

BDS BeiDou Navigation Satellite System

CCT Cognitive and Cooperative Tracking

c.d.f. cumulative distribution function

CRLB Cramér-Rao Lower Bound

DB Data Base

D-GPS Differential-GPS

DVB Digital Video Broadcasting

DVB-T Digital Video Broadcasting-Terrestrial

ECEF Earth Centered Earth Fixed

EGNOS European Geostationary Navigation Overlay Service

EKF Extended Kalman Filter

EP Expectation Propagation

EU European Union

FCC Federal Communications Commission

FG Factor Graph

FIM Fisher Information Matrix

GBAS Ground-based Augmentation System

GNSS Global Navigation Satellite System

GLONASS GLObalnaya NAvigatsionnaya Sputnikovaya Sistema

GPS Global Positioning System

GSM Global System for Mobile Communications

HC-EKF Hybrid-Cooperative Extended Kalman Filter

HC-PF Hybrid-Cooperative Particle Filter

HC-UKF Hybrid-Cooperative Unscented Kalman Filter

HC-LS Hybrid-Cooperative Least Squares

HF High-Frequency

H-SPAWN Hybrid Sum-Product Algorithm over a Wireless Network

IoT Internet of Things

IPS Indoor Positioning System

ISMB Istituto Superiore Mario Boella

IR-UWB Impulse Radio Ultra-Wide Band

KF Kalman Filter

LBS location-based services

LS Least Squares

LLS Linear Least Squares

LoS Line-of-Sight

MC Monte Carlo

MSAS Multi-functional Satellite Augmentation System

NLoS Non-Line-of-Sight

NSA Neighbors Selection Algorithm

OWR One-Way Ranging

p.d.f. probability distribution function

P Position

P2P Peer-to-Peer

PF Particle Filter

PT Position-Time

PV Position-Velocity

PVA Position-Velocity-Acceleration

PVT Position-Velocity-Time

RF Radio Frequency

RFID Radio Frequency IDentification

RMSE Root Mean Squared Errors

RSS Received Signal Strength

RSSI Received Signal Strength Indication

RTT Round-Trip Time

SBAS Satellite-Based Augmentation System

SNR Signal-to-Noise Ratio

SoO Signal-of-Opportunity

SPA Sum-Product Algorithm

TDoA Time-Difference-of-Arrival

ToA Time-of-Arrival

ToF Time of Flight

TS Time Slot

TWR Two-Way Ranging

UHF Ultra-High Frequency

UKF Unscented Kalman Filter

UMTS Universal Mobile Telecommunications System

UWB Ultra-Wide Band

WAAS Wide Area Augmentation System

WLAN Wireless Local Area Network

WSN Wireless Sensor Network

Part I

BASIC CONCEPTS

1 INTRODUCTION

1.1 BACKGROUND AND MOTIVATION

Nowadays, location-based services (LBS) have become a part of everyone's daily life. Positioning systems gain a lot of interest and efforts both in academic and industrial research. At the moment, lots of technologies can be exploited and mixed (e.g., ultrasound, laser scanner, infrared, radio frequencies, custom sensors, and camera vision). Each of them has addressed the aggregation of sensor data into location estimation via a suitable method. Positioning and tracking are crucial features in many ubiquitous computing and robotics applications where the knowledge of the location of the entities (i.e., people and objects) is required [8, 9]. In fact, the collected or communicated data is often useless if it is not associated to the location information.

At present, the most widely advanced positioning services have been thought for outdoor scenarios. Since 1990s, Global Navigation Satellite Systems (GNSSs) can provide accurate location estimation with global coverage and are utilized in many applications. For instance, Global Positioning System (GPS) is widely employed in navigation, mapping, environment protection. However, there are still some limitations of GNSS-based localization systems. One of the main problem is that thay may fail in some challenged area, for example, urban canyons, dense foliage and indoor environments. As it is well known to all, a GNSS receiver can be located when it can acquire at least four satellites [10]. In urban canyons or under dense foliage, the Line-of-Sight (LoS) communication links between the satellites and the receiver are often obstructed by tall buildings or dense foliage, resulting in not enough satellite pseudoranges for positioning. In indoor environments, the weak GNSS signal is not able to penetrate the concrete walls, causing almost no pseudorange for localization [1]. The solutions of these limitations have drawn great attention among industrial and scientific researchers.

For outdoors, different aiding or augmentation approaches have been proposed and developed. Among them, there are Satellite-Based Augmentation Systems (SBASs) like Wide Area Augmentation System (WAAS), Multifunctional Satellite Augmentation System (MSAS) and European Geostationary Navigation Overlay Service (EGNOS), or Ground-based Augmentation Systems (GBASs) like Differential-GPS (D-GPS) and Assisted-GPS (A-GPS).

1 Sometimes one can receive GPS signal through the window.

The aiding and augmentation approaches are far more than mature and some new emerging approaches can provide better performance of positioning accuracy and availability.

For indoors, a new type of localization system, namely Indoor Positioning System (IPS), has been designed to provide LBS for indoor environments, including asset tracking [11], intruder detection [12], healthcare monitoring [13], emergency 911 services [14]. An IPS is a network of devices that are used wirelessly to localize people or objects inside a building [15]. IPSs are based on some prior knowledge about position of special nodes, namely the anchor nodes, and are aimed at estimating position of one or more mobile nodes, whose positions are unknown, by processing ranging data collected and exchanged by both mobile and anchor nodes. From radio propagation point of view, indoor environment is extremely complex, since it is full of various obstacles, multipath and interference from other wireless devices. The IPS technology is an up-and-coming research topic of short range wireless communications.

The main objective of this doctorate thesis is to study and apply new localization scheme in wireless networks: hybrid and cooperative positioning approaches. The paradigm of this relies on two aspects. On one hand, different communication technologies, e.g., Wireless Sensor Network (WSN), Ultra-Wide Band (UWB), Wi-Fi, cellular networks, are exploited as Signal-of-Opportunity (SoO) approaches to overcome the limit of single one and increase the robustness the current localization system. On other hand, cooperation among the users within the network is adopted for data and information sharing, with the aim to further enhance the position estimate. In more details, this work covers the issues of how to fuse different observations, what data, when and where to communicate for cooperation, and in which way to use information.

1.2 PROBLEMS AND METHODOLOGIES

This thesis is focused on improving the positioning accuracy and availability of the current localization system. First, it studies the problem of data fusion from different communication technologies and the exchange of positioning information among mobile nodes. Then it investigates the various LBS requirements of different applications and proposes some advanced positioning algorithms.

In particular, we concentrate on the hybrid and cooperative paradigm in a wireless ad hoc or sensor network shown in Fig. 1.1, where the 'RF' stands for Radio Frequency (RF) device. In other words, the term 'RF 1' stands for the first RF device while the 'RF 2' stands for the second RF device. In this work, they could be a node of WSN, a Radio Frequency IDentification (RFID) device, a UWB transceiver, and a receiver or satellite of GNSS. Besides, the term 'A' and 'M' means anchor node and mobile node, respectively. As it can be observed, a mobile node consists of different RF devices so that it is

able to communicate with different RF anchors to collect mixed range measurements (the red and blue lines in Fig. 1.1). Moreover, it can range with other mobile neighbor and exchange positioning information (the purple arrow in Fig. 1.1). In this way, each mobile node has three range measurements so its position can be accurately inferred in a 2D plane. However, if only one RF technology is used, the mobile cannot be located since there are not enough measurements.

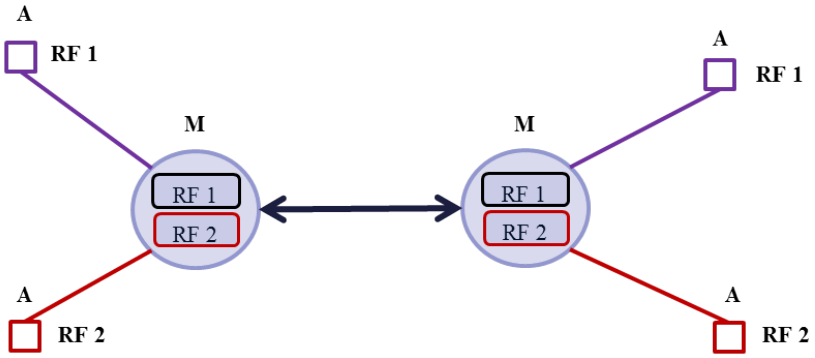

Figure 1.1: Hybrid and cooperative paradigm.

The hybrid and cooperative positioning strategy has been studied in the context of wireless network, assuming that the positioning estimation is not available for a single technique. This strategy is of special use in GNSS challenging area, like indoors and urban canyons. Sometimes there may be enough measures from one technology, but nevertheless this strategy can still improve the positioning accuracy by exploiting the redundant measurements. Furthermore, the joint use of different RF techniques can overcome the limits of the single one. In a word, the hybrid and cooperative strategy can improve the robustness of the localization system. It is worth reminding that the system complexity and cost are increased.

From the hybrid and cooperative strategy, this study proposes some hybrid cooperative solutions for network localization. First we present a comprehensive mathematical model for the hybrid cooperative positioning problem. Then we map this model to Bayesian filtering approach, such as Kalman Filter (KF) and Particle Filter (PF). KF [16] is a linear quadratic estimation and widely used in localization application. PF [17] is a sequential Monte Carlo (MC) method and is used for nonlinear/non-Gaussian estimation. The proposed solutions have been applied for different applications, for example, hybrid cooperative WSN-RFID indoor positioning and hybrid cooperative GNSS-terrestrial navigation.

Since indoor environments are many and variant, some work has been done to study some advanced localization algorithm with context awareness, like noise variance tracking and Non-Line-of-Sight (NLoS) detection. Factor Graph (FG), which is a bipartite graph that represents the statistical factorization of the problem variables [18], is applied to perform Bayesian

inference of marginal distributions by message passing according to the Sum-Product Algorithm (SPA).

Finally, all the proposed algorithms are tested by MC simulations in realistic scenarios, where the advantages and the limitations are analyzed for the later deployments. Some prototypes are developed to collect the real experimental measurements for performance evaluation.

1.3 LITERATURE VIEW

As mentioned before, the GNSSs-based positioning systems fail in some situations, indoor environments, urban canyons and wooded areas, etc, due to the blockage of the GNSS signal. In such conditions, some different augmentation systems have been studied and adopted. SBASs, such as WAAS, EGNOS and MSAS, use a number of known GNSS receiving stations to improve the positioning accuracy [19]. GBASs, such as D-GPS [20] and A-GPS [21], employ ground based networks to locate the users with enhanced performance. These approaches support wide-area or regional augmentation, and require large investment. The focus of this work is the aiding from other existing RF techniques.

In parallel, many hybrid positioning approaches are proposed in the literature with the adoption of different RF techniques. Hybrid positioning means the integration with different RF techniques, derived from the SoO. Many terrestrial communication systems can be used to aid GNSS, such as 2G/3G mobile communication systems, Digital Video Broadcasting (DVB) and Wireless Local Area Network (WLAN). The integration can be seen as a data fusion problem, which can be done in two ways: loose and tight hybridization. In loose hybridization, the fusion data are the position estimates from different systems, which means the hybridization could fail if one system cannot finish the position estimation. Nevertheless, in tight hybridization, the fusion data are the range measurements, which means the position can be decided if there are enough range measurements coming from the both systems. Due to this advantage, tight hybridization draws more attention among the researchers. In [22, 23], some hybrid positioning approaches are proposed by using the 2G Global System for Mobile Communications (GSM) network. In [24], a hybrid localization solution is studied based on GNSS and Universal Mobile Telecommunications System (UMTS). Deng et al [25] and Mensing et al [26] considered the 3G mobile network to improve GNSS localization in critical situations. De Angelis et al. [27] proposed a hybrid GNSS/cellular positioning system for vehicular navigation, which uses cellular network data to increase the location accuracy when the number of visible satellites is not adequate. With the availability of GPS receiver inside mobile phones, a new hybrid location system is proposed in [28]. Kovar et al. [29] proposed a hybrid hardware receiver, which exploits the pilot carriers of DVB signals for range measurements, achieving sub-meter positioning accuracies. Huang et al. [30, 31] explored the Digi-

tal Video Broadcasting-Terrestrial (DVB-T) signals as SoO approach to assist GNSS in hostile environment.

With the demand of LBS for indoors, many different IPSs are raised [32, 33, 34]. IPSs can also be classified according to the used position estimation technique.

WLAN is a widespread technology for geolocation due to the numerous presented networks [33]. Almost all the mobile devices, from laptop to smartphone and tablet, are able to communicate within this standard. Most of positioning methods in WLAN-based systems are dependent on the Received Signal Strength (RSS) for cost reasons, as this type of measurement is simple to implement in radio devices. Two common techniques to use RSS for localization are fingerprinting the RSS and conversion to distance. The fingerprinting approach is composed of two phases: in the offline phase, a database is built for the signal strength map of the coverage area; during the online phase, the positioning algorithm looks for the best matches between the current measurements and the stored values [35, 36, 37]. The main disadvantage of this method is the tiresome calibration of large amount of measurements for environmental change. Another approach involves the conversion of RSS to distance by using Friis equation [38] ,which establishes an exponential relation between the strength of a signal and the transmission distance. The main drawback of this approach is the variation of the signal strength due to channel fading in various propagation environments [39]. Not only for indoor positioning, WLAN is but also popular in hybrid positioning. Kwon et al. [40] proposed a hybrid algorithm for indoor positioning in WLAN. Singh et al. [41] proposed localization approach which uses WLAN in conjunction with GPS network. Yeh et al. [42] studied outdoor localization using GPS and WiFi networks.

UWB is a most promising RF technology for location-based application, with strong multipath resistance and building penetrability. It has recently gained lots of interest in positioning researches thanks to its theoretical ranging accuracy in the order of few centimeters [43]. The main issue of UWB is that there are few commercial solutions, resulting in the high cost of a single node and unsuitable for extensive deployments. Many works have been proposed for hybrid GNSS-UWB positioning solutions. Tan et al. [44] proposed a GPS and UWB integration approach for indoor localization, which could provide better positioning accuracy compared to the single UWB system. MacGougan et al. [45] applied UWB to assist GPS in hostile environment and they implemented a combined GPS+UWB positioning system with sub-meter accuracy [46, 47].

WSN is an emerging technology for environmental monitoring, surveillance, e-health, and manufacturing [48]. It is also popular in localization and lots of localization algorithms have been developed for indoors. Costa et al. [49] used distributed weighted multidimensional scaling approaches to locate the unknown nodes in sensor networks. Moore et al. [50] applied robust quadrilaterals for distributed localization. Meesookho et al.

[51] developed energy-based acoustic source positioning algorithms based on Least Squares (LS). Like other techniques, many hybrid positioning approaches have developed with WSN. Xu et al. [52] integrated satellite location and WSN , and seamlessly located the user between indoors and outdoors. Ren in [53] proposed a WSN-aided GPS location algorithm, using WSN to fast acquire the GPS signal.

A RFID system is able to automatically identify target tags and capture data in the interrogation range, which could be up to several meters. This capture can be explored as proximity information for localization and does not suffer from NLoS propagation and multipath. Some research has been done to investigate RFID technology for localization [54, 55], which used dense deployment of RFID readers. It is also possible to adopt the backscattered signal strength from the passive tag to locate the node, but it requires huge amount of experiments to calibrate the measurement model [56] and the positioning range is limited to a few meters. Active RFID tags were used in combination with GNSS and dead reckoning solutions for pedestrian navigation [57].

As increase in the mobile users, another SoO approach, cooperative localization in wireless networks, has received great attention over the last years [58, 59, 60]. In cooperative positioning, apart from range measurements with respect to anchors (i.e., nodes whose positions are perfectly known), unknown nodes perform range measurements also among themselves and exchange aiding data, such as estimated position and the estimated probability density function. The cooperation among mobile nodes is beneficial for network localization [60], where both positioning accuracy and availability can be improved. Cooperative localization allows a user of the network to voluntarily share key information with his neighbors for positioning purpose. In other word, all the users work together in a Peer-to-Peer (P2P) way to make range measurements and communication, which forms a map of the mesh network [58]. Cooperative positioning may provide similar performance of hybrid approach, but without any requirement of fixed infrastructure. Thus, cooperative positioning shows a promising prospect of future localization systems and can be addition to future augmentation systems. Furthermore, it can be employed together with hybrid positioning solutions to enhance the robustness the localization systems. Caceres et al. [61] proposed a hybrid GNSS-Time-of-Arrival (ToA) positioning approach base on cooperative Unscented Kalman Filter (UKF) and Sottile et al. [62] proposed a hybrid cooperative GNSS-terrestrial positioning algorithm based on PF. Moreover, Caceres et al. [63] investigated a more general hybrid positioning algorithm based on FG and SPA over a wireless network. Some more results of P2P cooperative positioning inside GNSS can be found in [64, 65].

1.4 CONTRIBUTION OF THIS THESIS

The outcome of this study is the design and analysis of several prototypes, which employ the advantages of different RF techniques, for instance, WSN, RFID, GNSS and UWB. These methods take into account the network topology, ranging method, wireless communication channel, computational capability of the devices, data fusion and information exchanging, with the aim to improve the current localization systems with higher accuracy and higher availability.

The main contributions of this thesis are:

- Development of a mathematical model for hybrid cooperative WSN-RFID positioning and design of the corresponding positioning algorithms (Chapter 3).
- Development of a prototype of hybrid WSN-RFID positioning system and verification of the real deployment (Chapter 4).
- Analysis of hybrid cooperative GNSS-terrestrial positioning algorithms in urban navigation (Chapter 5).
- Performing a hybrid GPS-UWB measurement campaign and testing the hybrid positioning algorithms with real measurements (Chapter 5).
- Development of a cognitive and cooperative tracking approach in wireless networks (Chapter 6).
- Design of a cooperative NLoS identification and positioning approach for network localization (Chapter 7).

2

OVERVIEW OF RANGING AND POSITIONING

In general, network-based positioning systems operate in two steps: *ranging* and *positioning*. Ranging performs the estimations of distance between two nodes of interest as ranging measurements, while positioning uses the measurements obtained from ranging to infer the locations of the unknown nodes. This chapter introduces the common ranging techniques and the corresponding hardware platforms used in this thesis. Moreover, it overviews the general position estimation techniques.

2.1 RANGING TECHNIQUES

2.1.1 *Ranging Methods*

Ranging is a process to determine the distance between two locations or positions. More in general, it is an estimation of position-related parameters. There are many ranging methods and this section gives a brief description of the used four ranging methods: RSS, ToA, Time-Difference-of-Arrival (TDoA), and proximity. .

2.1.1.1 *Received Signal Strength*

RSS, is a power indicator of the received RF signal, so it is also known as Received Signal Strength Indication (RSSI). Ranging estimation based on RSS, first introduced in [66], is most widely used ranging method, since it is relatively simple to be implemented in cheap devices. RSSI is available at almost all the wireless communication standards when each data packet is received. For example, it is directly known to users in the protocols of IEEE 802.11 wireless networking family.

Radio propagation in indoor environment usually suffers from multipath, attenuation from obstacles, interference and other factors. These make strong variability of the RSSI measurements and bring about the main drawback of RSS based ranging method—low accuracy.

Usually, the radio channel is modeled by using the *Log-normal shadowing path loss model* [67], Log-normal model for short. It represents the received signal power $\tilde{P}$, expressed in dBm, as a logarithmic function of the exact distance d between the two wireless agents involved in the ranging.

$$\tilde{P} = P_0 - 10\alpha \log_{10}(d/d_0) + X_\sigma, \tag{2.1}$$

where P_0 is the mean power (expressed in dBm) received at the reference distance d_0 (typically 1 meter), α is the path loss exponent determined by environment [68] and $X_\sigma \sim \mathcal{N}(0, \sigma^2_{dB})$ is additive Gaussian noise which models the shadowing effects.

It is worth mentioning that the Log-normal model is fully characterized by parameters α, P_0 and σ_{dB}. They can be estimated by performing some measurement campaigns in the environment of interest.

Given the parameters α, P_0 and σ_{dB}, the unbiased range estimator derived from Log-normal model (2.1) is [69]:

$$\hat{d} = K \cdot d_0 10^{\frac{P_0 - \hat{P}}{10\alpha}}, \tag{2.2}$$

where K is the bias factor depending on the channel model parameters α and σ_{dB}, $K = \exp\left(-\frac{1}{2}\left(\frac{(\ln 10)\sigma_{dB}}{10\alpha}\right)^2\right)$.

It can be proved that the error of range estimation $\hat{d} - d$ is proportional to the exact distance d [70]:

$$\sqrt{\text{var}\left(\hat{d} - d\right)} \geqslant \frac{(\ln 10)\,\sigma_{dB}}{10\alpha} \cdot d. \tag{2.3}$$

It can be observed from (2.3) that the accuracy of the RSS-based range estimator depends also on α and σ_{dB}. The accuracy of the range estimator degrades for high value of σ_{dB} and for low value of α.

Generally, RSS-based distance estimation depends more on the environment rather than on the adopted communication technology. For instance, in the indoor experimental environment [71] where RF channel model parameters are: $\alpha = 3.313$ and $\sigma_{dB} = 5.547$, the range error is $\sqrt{\text{var}\left(\hat{d} - d\right)} \geqslant 0.386 \cdot d$. Thus, in a room whose length is 20 meters, the range error can be as much as 7.7 meters.

2.1.1.2 *Time of Arrival*

The ToA ranging approach, also known as Time of Flight (ToF), is to measure the RF signal travel time between the transmitter and the receiver. Then the measured distance between the transmitter and the receiver is obtained by multiplying the signal propagation speed, i.e., the speed of light $c = 3 \cdot 10^8 m/s$. ToF can be estimated by using the two approaches: One-Way Ranging (OWR) and Two-Way Ranging (TWR).

OWR method measures the one-way ToF and its procedure is depicted in Fig. 2.1. Agent A sends to agent B a ranging packet, which includes the sending time stamp T_0. When agent B receives this packet and it takes the receiving time stamp T_1. Then the propagation time is estimated as $T = T_1 - T_0$. In this case, both A and B need to be synchronized with a common clock. Even a small synchronization error of 10 nanoseconds will leads to a ranging error of 3 meters. Since OWR method requires accurate

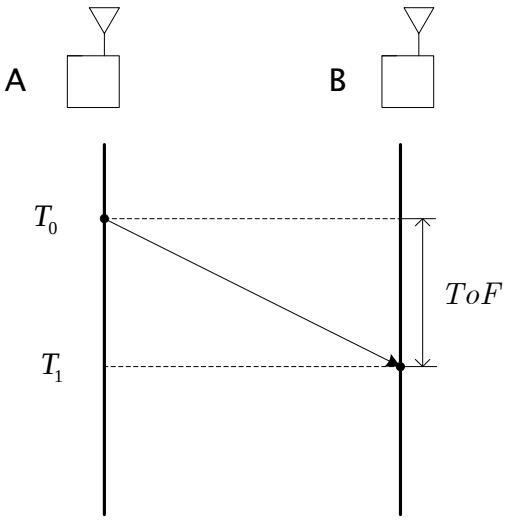

Figure 2.1: One way ranging.

time synchronization between transmitters and receivers, it is usually difficult to be implemented in network localization.

TWR approach measures the Round-Trip Time (RTT) of the RF signal between two transceivers. As depicted in Fig. 2.2, agent A sends at time T_0 a ranging request to agent B, who replies after the replying time, T_R. When the response is received at time T_1, agent A is able to determine the RTT as $T_1 - T_0$. Then the ToA is given by $[(T_1 - T_0) - T_R]/2$. In this case, the two agents are not required to be synchronized, since only the clock of agent A is used to estimate the ToA. Agent B, however, has to send packets back to agent A, which means more traffic is generated in the network.

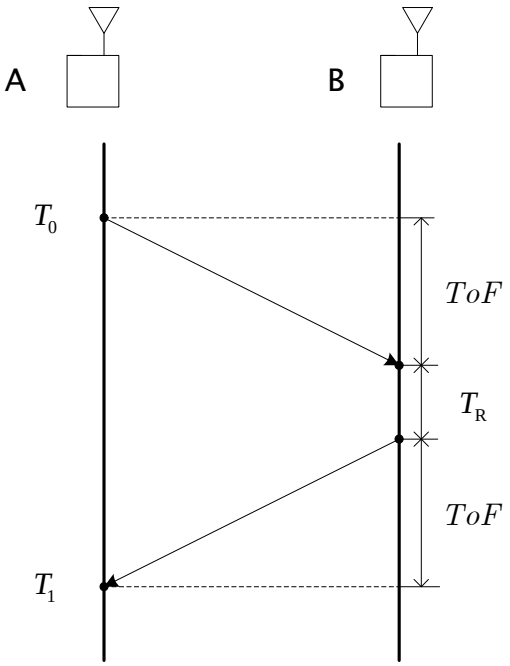

Figure 2.2: Two way ranging.

Cook et al. [72] and Poor in [73] showed the best achievable accuracy of ToA based distance estimate under single path Additive White Gaussian Noise (AWGN) channel satisfies the following inequality:

$$\sqrt{\text{var}\left(\hat{d} - d\right)} \geqslant \frac{c}{2\sqrt{2}\pi\sqrt{SNR}\beta}. \tag{2.4}$$

where $\hat{d}$ is the estimated distance between two stations while d is the corresponding exact distance. And c is the speed of light, SNR is the Signal-to-Noise Ratio (SNR), and β is the effective bandwidth of the transmission signal.

Hence, the ToA ranging accuracy is improved by increasing the SNR or the effective signal bandwidth. This is the main reason why UWB technology is widely used in time-based ranging method. More details about this can be found in the next section that introduces UWB sensors.

2.1.1.3 *Time Difference of Arrival*

TDoA technique is employed when some agents of the network are synchronized while the remaining are not. Usually, these agents are anchor nodes, since they are more powerful than mobile ones, making it possible to synchronize their clocks. A typical example like this is GPS, where all the anchors (satellites) are highly synchronized.

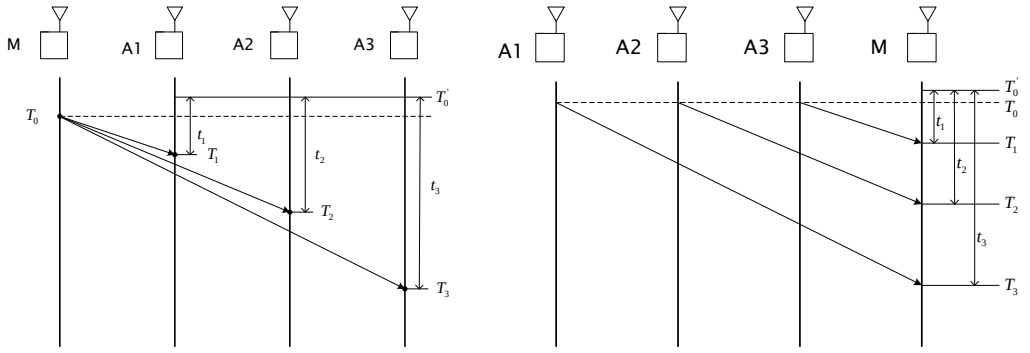

(a) Mobile ranging (b) Anchor ranging

Figure 2.3: Time-difference-of-arrival ranging.

Suppose in a network there are some mobile agents and some anchor agents which are synchronized to a common clock. The ranging procedure of TDoA is shown Fig. 2.3, where it presents two possible schemes of TDoA for three anchors and one mobile. In Fig. 2.3a, each of the anchor agents (A1, A2, A3) sends out a ranging massage including their common time stamp T_0 [1]. When the mobile M receives these messages, it can measure the

1 The time stamps can be different for different anchor agents. The time differences can be calculated in the same way, since they are synchronized. Here it is assumed that all the agents send out the ranging messages at the same time with aim to keep the simplicity of denotation.

different receiving time (T_1, T_2, T_3) and calculate the different ToFs (t_1, t_2, t_3) based on its own clock T_0'. Then, two independent TDoA measurements are estimated as $t_1 - t_2$ and $t_2 - t_3$. By using this subtraction, the clock bias between the anchors and mobiles can be removed.

In Fig. 2.3b, however, the mobile agent M sends out the ranging message at time T_0 and every anchor agent (A1, A2, A3) measures the receiving time (T_1, T_2, T_3). When the different receiving time becomes available, the different ToFs and TDoAs can be calculated like before. Finally, the different TDoA estimates are mapped into different distance differences by multiplying the speed of light.

As described before, the clock bias does not affect the ranging errors in TDoA method, since it is eliminated by subtracting the different ToF estimates. Moreover, the network traffic is minimized, since the ranging messages only go in one direction, either from anchor agents to mobile agents or the opposite way. These are two important advantage of TDoA based systems. Synchronization of the anchor agents, however, is still needed, and the ranging performance relies greatly on the synchronization of anchors. Hence, more efforts from the anchor agents are required to ensure the clock synchronization.

2.1.1.4 *Proximity*

Proximity is using the connectivity measurements for ranging and positioning. For some wireless devices, it is difficult to measure the distance or distance-based parameters. But if two devices can receive information from each other, for sure they are within the communication range. A typical application like this is RFID device. The RFID reader can detect the RFID tag within come distance.

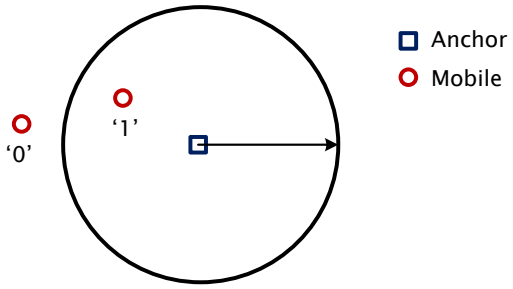

Figure 2.4: Binary measurements of connectivity.

Proximity method usually provides binary measurements, receiving or not receiving, which corresponds to be inside the connectivity range or outside that range. For simplicity, the transmitter is supposed to have omnidirectional antenna. In this case, the coverage area is circular. Fig. 2.4 shows an example of proximity method. If a mobile agent (red circle) are within the coverage area of the anchor agent (blue square), there is a proximity measurement, denoted by 1. If another mobile agent cannot receive message from the anchor agent, there is no proximity information, denoted

by 0. Proximity approach works good if the coverage area is small. In the general access control system, the detection range of High-Frequency (HF) badge is few centimeters, which means the ranging error is also few centimeters. Usually, the information from proximity measurement is limited, but it should be one of the most simple ranging method, only with binary measurements. In addition, almost no overhead is generated for ranging purpose, since the ranging can be done within the normal communication.

2.1.2 *Hardware Platforms*

There section introduces the used hardware platforms in this thesis. These platforms includes sensor boards of WSN and UWB, GPS receiver and RFID device.

2.1.2.1 *Wireless Sensor Network*

A WSN is a collection of large number of nodes organized into cooperative network [74]. Each node of the network has a very low-power microprocessor along with very constrained resources in terms of RAM and flash memory for storing data and the code. It also has a RF transceiver (generally with a omni-directional antenna) and power supply (e.g., batteries). A sensor node can accommodate different types of sensors that are capable of measuring or monitoring parameters of interest, such as temperature, sound, pressure. WSNs are widely used for military applications, transportation, medical and smart space. In typical WSN application, a series of nodes constitute a wireless ad-hoc network, supporting multi-hop routing algorithm and providing longer range commutations [75]. WSN communication standards includes ZigBee, IEEE 802.15.4 and 6LoWPAN.

Based on the different costs of the sensor platforms, WSN is able to implement RSS and ToA ranging. In this thesis TelosB mote platform is used for the WSN experimentation. It is an open-source platform designed for low-power research development and WSN experimentation [76]. A picture of TelosB sensor board is shown in Fig. 2.5. It is has the following important features:

- IEEE 802.15.4/ZigBee compliant transceiver
- Globally compatible with ISM band 2.4 to 2.4835 GHz
- High data rate up to 250 kps
- 8MHz TI MSP430 microcontroller with 10kB RAM
- Optional integrated temperature, humidity and light sensor
- TinyOS open-source operating systems

TelosB mote is small in size ($7 \times 3 \times 3$ cm with batteries) and can provide RSSI measurements up to 10 meters under LoS condition, where there is no obstacle between the transmitter and receiver.

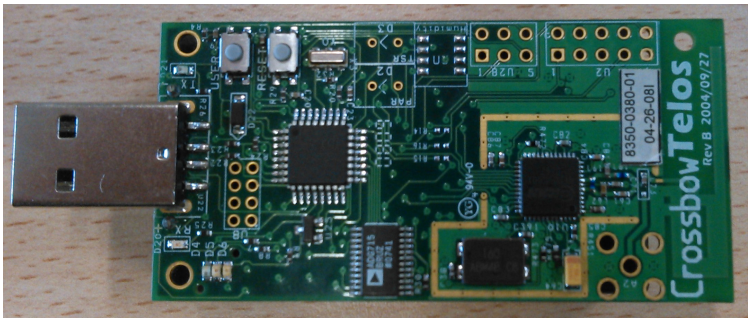

Figure 2.5: Telos mote platform.

2.1.2.2 *Ultra-Wide Band Sensor*

UWB is a radio technology used for short-range, high-bandwidth communications at very low energy level [77]. According to regulation of the US Federal Communications Commission (FCC), a UWB signal is defined as a signal with absolute bandwidth larger than 500 MHz or relative bandwidth larger than 20% of the center frequency. In 2002, FCC authorized the unlicensed use of UWB at frequency band from 3.1 to 10.6 GHz. The tranditional desgin of UWB systems adopt narrow time-domain pulse, whose dulatrion is on the order of nanosecond, to achieves this wide bandwidth. Since this method transmits impulse-like waveform, it is usually called Impulse Radio Ultra-Wide Band (IR-UWB).

As it can be observed from (2.4), the ranging accuracy of ToA method can be improved by increasing the effective signal bandwidth. Hence, UWB technology has the inherent advantage to provide the high accurate ToF measurement. Moreover, UWB technology better tolerates the multipath propagation, because it is able to separate the reflected signal from the direct signal. A UWB radio system has capability of determining the ToF of the transmission precisely. UWB ranging system can provide centimeter-accuracy ranging measurement under LoS conditions. Under NLoS condition, where the direct line between the transmitter and receiver is obstructed, the ranging performance may degrade severely, also depending on the materials of obstacles. The NLoS propagation of RF signal is a large challenge for UWB based localization systems.

In this thesis, a UWB module, from Time Domain (an American company), is used for experimental test and deployment. A photo of this module is shown in Fig. 2.6. The full name of this board is named as PulsON 400 (P400) ranging and communications module, which can provide advanced real-time ranging and communications in high multipath environments [78]. P400 applies coherent signal processing technique and spreads the signal energy over multiple pulses, with the aim to increase the energy per bit. Consequently, the SNR is increased and the communication range is extended. The key features of the P400 module is summarized as:

- Excellent performance in multipath and clutter environments

- Coherent signal processing with extending operating range
- Received signal waveform available to users
- Two-way ToF ranging method
- Coarse range estimate and recalibration
- Operating frequency from 3.1 to 5.3 GHz, with center at 4.3 GHz
- Three interfaces of Ethernet, Serial and USB

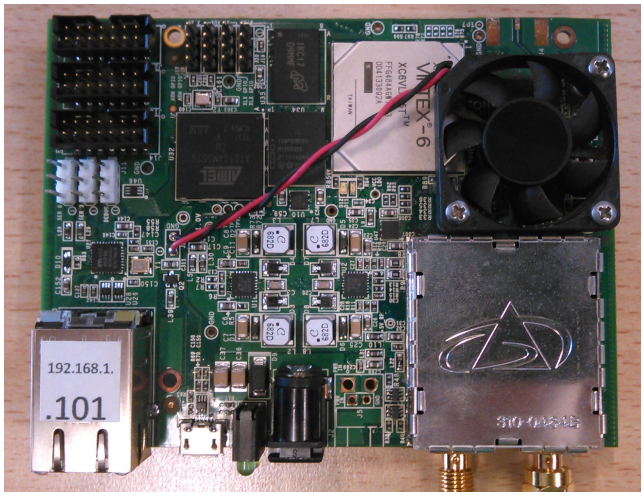

Figure 2.6: P400 UWB module.

The most important advantage of P400 is that it can provide excellent range measurements up to 100 meters in LoS condition. But it is large in size, with the dimension $11 \times 8 \times 9$ cm consisting of antenna and batteries. In addition, it is power hungry, with power consumption of 5 Watts.

2.1.2.3 *Global Navigation Satellite System*

A GNSS is a satellite system which provides autonomous geospatial positioning and navigation with global coverage. All the satellites are highly accurately synchronized and it periodically transmits time signals, allowing the electronic receivers to determine their location (longitude, latitude, and altitude) by using ranging methods of ToA and TDoA.

At present, the available global operational GNSSs are only the GPS from US and the GLObalnaya NAvigatsionnaya Sputnikovaya Sistema (GLONASS) from Russia. China has developed a regional navigation system and now is working on expanding it into the global BeiDou Navigation Satellite System (BDS). The European Union (EU) is developing another GNSS, Galileo positioning system, and has scheduled the global operation by 2020. Moreover, France, Japan and India are developing satellite navigation systems with regional coverage.

In this thesis, a training board of GNSS, called SAT-SURF, from the satellite navigation group of Istituto Superiore Mario Boella (ISMB), is used to collect the real pseudorange measurements from satellites. Fig. 2.7 shows a picture of SAT-SURF. As it can be seen right side of Fig. 2.7, it has two antenna port, one is for GPS antenna and the other is for GSM antenna. Here only the GPS port is used to provide pseudoranges for hybrid GNSS-terrestrial positioning.

Figure 2.7: SatSurf GPS receiver.

2.1.2.4 *Radio Frequency Identification*

RFID system consists of reader and tags. The reader, also known as interrogator, sends out a signal to query the zone and collects the reply from tags. The tag has their ID information stored in their memory circuit, which can be sent to the reader. The tag can be passive or active. Active tag has power supply(usually battery), and can transmit signal to the reader autonomously with large distance. Passive tag does not need battery or power supply. It can draw the signal power from the reader and backscatter their ID information to the reader. Usually, the reader is large in size and expensive while the tag is small and cheap, especially for passive tag.

In this work, some RFID devices are used for hybrid localization. Fig. 2.8 shows the HF RFID system, which is usually used for access control. It consists of reader (Fig. 2.8a) and badge (Fig. 2.8b). The reading range of this system is only a few centimeters, so one detection of badge can provide very accurate positioning information.

Fig. 2.9 presents the Ultra-High Frequency (UHF) RFID system. In particular, Fig. 2.9a shows the antenna of the reader, whose size is 50×20 cm, and Fig. 2.9b the passive tag with very small size. Due to the size of the UHF antenna, the reader can detect a tag within a approximated circular area whose radius is around 2 meters.

(a) HF badge reader

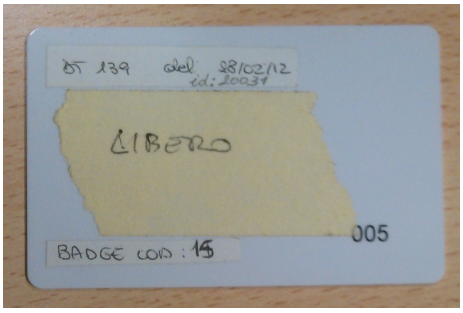

(b) HF badge

Figure 2.8: HF RFID devices.

(a) UHF reader antenna

(b) UHF tag

Figure 2.9: UHF RFID devices.

2.2 POSITIONING TECHNIQUES

After obtaining position-related signal parameters, the next step of localization is to estimate position based on those parameters. There are many positioning techniques and two of them are studied in this work.

2.2.1 *Geometric Approaches*

Geometric approaches exploit geometric relationships between different anchors and mobile to estimate the position of the mobile.

2.2.1.1 *Lateration*

Lateration uses the intersection of lines, curves, circles and sphere to determine the location in 2D or 3D space. When dealing with distance measurements from RSS and ToA, the mobile's position is the intersection of circles (2D localization) or sphere (3D localization) centered at the three anchors. An example of 2D lateration is shown in Fig. 2.10, where the intersection (small red circle) is the position of mobile agent.

When coping with TDoA measures, which corresponds to distance differences from anchors, the location is estimated as the intersection of hyperbolas with foci at the positions of anchors (see Fig. 2.11). It is worth mentioning that only two TDoAs are enough to locate the mobile in 2D

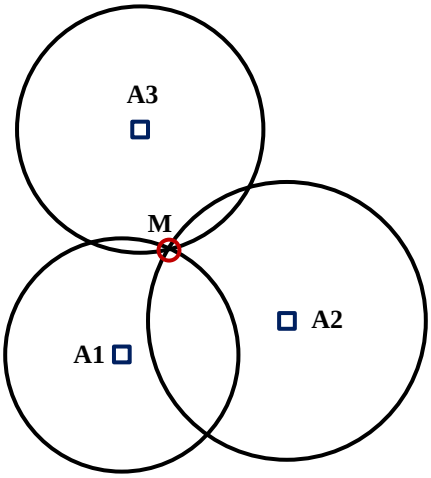

Figure 2.10: Lateration of three anchors based on RSS and ToA.

space, because the sign of the distance difference can determine which intersections to select. In practice there is always no existence of perfect intersection as Fig. 2.10 and 2.11. Some additional optimal strategies are taking into account to select the right location.

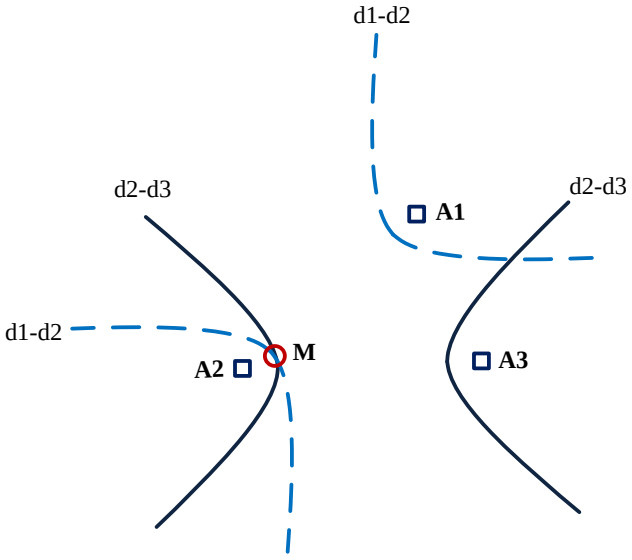

Figure 2.11: Lateration of three anchors based on TDoA.

2.2.1.2 *Proximity Localization*

The localization of proximity information can be also by using geometry of the anchors. Instead of using the intersection of lines, the intersection of coverage area can be exploited. Fig. 2.12 shows how to locate a mobile with proximity information. The mobile's position is considered as the the center of the overlapping area. As it can be seen, the localization error depends on the size of the coverage. The positioning error may be large, but it could be better than unavailability.

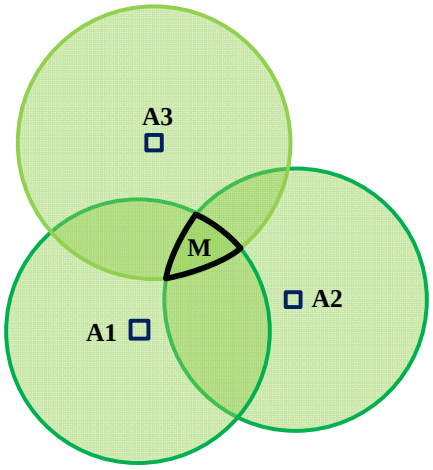

Figure 2.12: Locate the mobile with proximity information.

Although the proximity localization is not accurate, it can help to locate the mobile agents with other range measurements, when there are not enough measurements or these measurements are with large errors. Fig. 2.12 shows an example of proximity location. At a specific time, there are only two range measurements from two anchors (A1 and A2), resulting in an ambiguity of the position estimate. Fortunately, there is a proximity measurement from anchor A3, which loses the range measurements or maybe it can only provide proximity detection. By using the connectivity from anchor A3 (green circular area), the ambiguity of mobile's position is solved. As mentioned before, the RSS ranging measurements are not accurate, the adoption of proximity can improve the positioning performance [79].

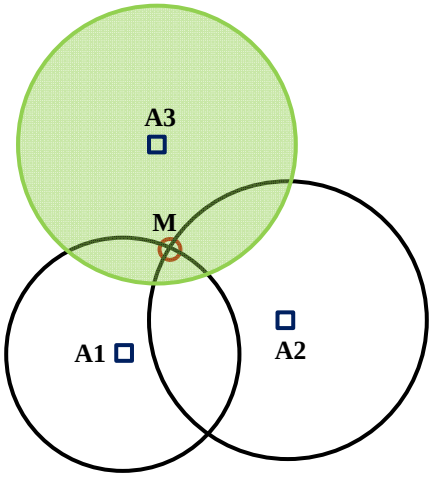

Figure 2.13: Proximity help locate the mobile.

2.2.2 *Bayesian Approaches*

In the geometrical localization, the statistics of the position-related signal parameters are not taken into account. The Bayesian positioning approach

considers the probability and statistics of these measurements and the involution of the mobile's positions, thus it is known as Bayesian tracking.

The Bayesian tracking approach models the dynamic positioning problem as a discrete-time stochastic process as follows:

$$\boldsymbol{x}^{(k)} = f^{(k)}\left(\boldsymbol{x}^{(k-1)}, \boldsymbol{\omega}^{(k-1)}\right), \tag{2.5}$$

where $\boldsymbol{x}^{(k)}$ and $\boldsymbol{x}^{(k-1)}$ are state vectors (positions and other parameters of interest, i.e., velocity and acceleration) at time step k and $k-1$ respectively, and $\boldsymbol{\omega}^{(k-1)}$ is the process noise from time step $k-1$ to k, which simulates the effects of mis-modeling and other unpredicted disturbances. $f^{(k)}(\cdot)$ is state transition function defined from time step $k-1$ to k. It can be a linear or non-linear function.

The relationship between the state and measurement is called observation model, expressed as

$$\boldsymbol{z}^{(k)} = h^{(k)}\left(\boldsymbol{x}^{(k)}, \boldsymbol{v}^{(k)}\right). \tag{2.6}$$

where $\boldsymbol{z}^{(k)}$ represents all available measurements (observations) at time step k and $\boldsymbol{v}^{(k)}$ is the measurement noise. $h^{(k)}(\cdot)$ is the observation function at time step k and could be also non-linear.

As it can be seen from (2.5), Bayesian tracking method models the dynamic problem as first order Markov chain. The combination of (2.5) and (2.6) leads to a Markov chain (Fig. 2.14), whose state $\boldsymbol{x}^{(k)}$ is not directly observable but can be indirectly inferred from the measurements.

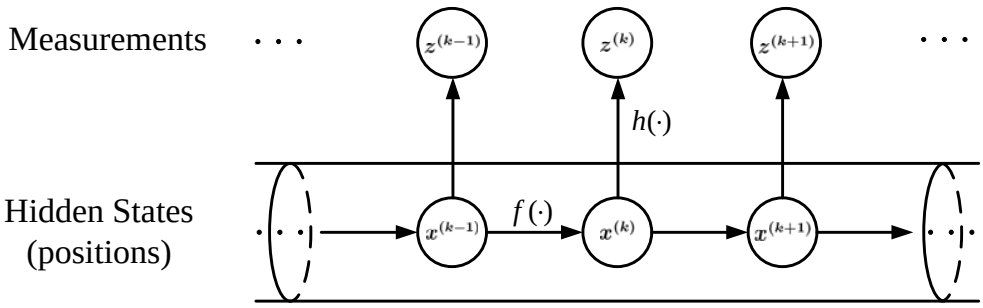

Figure 2.14: Hidden Markov model for Bayesian tracking.

From the Bayesian point of view, the tracking problem is to recursively estimate new state $\boldsymbol{x}^{(k)}$, taking into account all the available measurements $\boldsymbol{z}^{(1:k)}$ $(\boldsymbol{z}^{(1)}, \cdots, \boldsymbol{z}^{(k)})$, up to time step k. In other words, this problem is the calculation of the marginal distribution $p(\boldsymbol{x}^{(k)}|\boldsymbol{z}^{(1:k)})$, which in principle can be estimated by two stages: *prediction* and *update*. In prediction stage, the *a priori* probability distribution function (p.d.f.) $p(\boldsymbol{x}^{(k)}|\boldsymbol{z}^{(1:k-1)})$ of current state $\boldsymbol{x}^{(k)}$ is obtained. In update stage, the *a posteriori* p.d.f. $p(\boldsymbol{x}^{(k)}|\boldsymbol{z}^{(1:k)})$ is obtained.

Assume that the p.d.f. $p(\boldsymbol{x}^{(k-1)}|\boldsymbol{z}^{(1:k-1)})$ is available at time step k-1. The prediction of the *a priori* p.d.f. is obtained by using Chapman-Kolmogorov equation

$$\begin{aligned} p\left(\boldsymbol{x}^{(k)}|\boldsymbol{z}^{(1:k-1)}\right) &= \int p\left(\boldsymbol{x}^{(k)}, \boldsymbol{x}^{(k-1)}|\boldsymbol{z}^{(1:k-1)}\right) d\boldsymbol{x}^{(k-1)} \\ &= \int p\left(\boldsymbol{x}^{(k)}|\boldsymbol{x}^{(k-1)}, \boldsymbol{z}^{(1:k-1)}\right) p\left(\boldsymbol{x}^{(k-1)}|\boldsymbol{z}^{(1:k-1)}\right) d\boldsymbol{x}^{(k-1)} \\ &= \int p\left(\boldsymbol{x}^{(k)}|\boldsymbol{x}^{(k-1)}\right) p\left(\boldsymbol{x}^{(k-1)}|\boldsymbol{z}^{(1:k-1)}\right) d\boldsymbol{x}^{(k-1)}, \end{aligned} \tag{2.7}$$

where it adopts the property of first order Markov process:

$$p\left(\boldsymbol{x}^{(k)}|\boldsymbol{x}^{(k-1)}, \boldsymbol{x}^{(1:k-1)}\right) = p\left(\boldsymbol{x}^{(k)}|\boldsymbol{x}^{(k-1)}\right), \tag{2.8}$$

The p.d.f. $p(\boldsymbol{x}^{(k)}|\boldsymbol{x}^{(k-1)})$ depends only on the system transition function f_k and the statistics of process noise $\boldsymbol{\omega}^{(k-1)}$ (2.5). Here suppose that the initial p.d.f. $p(\boldsymbol{x}^{(0)}|\boldsymbol{z}^{(0)}) \equiv p(\boldsymbol{x}^{(0)})$, where $\boldsymbol{z}^{(0)}$ means no measurements available at the beginning.

When the new measurement $\boldsymbol{z}^{(k)}$ is available, the update can be carried out via Bayes' rule

$$\begin{aligned} p\left(\boldsymbol{x}^{(k)}|\boldsymbol{z}^{(1:k)}\right) &= p\left(\boldsymbol{x}^{(k)}|\boldsymbol{z}^{(k)}, \boldsymbol{x}^{(1:k-1)}\right) \\ &= \frac{p\left(\boldsymbol{z}^{(k)}|\boldsymbol{x}^{(k)}, \boldsymbol{z}^{(1:k-1)}\right) p\left(\boldsymbol{x}^{(k)}|\boldsymbol{z}^{(1:k-1)}\right)}{p\left(\boldsymbol{z}^{(k)}|\boldsymbol{z}^{(1:k-1)}\right)} \\ &= \frac{p\left(\boldsymbol{z}^{(k)}|\boldsymbol{x}^{(k)}\right) p\left(\boldsymbol{x}^{(k)}|\boldsymbol{z}^{(1:k-1)}\right)}{p\left(\boldsymbol{z}^{(k)}|\boldsymbol{z}^{(1:k-1)}\right)}, \end{aligned} \tag{2.9}$$

where the normalizing factor $p\left(\boldsymbol{z}^{(k)}|\boldsymbol{z}^{(1:k-1)}\right)$ can be calculated as

$$p\left(\boldsymbol{z}^{(k)}|\boldsymbol{z}^{(1:k-1)}\right) = \int p\left(\boldsymbol{z}^{(k)}|\boldsymbol{x}^{(k)}\right) p\left(\boldsymbol{x}^{(k)}|\boldsymbol{z}^{(1:k-1)}\right) d\boldsymbol{x}^{(k)}. \tag{2.10}$$

Note that in (2.10), $p\left(\boldsymbol{z}^{(k)}|\boldsymbol{x}^{(k)}\right)$ can be calculated by using the observation equation (2.6), knowing the p.d.f. of the measurement noise $\boldsymbol{v}^{(k)}$. In this way, the measurement $\boldsymbol{z}^{(k)}$ is used to correct the *a prior* p.d.f. and obtain the *a posterior* p.d.f.of current state. Thus the *update* stage is also called *correction*.

The two equations (2.7) and (2.9) form the basis of optimal Bayesian solution for dynamic systems. In general case, there is no optimal solutions for them because of the non-linearity of functions f and h and no knowledge of noise distribution $\boldsymbol{\omega}$ and $\boldsymbol{v}$.

Sometimes KF can provide optimal solution of the two equations, but the conditions are restricted to: linearity of both transition and observation functions and Gaussian distribution of both process noise and measurement noise. Usually, some sub-optimal approximation solutions are

adopted. Typically, there are two most widely adopted approaches for such approximation: direct and indirect. Extended Kalman Filter (EKF) makes a direct numerical approximation on the posterior distribution and provides efficient solutions for (2.7) and (2.9). The performance is good when the process model is nearly linear and the noise is almost Gaussian. For more general cases, PF is adopted to solve the two equations with non-linear systems and non-Gaussian noise. PF makes an indirect approximation of the posterior density function of the system state by using a set of particles. EKF and PF have their own advantages and are the most used algorithms for positioning. In this thesis, the implementation of both will be presented.

2.2.2.1 *Extended Kalman Filter*

EKF provides an efficient recursive solution for non-linear discrete filtering problems with low complexity [80], and it is widely used in positioning and tracking applications.

EKF models a dynamic system using the same equations of (2.5) and (2.6). But the process noise and the measurement noise are supposed to be Gaussian, that is, $\boldsymbol{\omega}^{(k)} \sim \mathcal{N}(0, \boldsymbol{Q}^{(k)})$, and $\boldsymbol{v}^{(k)} \sim \mathcal{N}(0, \boldsymbol{R}^{(k)})$. It estimates the *a posteriori* state vector by using a feedback control approach. First, the current state is predicted to produce the a *priori* estimate and then it is refined by using the feedback from the measurements. These two steps are also known as *predict phase*, and *update phase*.

Predict phase: In this phase, the EKF provides an estimate of both the a *priori* state $\hat{\boldsymbol{x}}^{(k|k-1)}$ and error covariance matrix $\boldsymbol{P}^{(k|k-1)}$. In particular, the estimation is based on the previous a *posteriori* estimates of both the state $\hat{\boldsymbol{x}}^{(k-1)}$ and the error covariance matrix $\boldsymbol{P}^{(k-1)}$, by using the following two equations:

$$\hat{\boldsymbol{x}}^{(k|k-1)} = f\left(\hat{\boldsymbol{x}}^{(k-1)}, 0\right), \tag{2.11}$$

$$\boldsymbol{P}^{(k|k-1)} = \boldsymbol{F}^{(k-1)}\boldsymbol{P}^{(k-1)}\boldsymbol{F}^{(k-1)\intercal} + \boldsymbol{W}^{(k-1)}\boldsymbol{Q}^{(k-1)}\boldsymbol{W}^{(k-1)\intercal}. \tag{2.12}$$

where $\boldsymbol{F}^{(k-1)} = \frac{\partial f}{\partial \boldsymbol{x}}\big|_{\hat{\boldsymbol{x}}^{(k-1)}}$ and $\boldsymbol{W}^{(k-1)} = \frac{\partial f}{\partial \boldsymbol{\omega}}\big|_{\hat{\boldsymbol{x}}^{(k-1)}}$ are Jacobian matrices of the transition function $f(\cdot)$ calculated at previous estimate $\hat{\boldsymbol{x}}^{(k-1)}$.

Update phase: During this procedure, EKF performs the feedback control, where both the state vector and the error covariance matrix are updated using new measurements. First, the optimal Kalman gain $\boldsymbol{K}^{(k)}$ and innovation vector $\tilde{\boldsymbol{y}}^{(k)}$ are calculated as follows:

$$\boldsymbol{K}_k = \boldsymbol{P}^{(k|k-1)}\boldsymbol{H}^{(k)\intercal}\left(\boldsymbol{H}^{(k)}\boldsymbol{P}^{(k|k-1)}\boldsymbol{H}^{(k)\intercal} + \boldsymbol{V}^{(k)}\boldsymbol{R}^{(k)}\boldsymbol{V}^{(k)\intercal}\right)^{-1}, \tag{2.13}$$

$$\tilde{\boldsymbol{y}}^{(k)} = \boldsymbol{z}^{(k)} - h\left(\hat{\boldsymbol{x}}^{(k|k-1)}, 0\right), \tag{2.14}$$

where $\boldsymbol{H}^{(k)} = \frac{\partial h}{\partial \boldsymbol{x}}\big|_{\hat{\boldsymbol{x}}^{(k|k-1)}}$ and $\boldsymbol{V}^{(k)} = \frac{\partial h}{\partial \boldsymbol{v}}\big|_{\hat{\boldsymbol{x}}^{(k|k-1)}}$ are Jacobian matrices of the observation function $h(\cdot)$ evaluated at current prediction $\hat{\boldsymbol{x}}^{(k|k-1)}$.

Then, the state estimate $\hat{\boldsymbol{x}}^{(k)}$ and error covariance matrix $\boldsymbol{P}^{(k)}$ are updated as follows:

$$\hat{\boldsymbol{x}}^{(k)} = \hat{\boldsymbol{x}}^{(k|k-1)} + \boldsymbol{K}_k \tilde{\boldsymbol{y}}^{(k)}, \tag{2.15}$$

$$\boldsymbol{P}^{(k)} = (\boldsymbol{I} - \boldsymbol{K}_k \boldsymbol{H}_k)\, \boldsymbol{P}^{(k|k-1)}. \tag{2.16}$$

where $\boldsymbol{I}$ is an identity matrix whose dimension is the same as $\boldsymbol{P}^{(k)}$.

In practice, it is impossible to know at each estimation time the exact value of the process noise $\boldsymbol{\omega}^{(k)}$ and measurement noise $\boldsymbol{v}^{(k)}$, the EKF approximates the vector state $\hat{\mathbf{x}}_{k|k-1}$ and the innovation vector $\tilde{\mathbf{y}}_k$ without them as (2.11) and (2.14). In general, the EKF requires an initialization step where both the state vector $\hat{\boldsymbol{x}}^{(0)}$ and the error covariance matrix $\boldsymbol{P}^{(0)}$ are set. After that, the recurrence can start according to the equations from (2.11) to (2.16).

2.2.2.2 *Particle Filter*

PF is a category of MC methods which recursively estimates the probability density of the state vector [81]. The probability density is approximated by a set of samples called particles $\left\{\boldsymbol{x}^{(k)^i}, w^{(k)^i}\right\}_{i=1}^{N}$, and each particle $\boldsymbol{x}^{(k)^i}$ (represented by a vector with the same size of the state vector) is associated a weight $w^{(k)^i}$. The posterior p.d.f. is approximated as

$$p\left(\boldsymbol{x}^{(k)}|\boldsymbol{z}^{(1:k)}\right) \approx \sum_{i=1}^{N} w^{(k)^i} \delta\left(\boldsymbol{x}^{(k)} - \boldsymbol{x}^{(k)^i}\right), \tag{2.17}$$

where $\delta(\cdot)$ is Dirac delta function, defined as $\delta(0) \to +\infty$ and $\int \delta(x)dx = 1$.

The weight $w^{(k)^i}$ is updated by importance sampling [82].

$$w^{(k)^i} \propto w^{(k-1)^i} \frac{p\left(\boldsymbol{z}^{(k)}|\boldsymbol{x}^{(k)^i}\right) p\left(\boldsymbol{x}^{(k)^i}|\boldsymbol{x}^{(k-1)^i}\right)}{q\left(\boldsymbol{x}^{(k)^i}|\boldsymbol{x}^{(0:k-1)^i}, \boldsymbol{z}^{(1:k)}\right)}, \tag{2.18}$$

where $p(\boldsymbol{x}^{(k)^i}|\boldsymbol{x}^{(k-1)^i})$ and $p(\boldsymbol{z}^{(k)}|\boldsymbol{x}^{(k)^i})$ represent the state transition and measurement update, corresponding to (2.5) and (2.6), respectively. And $q(\boldsymbol{x}^{(k)^i}|\boldsymbol{x}^{(0:k-1)^i}, \boldsymbol{z}^{(1:k)})$ is the importance density. Usually, the state transition probability function is chosen as the importance density to simply the weight updating:

$$w^{(k)^i} \propto w^{(k-1)^i} p\left(\boldsymbol{z}^{(k)}|\boldsymbol{x}^{(k)^i}\right). \tag{2.19}$$

The main drawback of this approach is the high level of computation complexity, which mainly depends on the number of particles and dimension of the state vector. Gustafsson et al. [83] proposed a framework of using PF for positioning and tracking problem, with high accuracy and low dimensional state.

Part II

HYBRID AND COOPERATIVE POSITIONING SOLUTIONS

3

HYBRID COOPERATIVE WSN-RFID POSITIONING

Nowadays indoor positioning applications have received great attentions among short range wireless communication systems. In particular, WSN is the most widely used technology for indoor localization as it is cheap and easy to deploy [84]. However, location accuracy is limited by the harsh propagation of the RF signals in indoor environments, for instance, caused by the presence of obstacles between wireless nodes, multi-paths, interference, etc. To overcome these effects and improve positioning accuracy, RFID technology is employed to assist the WSN-based positioning.

3.1 HYBRID WSN-RFID POSITIONING

As introduced before, a WSN node is able to accommodate different types of sensors that are capable of measuring or monitoring parameters of interest. WSNs are widely used for many applications, including indoor positioning. Since the indoor environment is harsh from the RF propagation point of view, also the resulting location accuracy is heavily affected. For instance, when a pair of nodes are under NLoS condition [85], the received signal is extremely attenuated. As a consequence, there may not be enough connectivity and thus ranging data to infer the target node's coordinates. Moreover, under indoor conditions, the signal could suffer from severe multi-path transmission which often leads to an overestimation of distances between WSN nodes. Thus, given the above mentioned limitations, in order to provide an accurate position estimation, the WSN based positioning needs some extra reference points, for instance, from other technologies. Considering cost and deployment requirements, the RFID technology has been selected as a suitable solution.

This section proposes two hybrid positioning approaches based both on WSN and RFID. One solution uses the EKF algorithm while the other one uses PF approach. Both methods are compared through Matlab simulations which demonstrate that in general the WSN-RFID hybrid approach is feasible and achieves good positioning estimation capabilities even under harsh indoor conditions.

3.1.1 *Hybrid Topology and Measurement Modeling*

The hybrid topology is depicted in Fig. 3.1, where squares represent WSN anchor nodes and crosses represent RFID anchors which are passive tags. The path with blue dots is the actual trajectory of the mobile node; the green circles represent the interrogation area of the RFID reader which is installed on the mobile node. We suppose that the reader has an omni-directional antenna and thus the interrogation area is a circle with radius d_r.

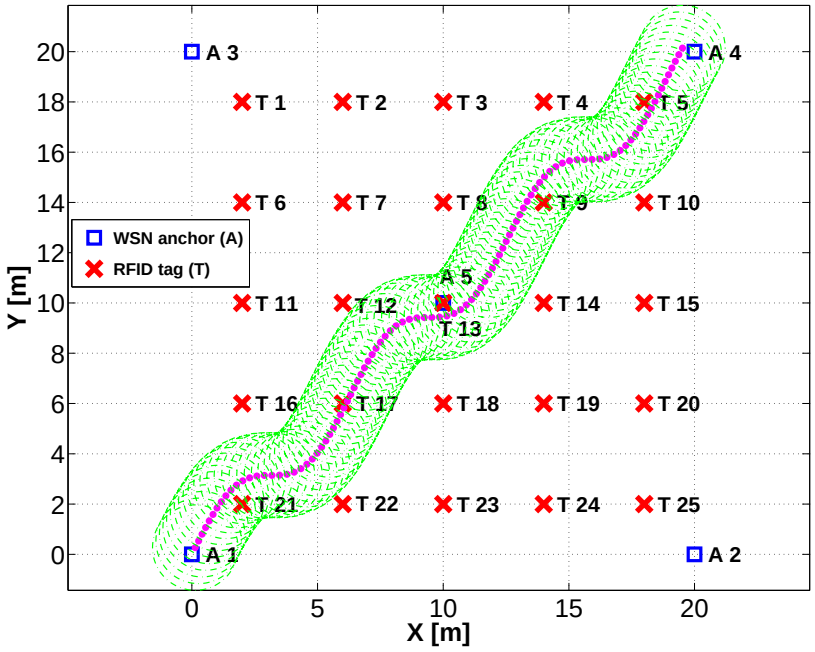

Figure 3.1: Hybrid WSN-RFID topology.

The mobile node is equipped with a WSN node and a RFID reader, so it is able to communicate with both the neighboring WSN anchor nodes and the anchor RFID tags. In this topology, the RFID deployment is composed of passive tags, which are very cheap and do not need any power supply, thus maintaining the low cost of the hybrid positioning approach.

Each anchor RFID tag can provides information '1' or '0' to the mobile reader depending on if the tag is inside or outside the reader coverage area. In order to integrate the RFID observation to the EKF equations, the RFID information is translated to a distance estimate. When the tag is inside the coverage area of the reader, we assume that the position of the mobile node is uniformly distributed within the circle centered at the tag's position. Therefore, the RFID information equal to '1' is converted to the average distance estimate $\tilde{d}_r = d_r/2$, i.e., equal to half the RFID reader interrogation radius, d_r. Moreover, we assume that the RFID based distance measurement is normally distributed as $\tilde{d}_r \sim \mathcal{N}\left(d_r/2, \sigma^2_{\text{RFID}}\right)$, where σ^2_{RFID} is a function of the radius d_r.

3.1.2 *Hybrid Tracking Algorithms*

3.1.2.1 *State Definition*

The performance and complexity of tracking algorithms depend heavily on how to model the system. In general, there are three widely used dynamic models [83, 86], Position (P), Position-Velocity (PV) and Position-Velocity-Acceleration (PVA). Here with aim to track a mobile node, only the PV model whose state vector is composed of position and velocity is taken into account. We suppose that the position and velocity are expressed in a 2-dimensional space using the Cartesian coordinate reference system. The position vector at the estimation time $t^{(k)}$ is defined as $\boldsymbol{p}^{(k)} = \left[x^{(k)}, y^{(k)}\right]$ and the velocity vector as $\boldsymbol{v}^{(k)} = \left[\dot{x}^{(k)}, \dot{y}^{(k)}\right]$, where $\dot{x}^{(k)}$, $\dot{y}^{(k)}$ represent the speed along the x and y axis, respectively. The PV model can be expressed by the two following equations:

$$\boldsymbol{x}^{(k)} = \left[\begin{array}{cc} \boldsymbol{p}^{(k)}, & \boldsymbol{v}^{(k)} \end{array}\right]^{\intercal}, \tag{3.1}$$

$$\boldsymbol{x}^{(k)} = \left[\begin{array}{cc} \boldsymbol{I}_2 & \triangle t^{(k)} \boldsymbol{I}_2 \\ 0_2 & \boldsymbol{I}_2 \end{array}\right] \boldsymbol{x}^{(k-1)} + \left[\begin{array}{c} \triangle t^{(k)^2} \boldsymbol{I}_2 \\ \triangle t^{(k)} \boldsymbol{I}_2 \end{array}\right] \boldsymbol{\omega}^{(k-1)}, \tag{3.2}$$

where $\triangle t^{(k)}$ is the time elapsed from the previous estimation time $t^{(k-1)}$ to the current one $t^{(k)}$, $\boldsymbol{I}_2$ and 0_2 are 2×2 identity matrix and zero matrix, respectively. $\boldsymbol{\omega}^{(k-1)} = [\ddot{x}^{(k-1)}, \ddot{y}^{(k-1)}]^{\intercal}$ is the unknown acceleration vector which models the process noise based on previous state $\boldsymbol{x}^{(k-1)}$. Notice that in the predict phase, the EKF can use (3.2) with $\boldsymbol{\omega}^{(k-1)} = 0$ to simply the estimation process.

3.1.2.2 *Hybridization with WSN Distance Measurements*

- Hybrid EKF with distance observation

In this case we suppose that there is distance measurements from WSN, which can be obtained by converting the RSS measures into distance. Typically, the distance measurements are modeled as exact distance plus a Gaussian noise:

$$\tilde{d}_a^{(k)} = d_a^{(k)} + e_{d_a}, \tag{3.3}$$

where $e_{d_a} \sim \mathcal{N}(0, \sigma_{\tilde{d}_a}^{(k)^2})$ is the noise and $d_a^{(k)}$ is the exact distance between the target node and the WSN anchor a at time $t^{(k)}$. Since the RFID-based observation is translated to a distance measurement, it can be processed in the same way as the WSN distance measurements.

Moreover, the following notations are used. At the estimation time $t^{(k)}$, the coordinates of the mobile are $\boldsymbol{p}^{(k)} = \left[x^{(k)}, y^{(k)}\right]$, the coordinates of WSN connected anchor nodes $\mathcal{A}^{(k)}$ are $\boldsymbol{p}_a = [x_a, y_a]$, for $a \in \mathcal{A}^{(k)}$, and the

coordinates of connected RFID anchors $\mathcal{R}^{(k)}$ are $\boldsymbol{p}_r = [x_r, y_r]$, for $r \in \mathcal{R}^{(k)}$. The observation vector $\mathbf{z}_k$ is defined as

$$\boldsymbol{z}^{(k)} = \left\{ \left\{ \tilde{d}_a^{(k)} \right\}_{a \in \mathcal{A}^{(k)}}, \left\{ \tilde{d}_r^{(k)} \right\}_{r \in \mathcal{R}^{(k)}} \right\}^T, \tag{3.4}$$

where $\tilde{d}_a^{(k)}$ is the WSN distance measurement defined in (3.3) and $\tilde{d}_r^{(k)}$ is the distance measurement from the RFID tag r, which can assume as $d_r/2$ or 0 according to the onserved information '1' or 'o', respectively.

The observation function h depends on the estimated distances between the mobile and anchors,

$$h\left(\hat{\boldsymbol{x}}^{(k|k-1)}\right) = \begin{bmatrix} \operatorname{dist}\left(\hat{\boldsymbol{p}}^{(k|k-1)}, \boldsymbol{p}_a\right) a \in \mathcal{A}^{(k)} \\ \vdots \\ \operatorname{dist}\left(\hat{\boldsymbol{p}}^{(k|k-1)}, \boldsymbol{p}_r\right) r \in \mathcal{R}^{(k)} \\ \vdots \end{bmatrix}, \tag{3.5}$$

where $\operatorname{dist}(\cdot)$ is the Euclidean distance between two positions, defined as

$$\operatorname{dist}(\boldsymbol{p}_1, \boldsymbol{p}_2) = \sqrt{(x_1 - x_2)^2 + (y_1 - y_2)^2}. \tag{3.6}$$

Consequentially, the Jacobian matrix is obtained by partly differentiating the h function with respect to the vector state:

$$\boldsymbol{H}^{(k)} = \begin{bmatrix} \frac{\hat{x}^{(k|k-1)} - x_a}{\operatorname{dist}\left(\hat{\boldsymbol{p}}^{(k|k-1)}, \boldsymbol{p}_a\right)} & \frac{\hat{y}^{(k|k-1)} - y_a}{\operatorname{dist}\left(\hat{\boldsymbol{p}}^{(k|k-1)}, \boldsymbol{p}_a\right)} & 0 & 0 \\ \vdots & \vdots & \vdots & \vdots \\ \frac{\hat{x}^{(k|k-1)} - x_r}{\operatorname{dist}\left(\hat{\boldsymbol{p}}^{(k|k-1)}, \boldsymbol{p}_r\right)} & \frac{\hat{y}^{(k|k-1)} - y_r}{\operatorname{dist}\left(\hat{\boldsymbol{p}}^{(k|k-1)}, \boldsymbol{p}_r\right)} & 0 & 0 \\ \vdots & \vdots & \vdots & \vdots \end{bmatrix}, \tag{3.7}$$

Suppose all the measurements are independent, the covariance matrix $\boldsymbol{R}^{(k)}$ is diagonal matrix as

$$\boldsymbol{R}^{(k)} = \operatorname{diag}\left(\sigma_{\tilde{d}_a}^{(k)^2} \cdots, \sigma_{\tilde{d}_r}^{(k)^2} \cdots\right). \tag{3.8}$$

where $\sigma_{\tilde{d}_a}^{(k)^2}$ and $\sigma_{\tilde{d}_r}^{(k)^2}$ are the corresponding measurement noise variance at current time $t^{(k)}$.

- Hybrid PF with distance observation

The first step consists in generating the *a priori* estimation for every particle by applying (3.2), where the unknown acceleration vector $\boldsymbol{\omega}^{(k)}$ is drawn from a Gaussian distribution.

The weight update step depends on the likelihood function $p(\boldsymbol{z}^{(k)}|\boldsymbol{x}^{(k)^i})$. Since range measurements are independent between each other, the likelihood function can be simply expressed as product of all the contribution of measurments:

$$p\left(\boldsymbol{z}^{(k)}|\mathbf{x}^{(k)^i}\right) = \prod_{a\in\mathcal{A}^{(k)}} p_{e_{d_a}}\left(\tilde{d}_a^{(k)} - \text{dist}\left(\boldsymbol{p}^{(k)^i}, \boldsymbol{p}_a\right)\right) \cdot \prod_{r\in\mathcal{R}^{(k)}} p_{e_r}\left(\tilde{d}_r^{(k)} - \text{dist}\left(\boldsymbol{p}^{(k)^i}, \boldsymbol{p}_r\right)\right). \tag{3.9}$$

where $p_{e_{d_a}}$ and p_{e_r} are the probability density functions of WSN range error $e_{d_a} \sim \mathcal{N}(0, \sigma^{(k)^2}_{\tilde{d}_a})$ and RFID range error $e_r \sim \mathcal{N}(0, \sigma^{(k)^2}_{\tilde{d}_r})$, respectively. $\boldsymbol{p}^{(k)^i}$ is the position component of the particle $\mathbf{x}^{(k)^i}$ and $\text{dist}(\boldsymbol{p}^{(k)^i}, \boldsymbol{p}_a)$ and $\text{dist}(\boldsymbol{p}^{(k)^i}, \boldsymbol{p}_r)$ are calculated using (3.6).

Resampling is adopted to eliminate low weight particles and to concentrate on high weight particles. Here we adopts a Gaussian resampling algorithm. The idea is to generate new particles with Gaussian distribution whose mean and variance are obtained from the input particles and their weights. The main advantage of this algorithm is the generation of new particles instead of repeating old ones.

3.1.2.3 *Hybridization of WSN RSS Measurements*

In this subsection, we consider RSS measurements from WSN for the hybridization.

- Hybrid EKF with RSS observation

Since the WSN measurements are RSS values, the observation vector $\boldsymbol{z}^{(k)}$ becomes:

$$\boldsymbol{z}^{(k)} = \left\{\left\{\tilde{P}_a^{(k)}\right\}_{a\in\mathcal{A}^{(k)}}, \left\{\tilde{d}_r\right\}_{r\in\mathcal{R}^{(k)}}\right\}^T, \tag{3.10}$$

where $\tilde{P}_a^{(k)}$ is the received signal power at time $t^{(k)}$ from the WSN anchor node a ($a \in \mathcal{A}^{(k)}$)and $\tilde{d}_r^{(k)}$ ($r \in \mathcal{R}^{(k)}$) is RFID observation as described in section 3.1.1.

Here the RSS measurements are modeled with the *log-normal shadowing path loss model* [67] which relates RSS with distance as:

$$\tilde{P}_a(d) = P_0 - 10\alpha \log_{10}(d_a/d_0) + e_{P_a}, \tag{3.11}$$

where P_0 is the mean power received at the reference distance d_0 (typically 1 meter), α is the path loss exponent and $e_{P_a} \sim \mathcal{N}\left(0, \sigma^2_{dB_a}\right)$ is an additive

Gaussian noise which models the shadowing effect. By applying the log-normal model, the hybrid observation function h and Jacobian matrix $\mathbf{H}_k$ are defined as follow:

$$h\left(\hat{\boldsymbol{x}}^{(k|k-1)}\right) = \begin{bmatrix} \hat{P}\left(\text{dist}\left(\boldsymbol{p}^{(k|k-1)}, \boldsymbol{p}_a\right)\right) a \in \mathcal{A}^{(k)} \\ \vdots \\ \text{dist}\left(\hat{\boldsymbol{p}}^{(k|k-1)}, \boldsymbol{p}_r\right) r \in \mathcal{R}^{(k)} \\ \vdots \end{bmatrix}, \tag{3.12}$$

$$\boldsymbol{H}^{(k)} = \begin{bmatrix} \frac{-10\alpha\left(\hat{x}^{(k|k-1)} - x_a\right)}{\ln(10)\text{dist}^2\left(\hat{\boldsymbol{p}}^{(k|k-1)}, \boldsymbol{p}_a\right)} & \frac{-10\alpha\left(\hat{y}_{k|k-1} - y_a\right)}{\ln(10)\text{dist}^2\left(\hat{\boldsymbol{p}}^{(k|k-1)}, \boldsymbol{p}_a\right)} & 0 & 0 \\ \vdots & \vdots & \vdots & \vdots \\ \frac{\hat{x}^{(k|k-1)} - x_r}{\text{dist}\left(\hat{\boldsymbol{p}}^{(k|k-1)}, \boldsymbol{p}_r\right)} & \frac{\hat{y}^{(k|k-1)} - y_r}{\text{dist}\left(\hat{\boldsymbol{p}}^{(k|k-1)}, \boldsymbol{p}_r\right)} & 0 & 0 \\ \vdots & \vdots & \vdots & \vdots \end{bmatrix}, \tag{3.13}$$

where the Euclidean distances $\text{dist}\left(\boldsymbol{p}^{(k|k-1)}, \boldsymbol{p}_a\right)$ and $\text{dist}\left(\boldsymbol{p}^{(k|k-1)}, \boldsymbol{p}_r\right)$ are calculated by using (3.6). The expected receive power $\hat{P}\left(\text{dist}\left(\boldsymbol{p}^{(k|k-1)}, \boldsymbol{p}_a\right)\right)$ is defined as

$$\hat{P}\left(\text{dist}\left(\boldsymbol{p}^{(k|k-1)}, \boldsymbol{p}_a\right)\right) = P_0 - 10\alpha \log_{10}\left(\text{dist}\left(\hat{\boldsymbol{p}}^{(k|k-1)}, \boldsymbol{p}_a\right)/d_0\right), \tag{3.14}$$

The error covariance matrix $\boldsymbol{R}^{(k)}$ is a diagonal matrix as the one defined in (3.8), but with different variances for WSN part.

$$\boldsymbol{R}^{(k)} = \text{diag}\left(\sigma^{(k)^2}_{\text{dB}_a} \cdots, \sigma^{(k)^2}_{\tilde{d}_r} \cdots\right). \tag{3.15}$$

- Hybrid PF with RSS observation

The PF formulations for the WSN-based RSS measurements is similar to the WSN-distance ones. The only difference is to substitute the likelihood of distance measure to that of power in (3.11), in order to calculate the expected received power $\hat{P}$. Thus the likelihood function becomes:

$$\begin{aligned} p\left(\boldsymbol{z}^{(k)}|\mathbf{x}^{(k)^i}\right) = & \prod_{a \in \mathcal{A}^{(k)}} p_{e_{P_a}}\left(\tilde{P}^{(k)}_a - \hat{P}\left(\text{dist}\left(\boldsymbol{p}^{(k)^i}, \boldsymbol{p}_a\right)\right)\right) \cdot \\ & \prod_{r \in \mathcal{R}^{(k)}} p_{e_r}\left(\tilde{d}^{(k)}_r - \text{dist}\left(\boldsymbol{p}^{(k)^i}, \boldsymbol{p}_r\right)\right). \end{aligned} \tag{3.16}$$

where $p_{e_{P_a}}$ is the probability density function of the RSS noise e_{P_a}. Remark that $e_{P_a} \sim \mathcal{N}(0, \sigma^2_{\text{dB}_a})$.

3.1.3 *Simulation of Hybrid WSN-RFID Positioning*

The performance of the proposed hybrid tracking algorithms has been evaluated through MC simulations. The selected topology is reported in Fig. 3.1, composed of 5 WSN anchors, and a total of 25 RFID anchor tags. Assume that the trajectory of the mobile node is a curve analytically composed of a line and a sinusoidal curve, and the nodes moves along the trajectory with a constant speed of 1.5 m/s. In order to evaluate the tracking performance on the whole plane, the trajectory is uniformly rotated 200 times in the interval $[0° - 360°]$ around its middle point. The time slot duration is $\Delta t = 200$ ms and a single trajectory contains 100 points. The tracking performance is evaluated as the Root Mean Squared Errors (RMSE) of the location errors as:

$$\mathrm{RMSE}_{\mathrm{loc}} = \sqrt{\frac{1}{L \cdot K} \sum_{l=1}^{L} \sum_{k=1}^{K} \left\| \hat{\boldsymbol{p}}_l^{(k)} - \boldsymbol{p}_l^{(k)} \right\|^2}. \tag{3.17}$$

where $\hat{\boldsymbol{p}}_l^{(k)}$ and $\boldsymbol{p}_l^{(k)}$ are the estimated position and the true one, respectively, at rotation l and time $t^{(k)}$. As it can been known from previous configuration, $L = 200$ is the number of rotated trajectories and $K = 100$ is the number of points in each trajectory.

The default setting parameters have been chosen as follows: WSN-based distance error standard deviation $\sigma_{\tilde{d}_a} = 2$ m $\forall n$; WSN-based RSS noise standard deviation $\sigma_{\mathrm{dB}_a} = 6$ dB $\forall a$; WSN radio coverage range is 15 m; the RFID reader radius $d_r = 2$ m; RFID-based distance error standard deviation $\sigma_{\tilde{d}_r} = d_r/2 \ \forall m$; for EKF, the initial position $\hat{\boldsymbol{p}}^{(0)}$ is set to the initial actual position, and the initial speed, $\hat{\boldsymbol{v}}^{(0)}$, is set to 0 m/s; for PF, initial particles are generated using a uniform distribution centered around the initial state used by EKF. The performance of the proposed hybrid algorithms are compared to a standard EKF which uses measurements only from the WSN nodes.

The simulated performance of the tracking algorithms is displayed in Fig. 3.2. The extreme environment, usually affected by severe NLoS and multipath, is modeled by using a large noise standard deviation and a short WSN radio coverage range. As it can be observed, the hybrid approaches outperforms the EKF based only on the WSN observations, and the accuracy improvement is more than 1 meter when the indoor parameters are extremely adverse. Moreover, the tracking performance for limited WSN coverage is considerable. In fact, the hybrid method is able to provide robust position estimations in case of reduced measurements from WSN anchors. It is worth observing that the improvement is not so evident when the WSN communication is good. In fact, WSN plays the leading role for determining positions of the mobile, while the RFID component plays a supporting role and has a positive effect on the final positioning accuracy when the WSN range measurements suffer.

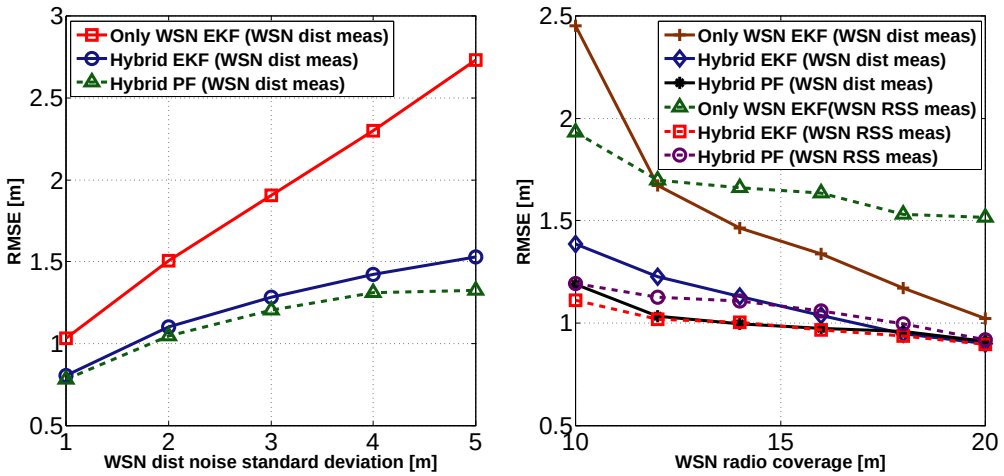

(a) WSN distance error std. (b) WSN radio coverage.

Figure 3.2: Simulation results for WSN parameters.

Different parameters of RFID have been also tested, and the relevant results are presented in Fig. 3.3. In particular, Fig. 3.3 shows the final positioning performance as a function of the RFID radio interrogation range, d_r (left side), and number of RFID anchors (right side). As it can be observed, the RFID coverage range does not affect performance as much as the number of RFID does, the larger the number of RFID anchors, the better the tracking performance. Moreover, increasing the number of RFID anchors is not expensive since the RFID tags are used as anchors. The only effort to be spent is on the deployment phase of tags and on the inserting of the corresponding exact positions into a database.

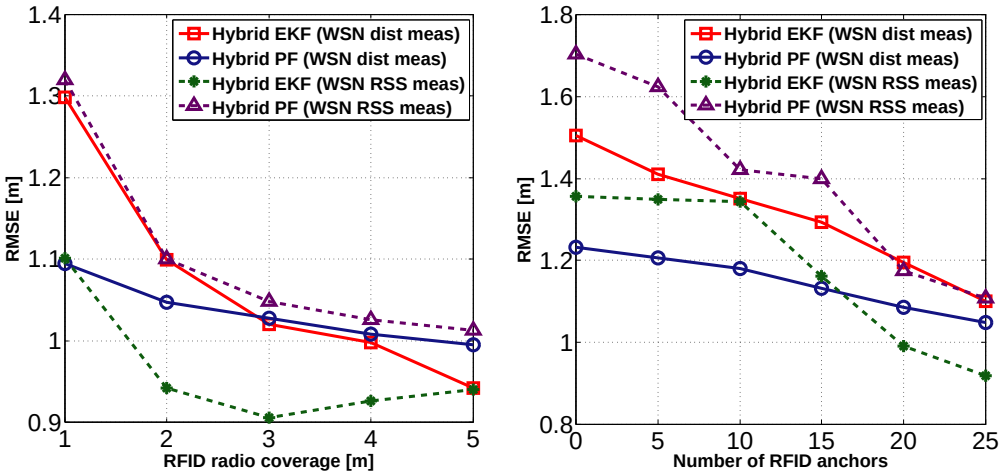

(a) RFID radio coverage. (b) Number of RFID anchors.

Figure 3.3: Simulation results for RFID parameters.

It can be also seen from Fig. 3.2 that the performance of the two hybrid tracking algorithms are different: PF is better when using distance measures are used while EKF is better when using RSS measurements. For real time positioning, EKF is more preferable due to its lower complexity.

This section proposed two hybrid positioning approaches, which adopt the RFID technology to assist single WSN positioning in harsh indoor environments, where the traditional WSN-based only positioning solutions suffer. In particular, the two algorithms, one based on EKF and the other one on PF, have been designed to be suitable for the WSN-RFID hybridization. Although the proposed solutions require new hardware (i.e., one RFID reader and a certain number of fixed tags deployed in the environment), the computational complexity is not so much increased compared to the WSN only positioning systems. The extra amount of calculations is proportional to the average number of RFID devices detected by the reader at each position calculation. Moreover, the simulation results proved that the hybrid algorithms show higher accuracy than the algorithms based only on WSN measurements. However, it is worth mentioning that the performance improvement is less evident as the the indoor channel condition is getting better.

3.2 HYBRID COOPERATIVE WSN-RFID POSITIONING

In this section we propose a novel hybrid and cooperative positioning approach based on EKF to localize mobile targets in indoors. The algorithm fuses both RSS measurements performed by nodes of a WSN and proximity information from RFID devices. With the aim to improve the positioning performance, the hybrid cooperative approach extends the hybrid (WSN-RFID) localization approach presented in section 3.1 by including the cooperative feature. In particular, the proposed algorithm supposes that unknown targets cooperate among them by exchanging positioning data. Moreover, an additional variance on WSN-based RSS measurements performed between unknown targets is introduced, which takes into account the uncertainties deriving from the mobile position estimates.

3.2.1 *Localization Environment*

We refer to a realistic positioning scenario depicted in Fig. 3.4 of size 50×50 m, where $A = 9$ fixed WSN anchors, $R = 8$ fixed RFID readers and $M = 4$ mobile targets are deployed. As it can be observed, WSN anchor nodes are placed according to a grid shape in order to maximize both positioning accuracy and availability, while the RFID readers are placed in each of the four main entrances and around the center of the environment.

The four mobile targets, which we want to localize and track, move along different trajectories represented by dotted lines in Fig. 3.4. Each mobile target is equipped with both a WSN node and a RFID tag. On one hand,

the mobile target uses the WSN node to perform RSS measurements with respect to its WSN neighbors, which could be either fixed anchors or other mobile WSN targets (note that the connectivity is calculated according to the communication distance, $d_{WSN} = 30$ m). On the other hand, the RFID tag attached to each mobile target is used to know whether the target is inside or outside the RFID readers' interrogation area modeled with a circle of radius $d_r = 6$m.

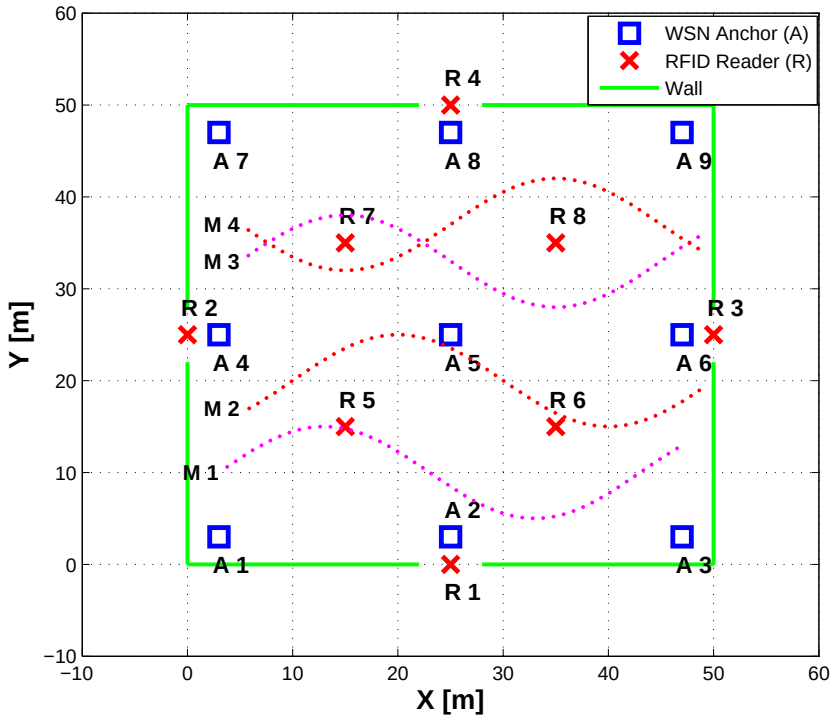

Figure 3.4: Hybrid WSN-RFID cooperative deployment.

Same as before, the RSS measurement is modeled by using the well known Log-normal model [67]. In particular, this model assumes that the received power is a function of the distance between the transmitter and receiver(see (3.11)). The RFID reader can also provide signal strength observation of backscattered signal from the tag, but it is not reliable for positioning purpose, because it is related to 4th power of the communication distance. Hence, we still use the RFID detection information as proximity data. A RFID observation is modeled as a constant distance measurement $\tilde{d}_r = d_r/2$ and it is Gaussian distributed with zero mean and variance depending on interrogation radius d_r.

3.2.2 *Hybrid Cooperative EKF Algorithm*

The design of the proposed algorithm, named as Hybrid-Cooperative Extended Kalman Filter (HC-EKF), can be subdivided into three parts: state modeling, hybridization and cooperation.

3.2.2.1 *State Modeling*

Since the final positioning accuracy and complexity strongly depend on the modeling of the system dynamics, a suitable state model is important to be chosen. In this work, we applied the PV model [86] which is often used in scenarios with mobility.

The PV model supposes that the target moves with constant velocity within the interval $\triangle t^{(k)}$ between two consecutive time steps k and $k-1$. The corresponding state vector is composed of both position and velocity components, $\boldsymbol{x}^{(k)} = [\boldsymbol{p}^{(k)}, \boldsymbol{v}^{(k)}]$, where $\boldsymbol{p}^{(k)}$ and $\boldsymbol{v}^{(k)}$ are position and velocity vectors, respectively, represented in the 2D Cartesian coordinate system (the extension to the 3D case is straightforward).

According to the PV model, the state transition function $f(\cdot)$ is a linear function of the state:

$$\hat{\boldsymbol{x}}^{(k|k-1)} = f\left(\hat{\boldsymbol{x}}^{(k-1)}, \boldsymbol{\omega}^{(k-1)}\right) = \hat{\boldsymbol{x}}^{(k-1)} + \boldsymbol{v}^{(k-1)} \cdot \triangle t^{(k)} + \boldsymbol{\omega}^{(k-1)}, \tag{3.18}$$

In this case, the process noise $\boldsymbol{\omega}^{(k-1)}$ models the unknown random accelerations that affect the target maneuvers. The acceleration components are modeled with zero mean and variances $[\sigma^2_{\ddot{x}}, \sigma^2_{\ddot{y}}]$, uncorrelated with time. Consequently, the covariance matrix $\boldsymbol{Q}^{(k-1)}$ can be expressed as:

$$\boldsymbol{Q}^{(k-1)} = \begin{bmatrix} \triangle t^{(k)^2} \boldsymbol{I}_2 \\ \triangle t^{(k)} \boldsymbol{I}_2 \end{bmatrix} \operatorname{diag}\left(\sigma^2_{\ddot{x}}, \sigma^2_{\ddot{y}}\right) \begin{bmatrix} \triangle t^{(k)^2} \boldsymbol{I}_2 \\ \triangle t^{(k)} \boldsymbol{I}_2 \end{bmatrix}^T. \tag{3.19}$$

where $\mathbf{I}_2$ is a 2×2 identity matrix and $\operatorname{diag}(\sigma^2_{\ddot{x}}, \sigma^2_{\ddot{y}})$ is a 2×2 diagonal matrix.

3.2.2.2 *Hybridization*

This section presents the hybridization part which consists in fusing the measurements from WSN and RFID. We denote with $\mathcal{A} = \{1, 2, \ldots A\}$, $\mathcal{M} = \{1, 2, \ldots M\}$ and $\mathcal{R} = \{1, 2, \ldots R\}$ the sets of fixed WSN anchors, WSN mobiles and fixed RFID readers, respectively, deployed in the environment. Moreover, we denote with $\mathcal{A}_m^{(k)} \subseteq \mathcal{A}$, $\mathcal{M}_m^{(k)} \subseteq \mathcal{M}$ and $\mathcal{R}_m^{(k)} \subseteq \mathcal{R}$ the sets of WSN anchors, WSN mobiles and RFID readers, respectively, connected to a generic mobile node m at time k.

Given the mobile node $m \in \mathcal{M}$, its hybrid observation vector can be written as:

$$\boldsymbol{z}_m^{(k)} = \left\{ \left\{ \tilde{P}_{a \to m}^{(k)} \right\}_{a \in \mathcal{A}_m^{(k)}}, \left\{ \tilde{P}_{n \to m}^{(k)} \right\}_{n \in \mathcal{M}_m^{(k)}}, \left\{ \tilde{d}_{r \to m} \right\}_{r \in \mathcal{R}_m^{(k)}} \right\}^T, \tag{3.20}$$

where $\tilde{P}_{a \to m}^{(k)}$ and $\tilde{P}_{n \to m}^{(k)}$ are the sets of RSS measurements performed by the mobile node m with respect to the connected WSN anchors and mobiles, respectively, while $\tilde{d}_{r \to m}^{(k)}$ is the set of RFID-based distances (i.e., proximity information).

The observation function related to the mobile node m can be written as follows:

$$h(\hat{\boldsymbol{x}}_m^{(k|k-1)}) = \begin{bmatrix} h_a\left(\hat{\boldsymbol{x}}_m^{(k|k-1)}\right) a \in \mathcal{A}_m^{(k)} \\ \vdots \\ h_n\left(\hat{\boldsymbol{x}}_m^{(k|k-1)}\right) n \in \mathcal{M}_m^{(k)} \\ \vdots \\ h_r\left(\hat{\boldsymbol{x}}_m^{(k|k-1)}\right) r \in \mathcal{R}_m^{(k)} \\ \vdots \end{bmatrix}. \tag{3.21}$$

where $h_a\left(\hat{\boldsymbol{x}}_m^{(k|k-1)}\right)$, $h_n\left(\hat{\boldsymbol{x}}_m^{(k|k-1)}\right)$, $h_r\left(\hat{\boldsymbol{x}}_m^{(k|k-1)}\right)$ are the observation functions which refer to the sets of connected WSN anchors, WSN mobiles and RFID readers, respectively, to mobile m at time k.

Let $\boldsymbol{p}_a^{(k)}$, $a \in \mathcal{A}_m^{(k)}$, be the position coordinates of the WSN anchor a connected to the mobile node m at time k. The corresponding observation function related to a generic connected WSN anchor node a is given by:

$$h_a\left(\hat{\boldsymbol{x}}_m^{(k|k-1)}\right) = P_0 - 10\alpha \log_{10}\left(\text{dist}\left(\hat{\boldsymbol{p}}_m^{(k|k-1)}, \boldsymbol{p}_a^{(k)}\right)/d_0\right), \tag{3.22}$$

where P_0, α and d_0 are the parameters of the Log-normal model. Moreover, the term $\text{dist}\left(\hat{\boldsymbol{p}}_m^{(k|k-1)}, \boldsymbol{p}_a^{(k)}\right)$ is the Euclidean distance between the current position of the mobile node m and the connected anchor node a, calculated as (3.6). Note that $\hat{\boldsymbol{p}}_m^{(k|k-1)}$ is the position component of the the priori state estimate $\hat{\boldsymbol{x}}_m^{(k|k-1)}$.

The corresponding contribution to the global Jacobian matrix $\boldsymbol{H}_m^{(k)}$ is obtained by partially differentiating (3.22) around $\hat{\boldsymbol{x}}_m^{(k|k-1)}$:

$$\boldsymbol{H}_a\left(\hat{\boldsymbol{x}}_m^{(k|k-1)}\right) = \begin{bmatrix} \dfrac{-10\alpha\left(\hat{\boldsymbol{p}}_m^{(k|k-1)} - \boldsymbol{p}_a^{(k)}\right)}{\ln(10)\,\text{dist}^2\left(\hat{\boldsymbol{p}}_m^{(k|k-1)}, \boldsymbol{p}_a^{(k)}\right)} & \mathbf{o} \end{bmatrix}. \tag{3.23}$$

where $\mathbf{o}$ is an 1×2 vector, which refers to the velocity component. Since there is no observation for the speed component, it has no contribution in the Jacobian matrix.

Similarly, let $\boldsymbol{p}_n^{(k)}$, $n \in \mathcal{M}_m^{(k)}$, be the position of the WSN mobile n connected to the mobile node m at time k. The corresponding observation function related to a generic connected WSN mobile node n is:

$$h_n\left(\hat{\boldsymbol{x}}_m^{(k|k-1)}\right) = P_0 - 10\alpha \log_{10}\left(\text{dist}\left(\hat{\boldsymbol{p}}_m^{(k|k-1)}, \boldsymbol{p}_n^{(k)}\right)/d_0\right), \tag{3.24}$$

It is worth observing that $\boldsymbol{p}_n^{(k)}$ is the position of a mobile neighbor which is unknown. Node m can use the received position estimate $\hat{\boldsymbol{p}}_n^{(k)}$ from node

n. Therefore, similar to (3.23), the corresponding contribution to $\boldsymbol{H}_m^{(k)}$ can be calculated as:

$$\boldsymbol{H}_n\left(\hat{\boldsymbol{x}}_m^{(k|k-1)}\right) = \left[\frac{-10\alpha\left(\hat{\boldsymbol{p}}_m^{(k|k-1)} - \hat{\boldsymbol{p}}_n^{(k)}\right)}{\ln(10)\,\mathrm{dist}^2\left(\hat{\boldsymbol{p}}_m^{(k|k-1)}, \hat{\boldsymbol{p}}_n^{(k)}\right)} \quad \mathbf{o}\right]. \tag{3.25}$$

Since $\hat{\boldsymbol{p}}_n^{(k)}$ is suffered from estimation errors, additional efforts have been taken to compensate uncertainty on it, which is explained in the next subsection.

Finally, let $\boldsymbol{p}_r^{(k)}$, $r \in \mathcal{R}_m^{(k)}$, be the coordinates of the RFID reader r connected to the mobile node m at time k. Since the RFID-based proximity information is translated into a distance, the corresponding observation function is given by the Euclidean distance:

$$h_r\left(\hat{\boldsymbol{x}}_m^{(k|k-1)}\right) = \mathrm{dist}\left(\hat{\boldsymbol{p}}_m^{(k|k-1)}, \boldsymbol{p}_r^{(k)}\right), \tag{3.26}$$

The contribution to the Jacobian matrix $\boldsymbol{H}_m^{(k)}$ is obtained as:

$$\boldsymbol{H}_n\left(\hat{\boldsymbol{x}}_m^{(k|k-1)}\right) = \left[\frac{\hat{\boldsymbol{p}}_m^{(k|k-1)} - \boldsymbol{p}_r^{(k)}}{\mathrm{dist}\left(\hat{\boldsymbol{p}}_m^{(k|k-1)}, \boldsymbol{p}_r^{(k)}\right)} \quad \mathbf{o}\right]. \tag{3.27}$$

Note that in the above equations, the subscript k used in $\boldsymbol{p}_a^{(k)}$ and $\boldsymbol{p}_r^{(k)}$ can be omitted as both WSN anchors and RFID readers have fixed positions.

3.2.2.3 *Cooperation*

The proposed algorithm adopts a cooperative approach. In fact, unknown mobile targets cooperate among them in order to improve their final position accuracy. It is worth noting from (3.20) that the unknown mobile target m uses not only measurements from the fixed nodes (i.e., both WSN anchors and RFID readers whose positions are perfectly known) but also RSS measurements from the neighboring unknown mobile targets, $\tilde{P}_{n\to m}^{(k)} (n \in \mathcal{M}_m^{(k)})$. Since the positions of the mobile neighbors are not known, the target m uses their position estimates sent over the air, (see (3.25)), which of course are affected by their position uncertainties. Therefore, in order to properly take as input these positioning data, the target node m, apart from the intrinsic uncertainty on the RSS measurements σ_{dB}^2, should take into account also additional uncertainties due to these neighbors' position estimates.

Let $e_{d_{n\to m}}^{(k)}$ be the distance error between nodes m and n deriving only from the position error of node n, denoted with $e_{p_n}^{(k)}$. We assume that $|e_{d_{n\to m}}^{(k)}| \approx |e_{p_n}^{(k)}|$ and $e_{p_n}^{(k)}$ is Gaussian distributed with zero mean and whose variance can be upper bounded by using the error covariance matrix $\boldsymbol{P}_n^{(k)}$ provided by the EKF running on node n:

$$\mathrm{Var}\left(e_{d_{n\to m}}^{(k)}\right) \approx \mathrm{Var}\left(e_{p_n}^{(k)}\right) \leqslant \mathrm{tr}\left(\mathcal{P}_n^{(k)}\right), \tag{3.28}$$

where $\mathcal{P}_n^{(k)}$ is the sub matrix of $\boldsymbol{P}_n^{(k)}$ which refers only to the position components.

Taking into account the distance error of the mobile target n introduced in (3.25), the RSS model can be rewritten as:

$$\begin{aligned}\tilde{P}_{n\to m}^{(k)} &= P_0 - 10\alpha \log_{10}\left(\frac{\hat{d}_{n\to m}^{(k)} + e_{d_{n\to m}}^{(k)}}{d_0}\right) + X_\sigma \\ &= P_0 - 10\alpha \log_{10}\left(\hat{d}_{n\to m}^{(k)}/d_0\right) + X_\sigma + X_{\sigma_{n\to m}}^{(k)}, \end{aligned} \tag{3.29}$$

where $\hat{d}_{n\to m}^{(k)}$ is the Euclidean distance calculated between the estimated positions of nodes m and n and $X_{\sigma_{n\to m}}^{(k)} = -10\alpha \log_{10}(1 + e_{d_{n\to m}}^{(k)}/\hat{d}_{n\to m}^{(k)})$ is the additional RSS noise contribution.

Denote with $X_{\sigma_{n\to m}}^{(k)} = X_\sigma + X_{\sigma_{n\to m}}^{(k)}$ the new additive noise on the RSS measurement with respect to the mobile node n. For simplicity, assume that this new noise satisfies Gaussian distribution. As it can be seen, the mean of $X_{\sigma_{n\to m}}^{(k)}$ is zero. The final objective is to find the variance, needed as input to the covariance matrix $\boldsymbol{R}_m^{(k)}$ of the observation vector. Since it is difficult to directly calculate the variance of $X_{\sigma_{n\to m}}^{(k)}$, we use the following approximation $\log_{10}(1+x) \approx x$ valid around $x = 0$ (i.e., for small values of $|e_{d_{n\to m}}^{(k)}/\hat{d}_{n\to m}^{(k)}|$). Consequently, $X_{\sigma_{n\to m}}^{(k)} \approx X_\sigma - 10\alpha e_{d_{n\to m}}^{(k)}/\hat{d}_{n\to m}^{(k)}$.

Based on the above approximation and assumptions, the variance of $X_{\sigma_{n\to m}}^{(k)}$ can be calculated as:

$$\begin{aligned}\sigma^2_{X_{\sigma_{n\to m}}^{(k)}} &= E\left(X_{\sigma_{n\to m}}^{(k)^2}\right) \approx \sigma_{dB}^2 + 100\alpha^2 \mathrm{Var}\left(e_{d_{n\to m}}^{(k)}\right)/\hat{d}_{n\to m}^{(k)^2} \\ &\leqslant \sigma_{dB}^2 + 100\alpha^2 \mathrm{tr}\left(\mathcal{P}_n^{(k)}\right)/\hat{d}_{n\to m}^{(k)^2}. \end{aligned} \tag{3.30}$$

Finally, the measurement noise covariance matrix for mobile m is given by:

$$\boldsymbol{R}_m^{(k)} = \mathrm{diag}(\underbrace{\ldots \sigma^2_{dB_a} \ldots}_{a\in\mathcal{A}_m^{(k)}} \underbrace{\ldots \sigma^2_{X_{\sigma_{n\to m}}^{(k)}} \ldots}_{j\in\mathcal{M}_m^{(k)}} \underbrace{\ldots \sigma^2_{\tilde{d}_{r\to m}} \ldots}_{r\in\mathcal{R}_m^{(k)}}). \tag{3.31}$$

It is worth mentioning that iterations can be adopted to make the position estimate converge. The designed HC-EKF algorithm is reported in pseudo code form as Alg. 3.1

3.2.2.4 *Complexity Analysis*

The computational complexity of EKF is mainly upon the matrix inversion and matrix multiplication. For each state estimate, in (2.13), matrix inversion is computed with asymptotic complexity $\mathcal{O}(\mathbb{R}^3)$ [87], where $\mathbb{R}$ is the dimension of measurement noise covariance $\boldsymbol{R}$ or the number of available

Algorithm 3.1: Hybrid-Cooperative EKF

input : Hybrid measurements $\boldsymbol{z}_m^{(k)}$ (3.20) and previous estimate $\hat{\boldsymbol{x}}_m^{(k-1)}$ $\forall m$

output: Updated estimate $\hat{\boldsymbol{x}}_m^{(k)}$ $\forall m$

for *timestep* $k = 1$ *to* K **do**
  $\forall m \in \mathcal{M}$: collect measurements $\tilde{P}_{a\to m}$ $\forall a \in \mathcal{A}_m^{(k)}$, $\tilde{P}_{n\to m}^{(k)}$ $\forall n \in \mathcal{M}_m^{(k)}$, $\tilde{d}_{r\to m}$ $\forall r \in \mathcal{R}_m^{(k)}$
  for *iteration* $it = 1$ *to* I **do**
    for *node* $m \in \mathcal{M}$ ***in parallel*** **do**
      Receive $\hat{\boldsymbol{p}}_n^{(k)}$ and $\mathrm{tr}\left(\boldsymbol{\mathcal{P}}_n^{(k)}\right)$ from all neighbors $n \in \mathcal{M}_m^{(k)}$
      Calculate noise covariance $\boldsymbol{R}_m^{(k)}$ using (3.31)
      Predict $\hat{x}_{k|k-1}^m$ and $\boldsymbol{P}_m^{(k|k-1)}$
      Compute $\tilde{\boldsymbol{y}}_m^{(k)}$ and $\mathbf{K}_m^{(k)}$
      Update state $\hat{\boldsymbol{x}}_m^{(k)}$ and error covariance $\boldsymbol{P}_m^{(k)}$
      Communicate $\hat{\boldsymbol{p}}_m^{(k)}$ and $\mathrm{tr}\left(\boldsymbol{\mathcal{P}}_n^{(k)}\right)$ to neighbors
    end
  end
end

measurements; in (2.16), matrix multiplication is computed with asymptotic complexity $\mathcal{O}(\mathbb{P}^3)$ [87], where $\mathbb{P}$ is the dimension of error covariance $\boldsymbol{P}$ or the dimension of the state vector. In the positioning applications, the number of measurements is usually larger than the dimension of state in order to solve the ambiguity of position estimate.

Hence, the complexity of EKF is mainly the computation of inverting matrices in our application. Let $\left|\mathcal{A}^{(k)}\right|$, $\left|\mathcal{M}^{(k)}\right|$, and $\left|\mathcal{R}^{(k)}\right|$ denote the cardinality of the corresponding sets $\mathcal{A}^{(k)}$, $\mathcal{M}^{(k)}$, and $\mathcal{R}^{(k)}$. The complexity of the proposed HC-EKF is asymptotically $\mathcal{O}\left((\left|\mathcal{A}^{(k)}\right| + \left|\mathcal{M}^{(k)}\right| + \left|\mathcal{R}^{(k)}\right|)^3\right)$. For the standard EKF algorithm, the used measurements are only in set $\mathcal{A}^{(k)}$, and the complexity is asymptotically $\mathcal{O}(\left|\mathcal{A}^{(k)}\right|^3)$. Therefore, the complexity of HC-EKF is increased $(1 + \frac{|\mathcal{M}^{(k)}|+|\mathcal{R}^{(k)}|}{|\mathcal{A}^{(k)}|})^3$ times with respect to the standard one. For example, suppose that at a specific time, there are two RSSI measures from anchors $\left|\mathcal{A}^{(k)}\right| = 2$, one RSSI measure from mobile node $\left|\mathcal{M}^{(k)}\right| = 1$, and one RFID observation $\left|\mathcal{R}^{(k)}\right| = 1$, the computational complexity of HC-EKF is increased by 8 times. It is worth reminding that the hybrid cooperative approach can still locate the mobile node in this case by using the observations from mobile neighbor and RFID technology.

3.2.3 *Simulation of Hybrid Cooperative WSN-RFID Positioning*

During simulations, we used the Log-normal model parameters extrapolated from a real experiment [71], where $P_0 = -49$ dBm, $d_0 = 1$ m, $\alpha = 3$, $\sigma_{dB} = 6$ dB. In total we tested four different versions of the EKF algorithm, namely HC-EKF, cooperative EKF (C-EKF) based only on WSN measurements, hybrid EKF (H-EKF) without cooperation and a standard EKF (S-EKF) based only on WSN without cooperation. The positioning results, evaluated after 100 MC runs, are displayed in Fig. 3.5 and Fig. 3.6. In particular, Fig. 3.5 presents the RMSE (defined in (3.17)) of each mobile, and Fig. 3.6 displays the cumulative distribution function (c.d.f.) of the localization errors and the overall RMSE.

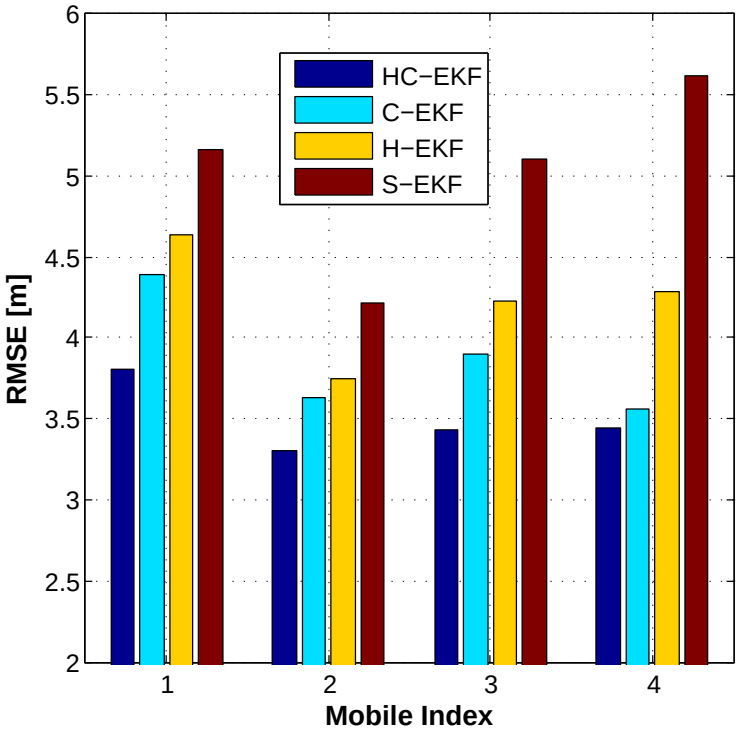

Figure 3.5: Tracking results of each mobile.

As it can be observed, the proposed HC-EKF algorithm, which includes both cooperation and RFID hybridization, outperforms the other three ones. In addition, we can observe that the C-EKF is slightly better than H-EKF. Thus, we can conclude that the proposed cooperation approach based only on WSN provides an improvement larger than the contribution provided by the hybridization only. That's because there are only few deployed RFID readers which provide sparse observations. Finally, the RFID hybridization algorithm (H-EKF) without cooperation outperforms the S-EKF using only WSN measurements without cooperation, which confirms the results reported in section 3.1.

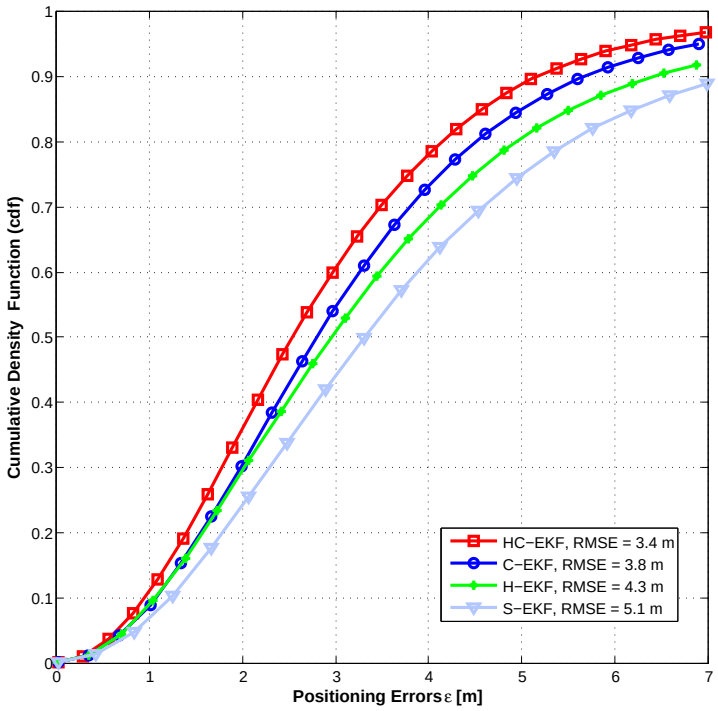

Figure 3.6: Performance comparison of different algorithms.

3.3 SUMMARY

This chapter presented an application of the EKF to the tracking problem in indoors. The proposed solution adopts the hybridization of measurements from both WSN and RFID devices. Moreover, it uses the cooperation among mobile targets to improve the final positioning accuracy. In fact, the designed HC-EKF algorithm takes into account the position estimates from mobile nodes and their uncertainties. Simulation results showed that the proposed algorithm outperforms the non cooperative one.

4

HYBRID WSN-RFID POSITIONING SYSTEM

This presents the design and evaluation of a hybrid system which combines WSN and RFID technologies to provide an indoor positioning service with the capability of feeding position information into a general-purpose Internet of Things (IoT) environment. Performance of the proposed system is evaluated by means of simulations and a small-scale experimental set-up. The performed analysis demonstrates that the joint use of heterogeneous technologies can increase the robustness and the accuracy of the indoor positioning systems.

4.1 SYSTEM ARCHITECTURE AND DESIGN

The proposed positioning system combines WSN and RFID in order to compensate the limitations of each technology. On one hand, the WSN provides a good radio coverage but with a low positioning accuracy due to the high noise on the RSSI measurements. On the other hand, the RFID technology provides the following: (1) in the case of HF, very precise positioning information but limited coverage and temporal discontinuity; (2) in the case of UHF, good coverage and reliability but high granularity of the location. The appropriate combinations of the two technologies could be a good strategy in building indoor positioning and tracking system with increased positioning accuracy and availability.

Fig. 4.1 presents the hybrid architecture of the hybrid positioning system, and the field data are collected by two different systems, WSN segment and RFID segment.

4.1.1 *WSN segment*

The WSN segment is a self-configuring, IPv6-based sensor network which have been implemented and tested on Telos rev.B [76] nodes as shown in Fig. 4.2. On the software side, each node runs a TinyOS operating system; on the hardware side, each node is equipped with a radio transceiver, a microcontroller and some on-board sensors (e.g., humidity sensors, temperature sensors and light sensors).

In the network level, out-of-band control messages are exchanged among the nodes to help each node to build its neighbor list and autonomously

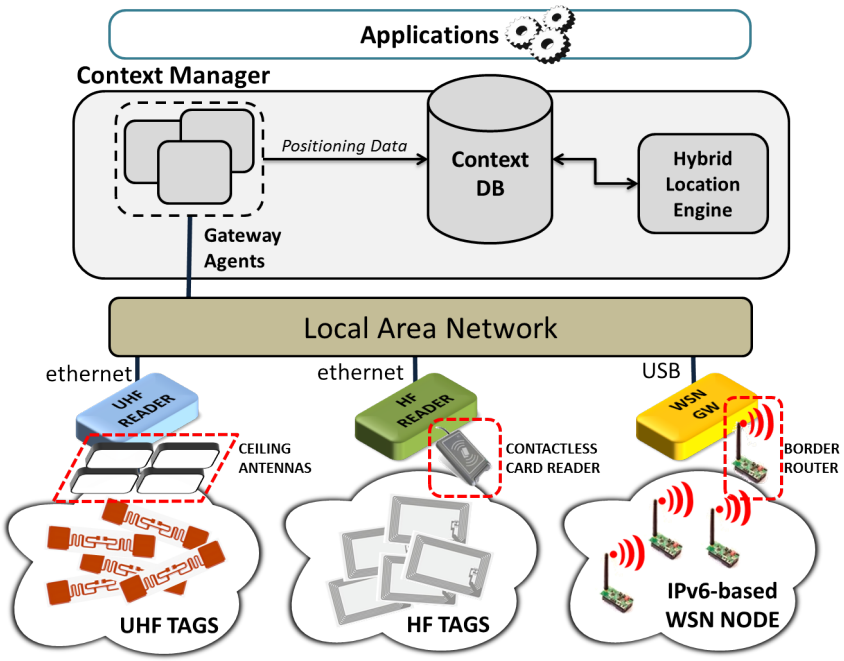

Figure 4.1: The proposed hybrid architecture.

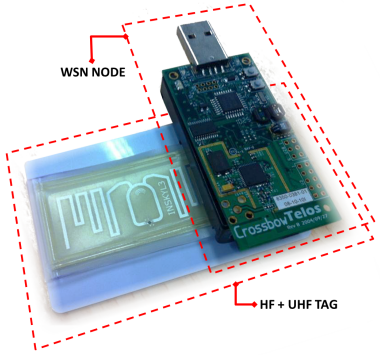

Figure 4.2: Hybrid node with multi-technology.

form the network. Each node periodically updates its neighbor list and dynamically builds an optimal route to every potential destination.

Within the WSN segment, the positioning data are collected in the following process:

1. The distances between the mobile node (node to be located) and other nodes (anchor nodes or any other mobile nodes) are measured in terms of the RSSI.

2. The measured RSSI values by the mobile node are directly sent to a fixed infrastructure, or forwarded by the router nodes (could be an anchor node or a mobile node), to a fixed infrastructure when a multi-hop transmission is required.

3. After being processed by the positioning algorithm that is running on the fixed infrastructure, the locating result is sent back to the requester (the mobile to be located).

In terms of communication, the WSN segment is divided into three levels:

- The main gateway, also called the concentrator
- The fixed gateway
- The network nodes

In order to obtain the RSSI information, each mobile node periodically broadcasts ranging requests, which are used by neighbor nodes to measure uplink RSSI. Anchor nodes reply in turn with a ranging response, including the measured uplink RSSI values. Finally, the mobile node measures all downlink RSSI, aggregates all ranging responses, and forwards all the uplink-downlink tuples to the WSNgateway, which is a simple commercial off-the-shelf low-power PC running Linux.

4.1.2 *RFID segment*

The RFID segment is composed of two systems, a UHF system and an HF system. They are independent from each other and provide separate detection for the RFID tags.

In the HF system, some contactless badge readers are placed at the room entrances, and they produce positioning information when a user registers or request access through a door. This information is extremely accurate, but could instantly become useless even over a short period of time. When the user enters or exits a room, this detection information should be fused with other information quickly.

The UHF system is composed of a RFID reader plus four compliant antennas deployed on the ceiling. Fig. 4.3 depicts the test-bed scenario while Fig. 4.4 provides a snapshot of the actual deployment (within labs of ISMB). Here, the typical 4-antennas/reader combination has been used, in order to simplify the field trial. A more complex antennas multiplexing can be used in an hypothetical wider deployment (at least 32 antennas/reader). The physical attributes, the relative position, and the power irradiation level of each antennas has been chosen to optimize the coverage area, trying to avoid the overlap of each antenna coverage range. It is impossible to avoid reading the same tag by different antennas, but the hybrid positioning algorithm has considered this as different range measurements.

Data collected by the two segments are preprocessed by specific gateways and then transferred through a local area network to a central entity named *context manager*, which is a virtually distributed entity capable of handling generalized context information extracted from different platform-specific components. Within the context manager, a virtual delegate named *gateway*

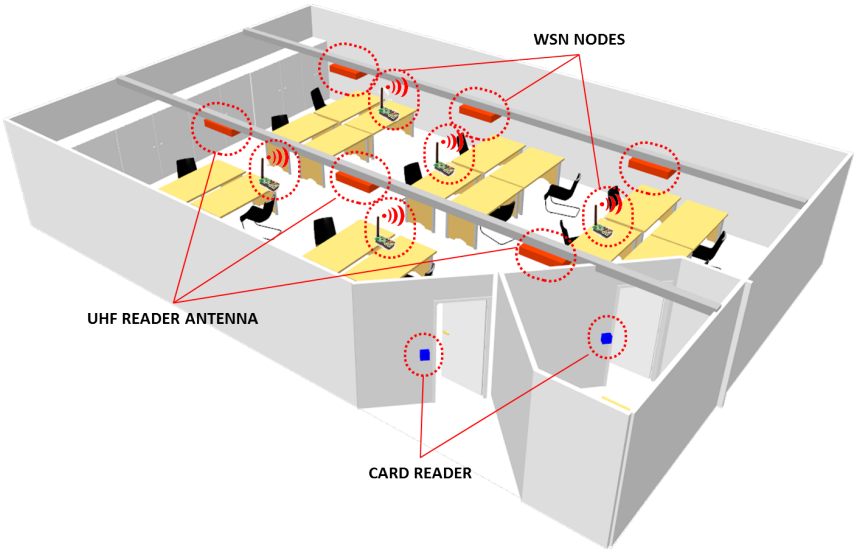

Figure 4.3: Hybrid WSN-RFID positioning system deployment.

Figure 4.4: The antennas of RFID reader on the ceiling.

agent is configured to filter all the data from the specific gateway and feed them into any subscribing entity, e.g., a system which is interested in receiving these specific data. Based on such data and configuration data hosted inside the context manager, the location engine (described in Section 4.1.3) is able to extract the physical location of objects (RFID tags and WSN nodes) associated with the sources of the physical-world events.

Since different types of techniques are adopted, the proposed system is classified as a hybrid scheme exploiting both indirect remote positioning systems and indirect self-positioning. Hence, the location engine is named as hybrid location engine.

4.1.3 *Hybrid location engine*

The hybrid location engine is the core of the positioning and tracking system. As it can be seen from Fig. 4.1, it is a centralized location engine where a hybrid positioning algorithm is implemented to periodically estimate the

positions of all the unknown mobile nodes. As shown in Fig. 4.2, a typical mobile node is equipped with three RF devices: a WSN node, a UHF tag, and an HF badge. Moreover, the system allows the existence of other combination of devices: two of the three different elements (e.g., a WSN node and an HF badge) or just with single device (e.g., a WSN node or a UHF tag).

As indicated in Figure 4.1, three different observations (RSSI measurements derived from WSN nodes, detection of events from UHF tags, and HF badges) are sent to a context Data Base (DB). Since the detection events are available at the corresponding readers, these data are not forwarded to the corresponding unknown mobile nodes, for instance, through the WSN technology, to implement a distributed positioning algorithm. On the contrary, in order to reduce communication latency and network traffic, all data, including also RSSI measurements from the WSN devices, are collected in the DB, then the hybrid location engine estimates the position of the mobile nodes in a centralized way.

The main task of the hybrid location engine is to estimate the positions of mobiles. But some other tasks, for instance, reading location information of anchors and measurements for mobile nodes, are done to accomplish this task. In every ΔT_p seconds, it completes the following processes:

1. **Location information reading**. At the beginning of each time step ΔT_p, the hybrid location engine queries the DB about the location information for all the devices. In more detail, the location information includes the unique device ID and the corresponding device category (e.g., WSN node, RFID tag or badge). For simplicity, the device ID is a five-digit number and is general for all the device. For each device there is a flag which indicates if it is *fixed* or *mobile*. A fixed device may be either a WSN anchor, a UHF antenna, or a badge reader whose positions are perfectly known and are stored in the DB; while a mobile device is a movable node whose position is not known. In addition, the device association information is read too. As mentioned above, a mobile node may be equipped with different RF devices and the association information specifies how different devices are binded with together. The association information is useful, since in the DB an observation (a RSSI measurement and a detection of RFID tag or badge) is only related to a single device.

   Note that this information reading step is performed at each ΔT_p, because the network topology may change with time, for example, node changing (e.g., a new node joins the network, a node leaves, or the known position changes), association changing (e.g., new devices are binded together or the old association changes), or role changing (e.g., a mobile node becomes an anchor node or an anchor node becomes a mobile node). By doing this, the location engine is able to follow the latest change of network topology and to have the capability of good position estimates.

2. **Measurements reading**. During this step, the hybrid location engine reads all the available observations from DB. These observations could be RSSI, RFID detection events, and the time interval is chosen from some previous time to current time $t^{(k)}$, that is, $[t^{(k)} - \Delta T_{DB}, t^{(k)}]$, where ΔT_{DB} is the width of the temporal window. In general, ΔT_{DB} is set equal to position update time step ΔT_p, so that all the observations are used only once. It is worth mentioning that ΔT_{DB} could be larger or smaller than ΔT_p. Sometimes, there may be not enough RSSI observations for an unknown node in low dynamic scenario, and ΔT_{DB} is set larger than ΔT_p in order to use the previously collected measurements. On the contrary, there may be too many RSSI observations for a mobile node in high dynamic scenario, and ΔT_{DB} is set smaller than ΔT_p in order to use the freshest measurements. In principle, ΔT_{DB} is chosen, depending on the prior knowledge of mobility degree of the unknown nodes.

   In practice, it may happen that more than one measurement is available between two WSN nodes at certain times. In this case, a weighted average scheme is applied, and the weight associated to a measurement is calculated according to an exponential function which takes as input the time difference between the current time $t^{(k)}$ and the time stamp attached to this measurement. In other words, much lower weight is assigned to the old measurement while much higher weight is assigned to the new one. For the multiple detections of RFID devices, however, weighted average is not necessary, because only the freshest one is used. It is supposed that this detection is exceedingly reliable and the old detection event can be neglected.

3. **Position estimation**. In this step the location engine estimates the positions of mobile nodes by using location information and measurements which are provided by the previous two steps. Moreover, a cooperation scheme is applied where the location engine, apart from RSSI measurements from anchors, uses also RSSI measurements performed between mobile nodes, since two mobile WSN nodes are able to communicate with each other and to perform corresponding RSSI observations. The adoption of cooperation improves not only the positioning accuracy but also system robustness (i.e., position estimation availability), as more measurements are available to localize the mobile nodes. Nevertheless, the cooperation can be merely applicable to mobile nodes equipped with WSN devices, because both RFID tag and badge are passive devices and cannot communicate with other passive devices for range or range-related observations. Since the HF badge can be detected by the reader in a very short distance (e.g., a few centimeters), this badge detection event can be seen as quite accurate localization information. In principle, whenever an HF badge is detected, the estimated position of the associated mobile node is set

Algorithm 4.1: Hybrid WSN-RFID location engine

```
repeat
    Read location information from DB
    Extract all the measurements from DB within the interval
    [t^(k) − ΔT_DB, t^(k)]
    for m = 1 to M {mobile index} do
        if there are HF-badge events for m then
            Set estimated position of m to the location of the HF badge
            reader according to the latest detection event
        else
            Select measurements related to mobile m
            Select reference location information according to the selected
            measurements
        end
        if there are measurements for m then
            Estimate the mobile's position using HC-EKF
        else
            Position estimation is not available and do not do any estimate
        end
        Display the estimated position on the map
        Upload the estimated position to the DB
    end
    Pause if ΔT_p is not fully consumed
until stop
```

to the reader's position, and other observations (e.g., RSSI or tag detections) are ignored. Since the badge readers are only installed at the door, mainly for the purpose of access control, they provide only sporadic detection events. In most of the time, the hybrid location engine relies on RSSI measurements from WSN devices and UHF tag detection events for localization.

In order to have a good estimate of a mobile's position, the location engine adopts a hybrid cooperative tracking algorithm, namely HC-EKF, which takes into account all the available observations, that is, RSSI measurements performed between WSN nodes (i.e., WSN mobiles to WSN anchors orWSN mobiles to WSN mobiles) and tag detection events. More details of the adopted HC-EKF is presented in Chapter 3. At the end of the estimation process, all the estimated positions are displayed on the map and are uploaded to the DB with a time stamp.

The periodic repetitions of these three steps form the whole procedure of the hybrid location engine, which can be summarized as pseudocode as Alg. 4.1.

4.2 SIMULATION AND EXPERIMENTAL RESULTS

The performance of the proposed tracking system is first evaluated through realistic simulations and then by means of real experiment deployment.

The selected validation scenario is based on the Laboratory of Pervasive Radio Technologies at ISMB (Turin, Italy) and is composed of two adjacent rooms, namely, room 1 and room 2, which are connected by a corridor (see in Fig. 4.5). This is a typical office-environment scenario with building structure mainly composed of metal and the size of it is about 25 × 12 m. In Fig. 4.5, the blue and the red rectangles inside room 1 and room 2 represent the tables and those at the edges represent the walls, which are made of wood and metal and whose material properties are not considered yet. Our work is concentrated on the realization of the hybrid WSN-RFID localization system. These tables and walls are plotted to provide apparent references to the estimated positions.

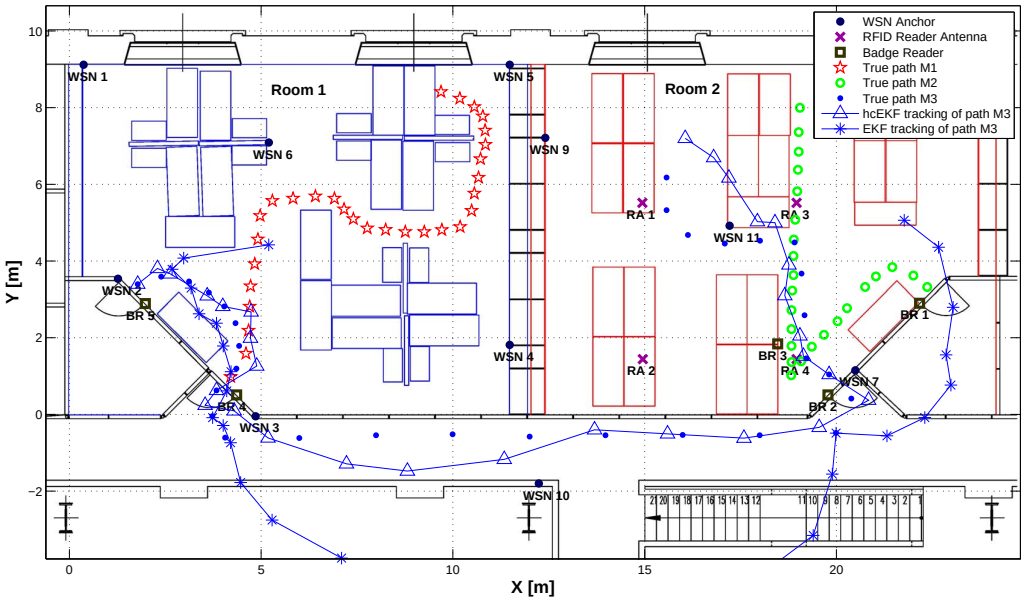

Figure 4.5: Simulation scenario and the trajectories.

4.2.1 *Simulation results*

In the simulation scenario, the following deployment of devices is adopted. Eleven WSN anchor nodes (WSN 1 to 11 in Fig. 4.5) are placed around the rooms to optimize the geometry distribution for positioning; four UHF RFID antennas (RA 1 to 4 in Fig. 4.5) are deployed only in room 2; five badge readers (BA 1 to 5 in Fig. 4.5) are installed at the doors to provide access control; three hybrid mobile nodes are considered; and all of them are equipped with three devices as Fig. 4.2.

Three different trajectories have been considered, and the three mobile nodes moved along them respectively. Fig. 4.5 shows the exact positions of three paths: the first one is in room 1 and is represented by red pentagrams and mobile; the second one is in room 2 and is represented by green circles; the third one connects from room 1 to room 2 through the corridor and is represented by blue dots.

The RSSI measurements are generated by using the Log-normal model reported in (2.1). The model parameters are from an experiment carried out in [71], in more details, $P_0 = -49$, $\alpha = 3.3$, and $\sigma_{dB} = 5.5$. The sensitivity of the WSN receiver is set to -90 dBm, which determines the connectivity of two WSN nodes. A badge event is generated by the badge reader when a badge passes through the doors. A tag detection event is provided by the UHF antenna when a passive tag is within the coverage area, which is modeled as a circle with radius $r = 2$ m.

One hundred MC simulations have been performed to provide steady statistics. The tracking performance is evaluated as RMSE given in (3.17). Moreover, four different tracking algorithms have been tested for comparison: the HC-EKF which uses all the available measurements, the H-EKF which uses RSSI from WSN anchors and detection events from RFID, the C-EKF which uses only RSSI measures from WSN, and the S-EKF (standard, non-cooperative and non-hybrid) which uses only RSSI measurements from WSN anchors.

Fig. 4.5 shows the tracking result of one realization, where only the estimated positions of HC-EKF and S-EKF related to mobile node M3 are plotted to avoid an overcrowded figure. Thanks to the badge detection, the HC-EKF is accurately initialized, while the S-EKF has to be initialized to the coordinates of the scenario's center because it only uses the RSSI measures. When M3 is in the corridor, the S-EKF diverges due to the bad geometry of the WSN anchor deployment while the HC-EKF is able to follow the real trajectory thanks to hybridization of RFID detection and the cooperation with the other mobile nodes. When M3 approaches room 2, the S-EKF diverges again while the HC-EKF is still able to track the mobile by fusing measurements from badge reader and tag reader.

Fig. 4.6 shows the simulated tracking performance in terms of c.d.f. and RMSE of the positioning errors. It can be observed that the HC-EKF, which fuses hybrid measurements of RSSI from WSN and detection events from RFID and adopts cooperation among mobile nodes, shows the best tracking performance, i.e., best c.d.f. curve and smallest RMSE. The H-EKF outperforms the C-EKF, which indicates that the integration of RFID technology can overcome the inherent disadvantages of RSSI localization. The C-EKF and S-EKF have similar performance, because there are lots of anchors nodes that provide enough RSSI measures and the gain of cooperation is not obvious.

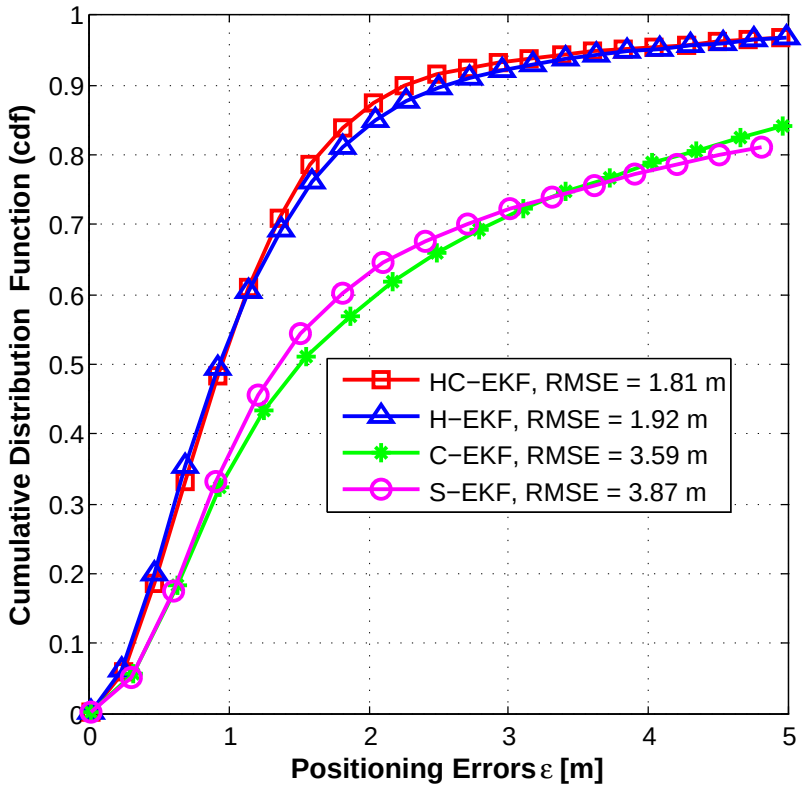

Figure 4.6: Simulated tracking performance.

4.2.2 *Experimental results*

Due to the lack of devices, the availability of WSN devices was not sufficient to allow a full deployment as the simulation. The experiment was carried out only in room 2, and the RF devices were only deployed in room 2 as Fig. 4.5. In total, five WSN nodes (WSN 1 to 5), four RFID antennas (RA 1 to 4), and three badge readers (BA 1 to 3) were deployed. A mobile equipped with the previously mentioned RF devices did a pedestrian movement along a zigzag trajectory in the experimental area.

Before tracking the mobile, some RSSI measurements have been taken to calibrate the Log-normal model in (2.1). The relative results are shown in Fig. 4.7. Based on these measurements, the model parameters is chosen as $P_0 = -50.8$, $\alpha = 1.3$, and $\sigma_{dB} = 6.1$. These parameters indicate that the environment is harsh and the RSSI measurements is quite noisy, posing a challenge for tracking.

The final experimental results are presented in Fig. 4.8, where the left part shows the tracking result of only WSN measurements and the right part shows that of hybrid tracking. Since the RSSI measurements contained large noise, we adopt an optimization method that corrects the bad position estimate to the position of RFID reader when RFID detection is available. Moreover, the measurement availability and RMSE are reported in the upper part.

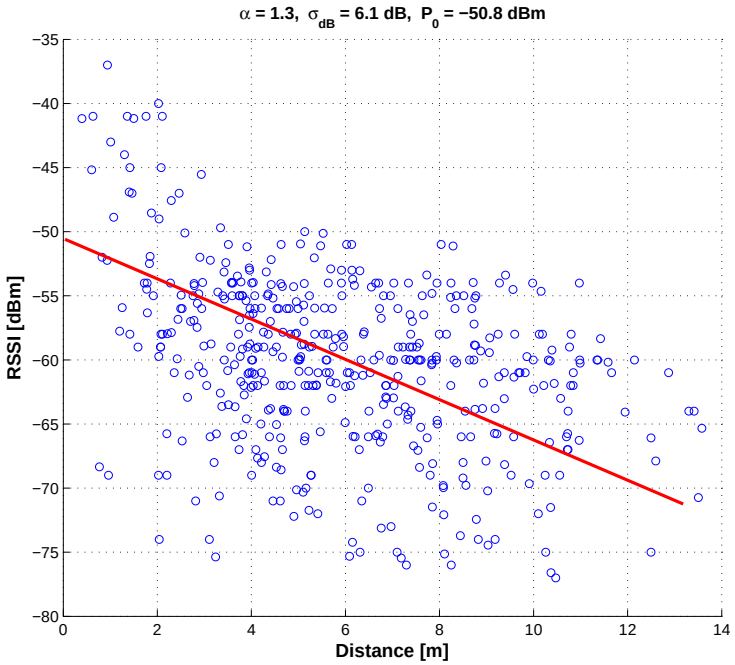

Figure 4.7: RSSI Channel model based on the measured values.

Due to the large noise on the RSS measurements, the tracking trajectory has large errors and the performance is worse than the simulation. By fusing the observations from RFID technology, the hybrid tracking algorithm is able to track better the maneuvers of mobile, which is consistent with the simulation result. As a result of high packet loss rate, sometimes there is no RSSI measurement to be used to track the mobile, and the observation from RFID can slightly improve system availability. The adoption of hybridization provides improvement of 1.6 m in RMSE and of 4% in availability.

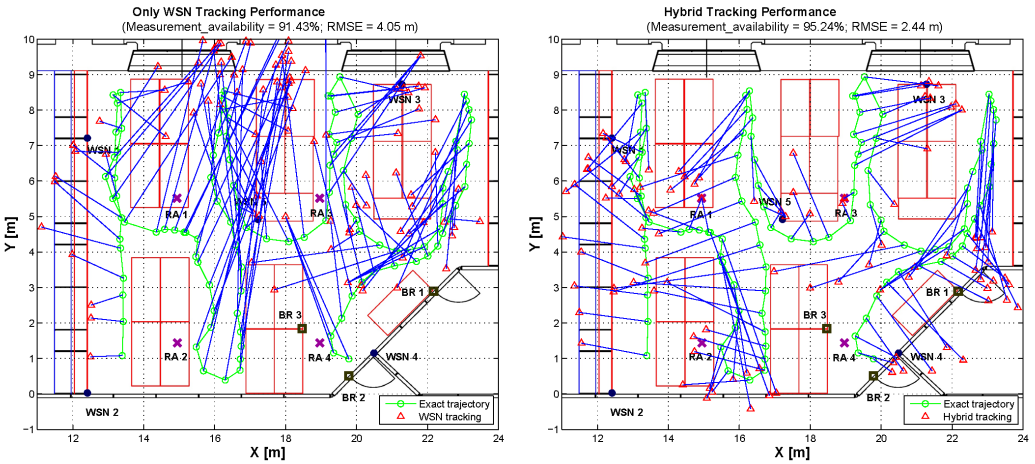

Figure 4.8: Experimental tracking results.

4.3 SUMMARY

This section presented a hybrid WSN-RFID system for tracking people and objects in indoor scenarios. The joint use of heterogeneous technologies can overcome the limitations of each other: WSN system provides adequate RSSI observations but with large errors, and RFID system provides accurate detections but with sparse observations. Thanks to the hybridization of RFID measurements and cooperation among mobile nodes, the proposed positioning solution based on EKF is able to increase the robustness and accuracy of indoor positioning systems in harsh propagation conditions. Simulation and experimental results showed that the hybrid configuration outperformed the set-ups employing single technology.

5

HYBRID COOPERATIVE GNSS-TERRESTRIAL NAVIGATION

5.1 HYBRID COOPERATIVE URBAN NAVIGATION

Urban canyons have proven to a big challenge for GNSS. In this section we adopt the hybrid and cooperative positioning approaches to assist GNSS in urban navigation. The presented algorithms fuse pseudorange measurements from satellites and terrestrial range measurements from terrestrial receivers. Furthermore, they adopt full cooperation among mobile agents to increase the SoO for terrestrial ranging and to reduce the number of the fixed terrestrial infrastructures.

5.1.1 *Problem Formulation*

The UWB augmentation has the advantage of low cost, low complexity and multipath resistant. However, it requires fixed infrastructure and has limited operational range. The concept of cooperative positioning can be enhanced in urban navigation. Cooperation among vehicles can increase both positioning accuracy and availability. It can be used accurately localize the vehicles without additional fixed devices.

5.1.1.1 *Scenario Description*

Fig. 5.1 presents the hybrid and cooperative architecture for vehicles. Each vehicle carries GNSS receiver and terrestrial transceiver. The former one is used to receive pseudorange. The latter one is used for terrestrial ranging and communication. All the vehicles compose a P2P vehicular network and one of them is a single peer. As it can been seen, each vehicle can only seen two satellites due to blockage of the buildings. By the adoption of hybrid and cooperative scheme, every vehicle can be located.

Here we consider a vehicular network with V vehicles and S satellites. $\mathcal{V}$ and $\mathcal{S}$ denote the set of peer agents and the set of satellites, respectively. For a particular vehicle peer $v \in \mathcal{V}$ at a specific Time Slot (TS) t_k, $\mathcal{V}_v^{(k)}$ denotes the subset of neighboring peers it can communicate with and $\mathcal{S}_v^{(k)}$ denotes the subset of satellites it can see from sky. We focus on the 3D Earth Centered Earth Fixed (ECEF) reference system, and the position variables at t_k can be expressed as $\boldsymbol{p}_j^{(k)} = \left[x_j^{(k)} y_j^{(k)} z_j^{(k)}\right]$, where j can be either a peer or a satellite.

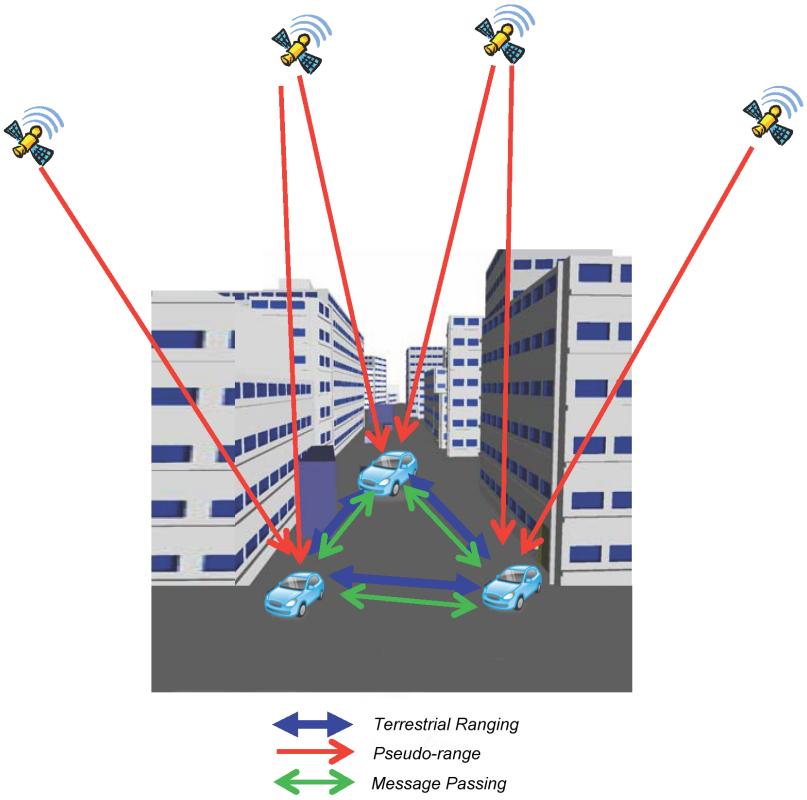

Figure 5.1: Hybrid and cooperative architecture of vehicles.

Moreover, we denote $\delta_v^{(k)}$ as the clock bias of peer v at time t_k with respect to the GNSS time. This bias is expressed the in meters $b_v^{(k)} = c \cdot \delta_v^{(k)}$, by multiplying the speed of light c. Therefore, the state vector of each peer v at every TS t_k is defined as:

$$\mathbf{x}_v^{(k)} \triangleq [\boldsymbol{p}_v^{(k)} \; b_v^{(k)}]^\mathsf{T}. \tag{5.1}$$

In the urban canyon scenarios, each peer v can perform are two types of measurements at each TS:

- **Satellite pseudorange measurements** represent the distances from satellites

$$\rho_{sv}^{(k)} = \left\| \boldsymbol{p}_s^{(k)} - \boldsymbol{p}_v^{(k)} \right\| + b_v^{(k)} + \xi_{sv}^{(k)}, \tag{5.2}$$

  where the symbol $\|\cdot\|$ is the norm of a vector and in positioning it is Euclidean distance operator. $\xi_{sv}^{(k)}$ $(s \in \mathcal{S})$ is the measurement noise on pseudorange.

- **Terrestrial range measurements** represent the distance measurements between peers:

$$r_{nv}^{(k)} = \left\| \boldsymbol{p}_n^{(k)} - \boldsymbol{p}_v^{(k)} \right\| + \zeta_{nv}^{(k)}, \tag{5.3}$$

where n is the neighbor peer of v ($v, n \in \mathcal{M}$), and $\zeta_{nv}^{(k)}$ is the corresponding measurement noise.

In (5.2), pseudorange measurements are affected by the additional bias $b_v^{(k)}$ due to the clock difference between the satellites and the vehicle. In (5.3), however, terrestrial measurements are assumed with no bias, since some methods can be used to avoid this problem, e.g., two-way time of flight.

Based on the previous description, the available measurements $\boldsymbol{z}_v^{(k)}$ can be divided into two subsets: pseudoranges from visible satellites $\boldsymbol{\rho}_v^{(k)} \triangleq \left\{ \rho_{sv}^{(k)} \mid s \in \mathcal{S}_v^{(k)} \right\}$ and terrestrial ranges from neighboring vehicles $\boldsymbol{r}_v^{(k)} \triangleq \left\{ r_{nv}^{(k)} \mid n \in \mathcal{V}_v^{(k)} \right\}$, that is, $\boldsymbol{z}_v^{(k)} = \left\{ \boldsymbol{\rho}_v^{(k)}, \boldsymbol{r}_v^{(k)} \right\}^T$, where the superscript T means transpose. Moreover, we define the set of exact satellites' positions $\boldsymbol{S}_v^{(k)} \triangleq \left\{ \boldsymbol{p}_s^{(k)} \mid s \in \mathcal{S}_v^{(k)} \right\}$ and the set of exact neighboring peers' positions $\boldsymbol{\mathcal{P}}_v^{(k)} \triangleq \left\{ \boldsymbol{p}_n^{(k)} \mid n \in \mathcal{V}_v^{(k)} \right\}$.

Given the previous sets of parameters, the positioning problem is to estimate the state vector of each peer $\mathbf{x}_v^{(k)}$ (or the position vector $\mathbf{p}_v^{(k)}$). It is worth reminding that the exact positions of neighbors may be not available when the neighbor is vehicular. In this case, the distribution of the position estimates $\hat{\boldsymbol{\mathcal{P}}}_v^{(k)} \triangleq \left\{ \hat{\boldsymbol{p}}_n^{(k)} \mid n \in \mathcal{V}_v^{(k)} \right\}$ are communicated to neighbors.

5.1.1.2 *State Model*

The dynamic behavior of a peer's state is modeled by

$$\mathbf{x}_v^{(k)} = f\left(\mathbf{x}_v^{(k-1)}, \boldsymbol{\omega}_v^{(k)} \right), \tag{5.4}$$

where $f(\cdot)$ is the system state transition function that indicates the evolution of system states[1]. The *process noise vector* $\boldsymbol{\omega}_v^{(k)}$ is the process noise that models the non-linearities and perturbations on the system. In fact, it is difficult to model these behaviors. For simplicity, $\boldsymbol{\omega}_v^{(k)}$ is usually modeled as Gaussian with zero mean and covariance matrix $\mathbf{Q}_v^{(k)}$, that is, $\boldsymbol{\omega}_v^{(k)} \sim \mathcal{N}(0, \mathbf{Q}_v^{(k)})$.

The choice of state transition function depends on the system maneuvers. In this work, we only consider Position-Time (PT) model instead of Position-Velocity-Time (PVT), in oder to limit the number of unknowns to 4 instead of 8 needed by the PVT model. The PT model is given by

$$\boldsymbol{x}_v^{(k)} = \mathbf{I}\boldsymbol{x}_v^{(k-1)} + \Delta t_k \mathbf{I}\boldsymbol{\omega}_v^{(k)}, \tag{5.5}$$

$$\mathbf{Q}_v^{(k)} = \text{diag}\left(\left[{\sigma_{\dot{x}_v}^{(k)}}^2 \; {\sigma_{\dot{y}_v}^{(k)}}^2 \; {\sigma_{\dot{z}_v}^{(k)}}^2 \; {\sigma_{\dot{b}_v}^{(k)}}^2 \right] \right), \tag{5.6}$$

where $\mathbf{I}$ is the identity matrix of size 4×4, which is the Jacobian matrix of state transition function f. Δt_k is the elapsed time between the two TSs

1 We assume the system state has the property of first- order descrete Markov process. The current state is only related to the previous one.

t_{k-1} and t_k. The noise covariance $\mathbf{Q}_v^{(k)}$ is proportional to the velocity of the vehicle.

5.1.1.3 *Observation Model*

Since hybrid measurements are adopted, the observation function $h(\cdot)$ is composed of equations (5.2) and (5.3) based on the arranged elements in observation vector $\boldsymbol{z}_v^{(k)}$:

$$\boldsymbol{z}_v^{(k)} = h\left(\boldsymbol{x}_m^{(k)}, \boldsymbol{\mathcal{P}}_v^{(k)}, \boldsymbol{S}_v^{(k)}, \boldsymbol{\nu}_v^{(k)}\right). \tag{5.7}$$

where $\boldsymbol{\nu}_v^{(k)} \sim \mathcal{N}(0, \mathbf{R}_v^{(k)})$ is the hybrid measurement noise vector. $\mathbf{R}_v^{(k)}$ is the covariance matrix and it is a function of pseudorange noise $\xi_{sv}^{(k)}$ and terrestrial range noise $\zeta_{nv}^{(k)}$.

We assume the satellite pseudorange measurements are independent and the noise is Gaussian, that is, $\xi_{sv}^{(k)} \sim \mathcal{N}(0, {\sigma_{sv}^{(k)}}^2)$. Furthermore, we assume the terrestrial range measurements are independent and the noise is also Gaussian with symmetric variance, that is, $\zeta_{nv}^{(k)}, \zeta_{vn}^{(k)} \sim \mathcal{N}(0, {\sigma_{nv}^{(k)}}^2)$.

Under such assumptions, the covariance matrix $\boldsymbol{R}_v^{(k)}$ can be defined as

$$\boldsymbol{R}_v^{(k)} \triangleq \operatorname{diag}\left(\left\{{\sigma_{sv}^{(k)}}^2, {\sigma_{nv}^{(k)}}^2 \mid s \in \mathcal{S}_v^{(k)}, n \in \mathcal{V}_v^{(k)}\right\}\right). \tag{5.8}$$

Note that the elements in (5.8) are arranged based on the measurement order of $\boldsymbol{z}_v^{(k)}$.

5.1.2 *Hybrid Cooperative Positioning Algorithms*

We consider the following four hybrid and cooperative positioning algorithms: Hybrid-Cooperative Particle Filter (HC-PF), Hybrid Sum-Product Algorithm over a Wireless Network (H-SPAWN), Hybrid-Cooperative Unscented Kalman Filter (HC-UKF), Hybrid-Cooperative Least Squares (HC-LS).

5.1.2.1 *Hybrid Cooperative Particle Filter*

The HC-PF is first presented in [62] and is the main algorithm for this analysis. It uses hybrid measurements to represent the likelihood function of particles.

$$\begin{aligned} p\left(\boldsymbol{z}_v^{(k)} \middle| {\boldsymbol{x}_v^{(k)}}^i\right) = &\prod_{s \in \mathcal{S}_v^{(k)}} p_{sv}\left(\rho_{sv}^{(k)} - \left\|\boldsymbol{p}_s^{(k)} - {\boldsymbol{p}_v^{(k)}}^i\right\| - {b_v^{(k)}}^i\right) \cdot \\ &\prod_{n \in \mathcal{V}_v^{(k)}} p_{nv}\left(r_{nv}^{(k)} - \left\|\hat{\boldsymbol{p}}_n^{(k)} - {\boldsymbol{p}_v^{(k)}}^i\right\|\right), \end{aligned} \tag{5.9}$$

where p_{sv} and p_{nv} are the likelihood function of satellite pseudorange noise ξ_{sv} and terrestrial range noise ζ_{nv}, respectively.

Since it is difficult to communicate and share the particle representation to neighbors, the HC-PF adopts Gaussian approximation. A peer would broadcast to neighbors its position estimate and the trace of the covariance matrix. The uncertainty on neighbor peer's position is interpreted as additional noise on the terrestrial range measurement. A safe worst-case approximation is to consider the variance of this noise as the trace of the position estimated covariance matrix. We suppose it is uncorrelated to the intrinsic measurement noise ζ_{nv}. Then the variance of measurement noise from a neighbor n ($n \in \mathcal{V}_v^{(k)}$) is given by

$$\hat{\sigma}_{nv}^{(k)^2} = \sigma_{nv}^{(k)^2} + \mathrm{tr}\left(\hat{\boldsymbol{P}}_n^{(k)}\right). \tag{5.10}$$

The HC-PF algorithm for hybrid cooperative positioning is described as pseudo code in Alg. 5.1. At every TS, each peer v ($v \in \mathcal{V}$) makes position estimate, taking into account the new available measurements $\boldsymbol{z}_v^{(k)}$ and the positioning data (positioning estimates $\hat{\boldsymbol{\mathcal{P}}}_v^{(k)}$, traces of the covariance matrices $\hat{\mathfrak{T}}_v^{(k)}$) from neighbors. Note that iterations are performed within the TS to improve the positioning performance.

5.1.2.2 *Hybrid Cooperative Least Square*

The HC-LS is extended version of cooperative least square algorithms in [60], in order to take into account pseudorange measurements and to estimate the bias variable. The LS estimate of $\boldsymbol{x}_v^{(k)}$ is obtained by solving the following optimization problem:

$$\hat{\boldsymbol{x}}_v^{(k)} = \arg_{\boldsymbol{x}_v^{(k)}} \min \left\| \boldsymbol{z}_v^{(k)} - h\left(\boldsymbol{x}_v^{(k)}, \boldsymbol{S}_v^{(k)}, \hat{\boldsymbol{\mathcal{P}}}_v^{(k)}\right) \right\|^2, \tag{5.11}$$

It is difficult to exactly solve equation (5.11). One approach is an iterative linearization of the cost function to the first order Taylor series expansion around the *a priori* estimate $\hat{\boldsymbol{x}}_v^{(k|k-1)}$ as

$$\boldsymbol{z}_v^{(k)} \approx h\left(\hat{\boldsymbol{x}}_v^{(k|k-1)}, \boldsymbol{S}_v^{(k)}, \hat{\boldsymbol{\mathcal{P}}}_v^{(k)}\right) + \left.\frac{\partial h}{\partial \boldsymbol{x}}\right|_{\hat{\boldsymbol{x}}_v^{(k|k-1)}} \left(\boldsymbol{x}_v^{(k)} - \hat{\boldsymbol{x}}_v^{(k|k-1)}\right), \tag{5.12}$$

which can be rewritten into matrix form

$$\Delta \boldsymbol{z}_v^{(k)} = \mathbf{H}_v^{(k)} \Delta \boldsymbol{x}_v^{(k)}, \tag{5.13}$$

where $\Delta \boldsymbol{z}_v^{(k)} = \boldsymbol{z}_v^{(k)} - h\left(\hat{\boldsymbol{x}}_v^{(k)^-}, \boldsymbol{S}_v^{(k)}, \hat{\boldsymbol{\mathcal{P}}}_v^{(k)}\right)$ and $\Delta \boldsymbol{x}_v^{(k)} = \left(\boldsymbol{x}_v^{(k)} - \hat{\boldsymbol{x}}_v^{(k|k-1)}\right)$. $\mathbf{H}_v^{(k)} = \left.\frac{\partial h}{\partial \boldsymbol{x}}\right|_{\hat{\boldsymbol{x}}_v^{(k|k-1)}}$ is the Jacobian matrix of observation function. The new state is updated by solving the following weighted linear system:

$$\hat{\boldsymbol{x}}_v^{(k)} = \hat{\boldsymbol{x}}_v^{(k|k-1)} + \left(\mathbf{H}_v^{(k)^T} \mathbf{W} \mathbf{H}_v^{(k)}\right)^{-1} \mathbf{H}_v^{(k)^T} \mathbf{W} \Delta \boldsymbol{z}_v^{(k)}. \tag{5.14}$$

Algorithm 5.1: Hybrid-Cooperative Particle Filter

input : $\left\{\boldsymbol{x}_v^{(k-1)^i}\right\}_{i=1}^{N}$, $\boldsymbol{z}_v^{(k)}$, $\boldsymbol{S}_v^{(k)}$ $\forall v$

output: $\left\{\boldsymbol{x}_v^{(k)^i}\right\}_{i=1}^{N}$, $\hat{\boldsymbol{x}}_v^{(k)}$ $\forall v$

for *time slot* $k = 1$ *to* K **do**
  for *vehicle* $v \in \mathcal{V}$ ***in parallel*** **do**
    for *iteration* $it = 1$ *to* N_{itr} **do**
      Receive positioning data $\hat{\mathcal{P}}_v^{(k)}$, $\hat{\mathcal{T}}_v^{(k)}$
      Update noise covariance matrix $\mathbf{R}_v^{(k)}$
      for *particle* $i = 1$ *to* N **do**
        Draw $\boldsymbol{\omega}_v^{(k)^i} \sim \mathcal{N}\left(0, \mathbf{Q}_v^{(k)}\right)$
        Update particles $\boldsymbol{x}_v^{(k)^i} = \mathbf{I}\boldsymbol{x}_v^{(k-1)^i} + \Delta t_k \mathbf{I}\boldsymbol{\omega}_v^{(k)^i}$
        Update weights $\tilde{w}_v^{(k)^i} = p\left(\boldsymbol{z}_v^{(k)} \middle| \boldsymbol{x}_v^{(k)^i}\right)$ using (5.9)
      end
      Compute total weight $W = \sum_{i=1}^{N} \tilde{w}_m^{(k)^i}$
      for *particle* $i = 1$ *to* N **do**
        Normalize weights $w_v^{(k)^i} = \tilde{w}_v^{(k)^i}/W$
      end
      Estimate peer's state $\hat{\boldsymbol{x}}_v^{(k)} = \sum_{i=1}^{N} w_v^{(k)^i} \boldsymbol{x}_v^{(k)^i}$
      Calculate the state covariance matrix
      $\hat{\boldsymbol{\Sigma}}_{\boldsymbol{x}_v}^{(k)} = \frac{\sum_{i=1}^{N} w_v^{(k)^i}\left(\boldsymbol{x}_v^{(k)^i} - \hat{\boldsymbol{x}}_v^{(k)}\right)\left(\boldsymbol{x}_v^{(k)^i} - \hat{\boldsymbol{x}}_v^{(k)}\right)^T}{1 - \sum_{i=1}^{N}\left(w_v^{(k)^i}\right)^2}$
      Communicate $\hat{\boldsymbol{p}}_v^{(k)}$ and $\mathrm{tr}\left(\hat{\boldsymbol{\Sigma}}_{\boldsymbol{x}_v}^{(k)}\right)$ to neighbors $n \in \mathcal{V}_v^{(k)}$
      Resample $\left\{\boldsymbol{x}_v^{(k)^i}\right\}_{i=1}^{N} \sim \mathcal{N}\left(\hat{\boldsymbol{x}}_v^{(k)}, \hat{\boldsymbol{\Sigma}}_{\boldsymbol{x}_v}^{(k)}\right)$
    end
  end
end

where $\mathbf{W}$ is a diagonal matrix whose elements are given by the inverse of the measurement variances. Since it is hard to estimate the uncertainty on the vehicle's position, the safest option is to give considerable weight to the pseudoranges no matter how good is the terrestrial ranging technology. In the HC-LS algorithm, only the position estimates are communicated to neighbors.

Due to the space limit, the detailed formulae of HC-UKF and H-SPAWN are not described here, which can be found in [61] and [63], respectively. For HC-UKF, the cooperative positioning data are still position estimates and the corresponding traces of covariance matrices. For H-SPAWN, the exchanging data are parametric Belief Propagation (BP) which approximates the messages as known 'distribution families'.

5.1.3 *Simulation of Urban Navigation*

5.1.3.1 *Simulation Scenario*

The simulation tool proposed in [88] has been used to simulate the performance of different algorithms. The scenario is depicted as 2D view in Fig. 5.2 where 25 unknown vehicles are deployed in an urban environment composed of three blocks per side. The main simulation parameters for this scenario are listed in Table 5.1.

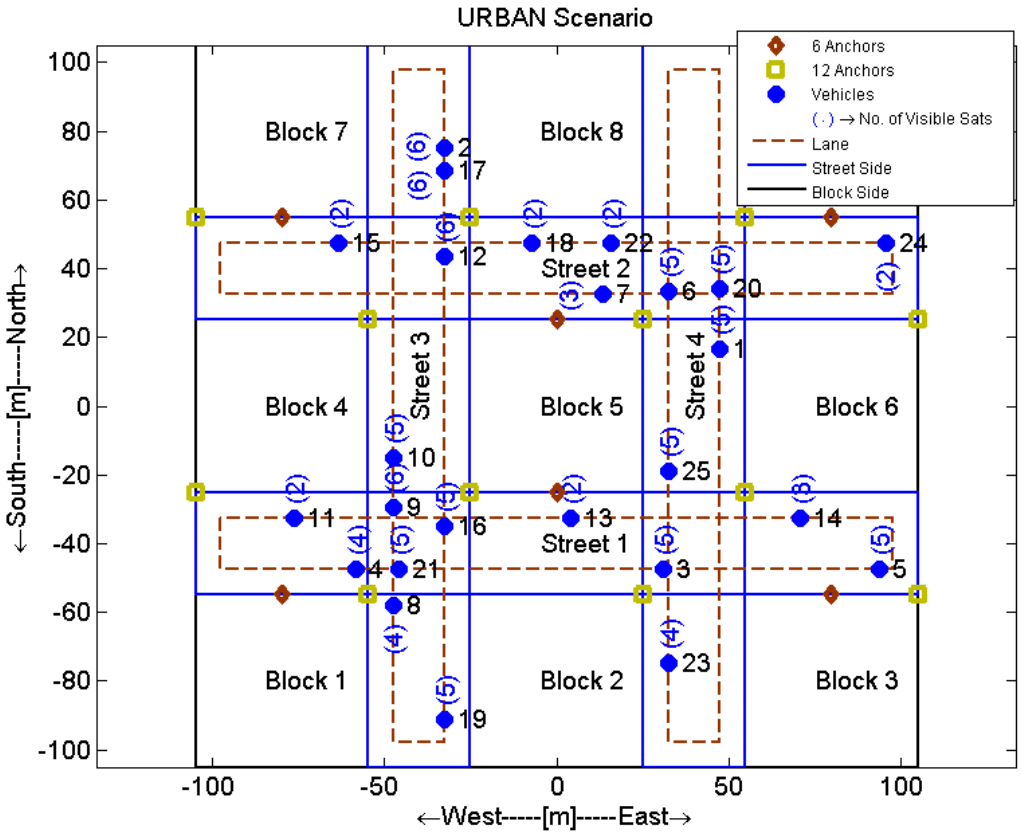

Figure 5.2: 2D view of the simulated vehicular network.

In particular, the center of the urban canyons is chosen as the city center of Singapore, 1.2831° latitude, in order to have better satellite visibility. The pseudo range measurements are generated based on the real GPS orbits and the vehicles' positions in the environment. The bias is considered as randomly within the interval of 5 milliseconds, corresponding the duration of one GPS C/A code. we assume that the blocks would completely obstructs the GPS signal, hence, the satellites are visible only from certain parts of the streets.

Three configurations of anchor nodes (0,6,12) are used to provide performance comparisons of cooperation. The horizontal positions of the anchor nodes are uniformly chosen within the environment while the vertical heights are randomly chosen between 5 and 10 meters. The communication range of terrestrial technique is 80 meters, which is typical value for

Table 5.1: Simulation parameters for urban navigation.

Parameter	Value	Units
Number of blocks per side	3	-
Blocks size	50	[m]
Street width	30	[m]
Building height	40	[m]
Urban environment latitude	1.2831 N	[degree]
Number of unknown peers	25	-
Number of anchor peers	0,6,12	-
Number of aiding peers	0	-
Connectivity radius	80	[m]
Std ranging error	0.2	[m]
Bias ranging error	0	[m]
Peer mobility	Vehicular	-
Route speed	10	[m/sec]
Flip speed	2	[m/sec]
Peer type	mass market	-
Wireless networking	asynch.	-
Number of time slots	40	-
Number of position iterations	3	-
Time slot width	1	[sec]
Number of Montecarlo simulations	100	-
Min max bias generation	150000	[m]
Initial guess peers' positions	uniform	-

UWB transceivers [78]. Since we consider the positioning of vehicles on flat ground, only the horizontal errors are considered.

5.1.3.2 *Simulation Results*

Since all the vehicles are on a plain city, we only consider the horizontal localization performance. Fig. 5.3 shows the evolution of the global positioning errors, which confirms the results observed in the c.d.f. plot. As it can be observed, all the algorithms shows good positioning availability due to the peer cooperation. Neither HC-UKF nor H-SPAWN show good convergence, mainly because they are not properly tuned for the urban mobility scenario. It can be observed that after the tenth time slot, errors remain stable around 25 m for H-SPAWN while it goes below 10 m for HC-UKF. The HC-PF instead, is able to track all vehicles and achieves a final accuracy of about 5 m. In the HC-LS algorithm, large oscillations are observed, which may be driven by few peers with large errors, because they may have lost some key satellites or peers.

Fig. 5.4, confirms the results observed in the RMSE plot, where HC-PF outperformed all the studied algorithms, while HC-UKF and surprisingly the

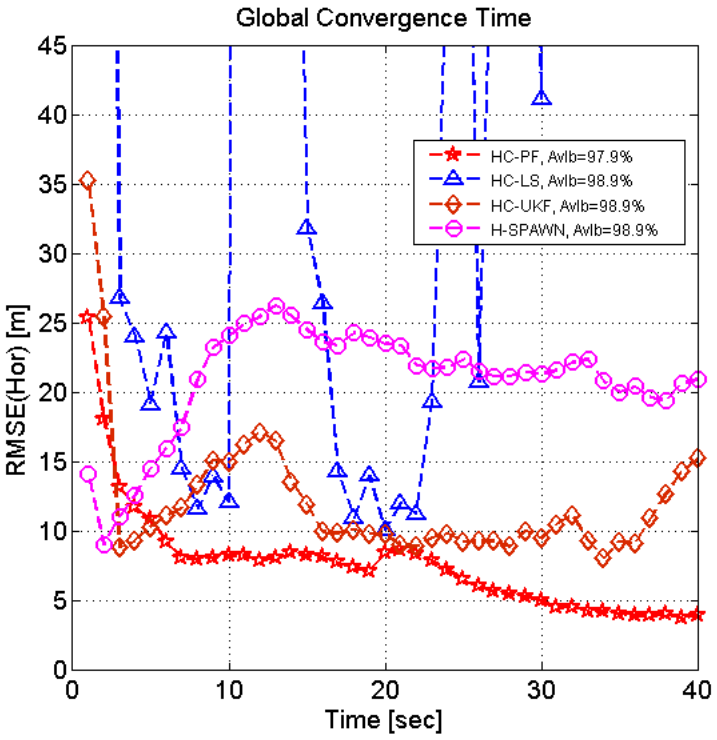

Figure 5.3: Positioning error evolution for different algorithms.

HC-LS obtained similar performance, even if the latter one exhibits more outliers. H-SPAWN seems to be the algorithm more affected by mobility, probably because its parameters, in particular the process noise model, was not properly tuned for these conditions.

Fig. 5.5 and Fig. 5.6 present the performance of the HC-PF algorithm under the configuration of $\{0, 6, 12\}$ anchor peers. Moreover, we test the hybrid algorithms without cooperation, i.e., only pseudorange measurements and terrestrial measurements from anchors are used. Note that the case with 0 anchor and no-cooperation corresponds to the case of GPS-only positioning.

As showed in Fig. 5.5, cooperation significantly improves both positioning availability and accuracy. Without fixed infrastructure (i.e., no anchor), cooperative positioning can significantly reduce positioning errors from 10 m (GPS-only) to 4 m. Moreover, the position estimate availability is increased by 19%. With 6 anchors, the final positioning error is around 2 m and the gain of cooperation is still considerable, more or less 3 m. With 12 anchors, the positioning error is very low, 0.8 m. Note that in this case the benefit of cooperation is not so evident, only around 0.3 m. Another advantage of cooperation is the fast convergence. In fact, the cooperative version of HC-PF converges within 10 TSs. It is worth observing that after 30 TSs, the cooperative localization with 0 anchor outperforms the non-cooperative lo-

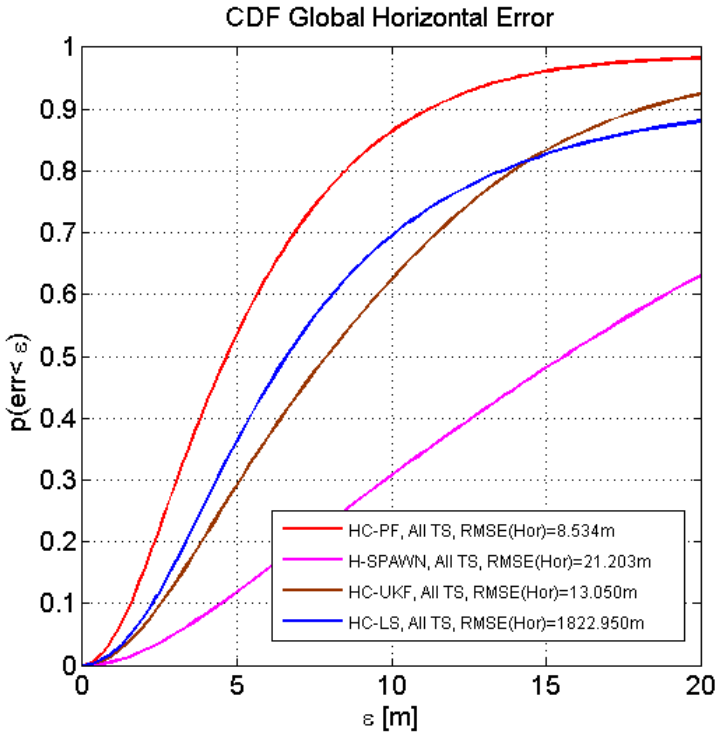

Figure 5.4: Horizontal positioning errors.

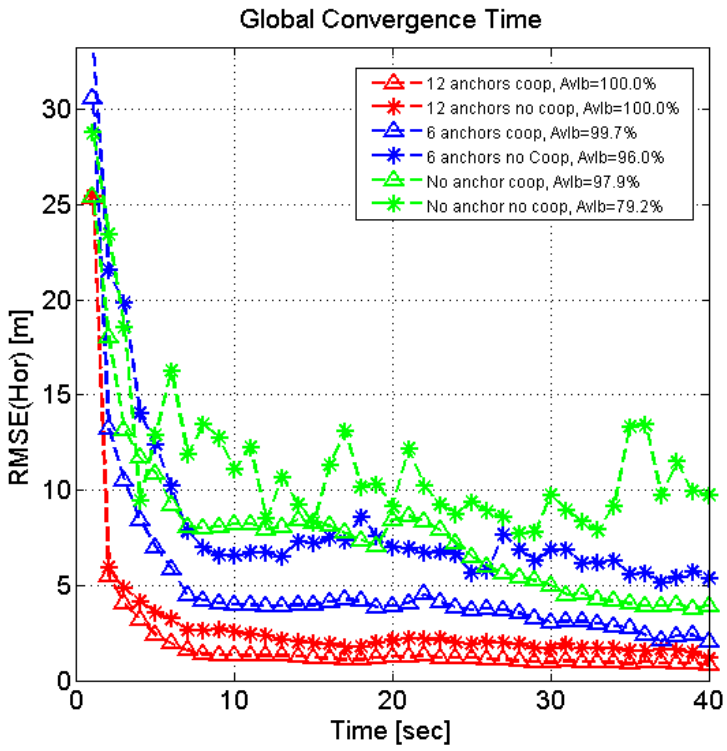

Figure 5.5: Convergence of the horizontal errors for HC-PF.

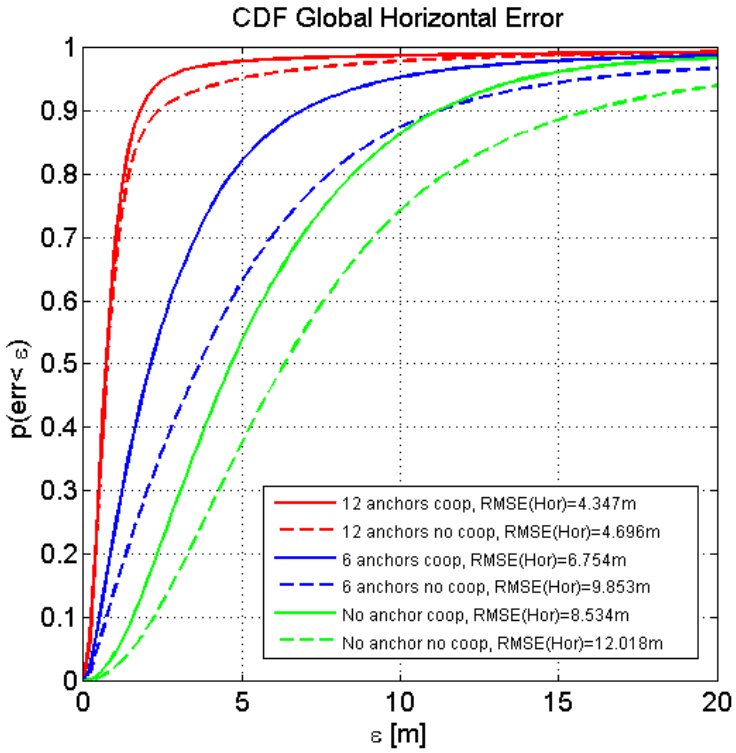

Figure 5.6: Positioning performance of HC-PF for different anchor settings .

calization with 6 anchors because more information is avaible thanks to the cooperation.

Fig. 5.6 presents the c.d.f. of different anchor setting, and it confirms the results in Fig. 5.5. With 12 anchors, the gain of cooperation can be neglected, while for 6 and 0 anchors, the cooperation shows great benefits.

Since installing a fixed UWB infrastructure in urban environment is expensive, the hybrid and cooperative localization without anchors can be a good candidate for urban navigation. Since the simulated area is close to equator, where the satellite visibility is the best, the gain of terrestrial hybridization and vehicle cooperation would be more in high altitude areas.

5.2 Hybrid GPS-UWB Indoor Navigation

As mention before, indoor navigation is a special challenge for GNSS. A hybrid navigation experiment to evaluate the was carried out to evaluate the proposed hybrid and cooperative positioning approaches. The corresponding experimental results are presented in this section.

5.2.1 *Localization Environment*

In the experiment, the mobile was composed of a GPS receiver (Fig. 2.7), a UWB device (Fig. 2.6) and a laptop, and it was placed on a small cart with purpose of convenient movement. A picture of the mobile station is shown in Fig. 5.7. Due to the lack of equipments, only one mobile node is available so only the hybrid positioning can be employed.

Figure 5.7: A picture of the mobile station.

The environment was chosen as the entrance of ISMB, whose map is shown in Fig. 5.8. As it can be seen, it consists of indoors and outdoors. Different walls separate the indoor part into three rooms and a corridor. Four UWB nodes (101-104 in Fig. 5.8) were deployed as anchors to provide terrestrial ranges for the mobile. These walls are made of wood, concrete and metal, and could block the signals of GPS and UWB. Therefore, in the outdoor, the UWB mobile could receive at most two ranges from anchors; in the indoor, the GPS receiver could only see satellites close to the door.

5.2.2 *Static Positioning*

First, we tested the positioning performance of the static points. Fig. In total, there are 16 points used to collect the real measurements. Some of them (P1-P8) are deep doors, some of them(P12-P14) are light indoors and the remaining are outdoors.

Due to the space limit, only results of some typical points are presented here. Fig. 5.10 presents positioning results of point 9 in Fig. 5.9, which shows the results of three configurations of the positioning algorithm, that is, GPS only, UWB only, GPS + UWB. Moreover, it shows the evolution of the positioning error in 100 seconds. As it can be observed from Fig. 5.10,

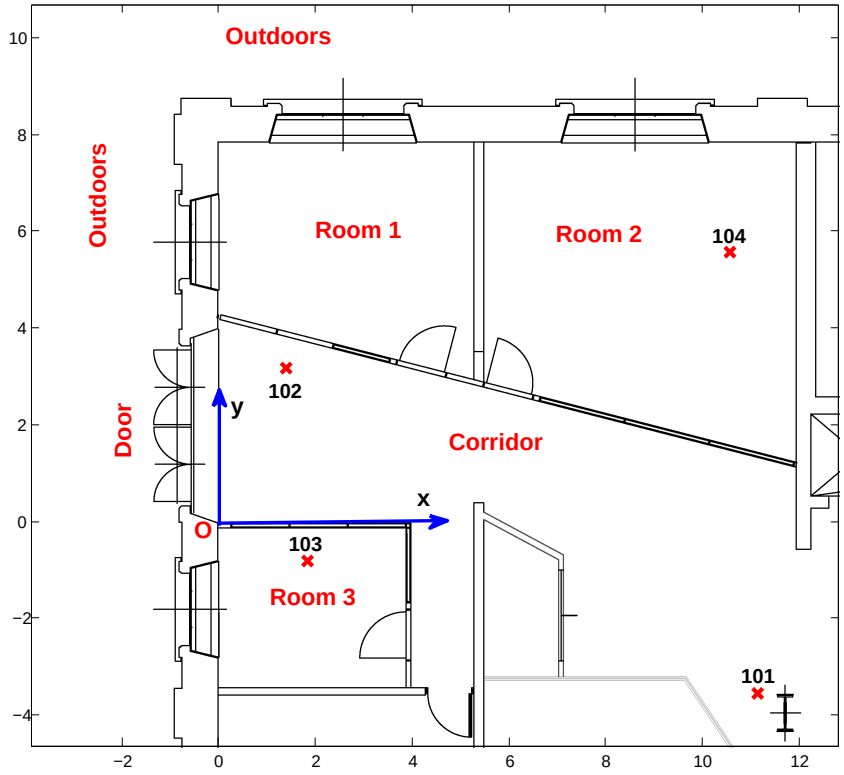

Figure 5.8: Map of ISMB entrance.

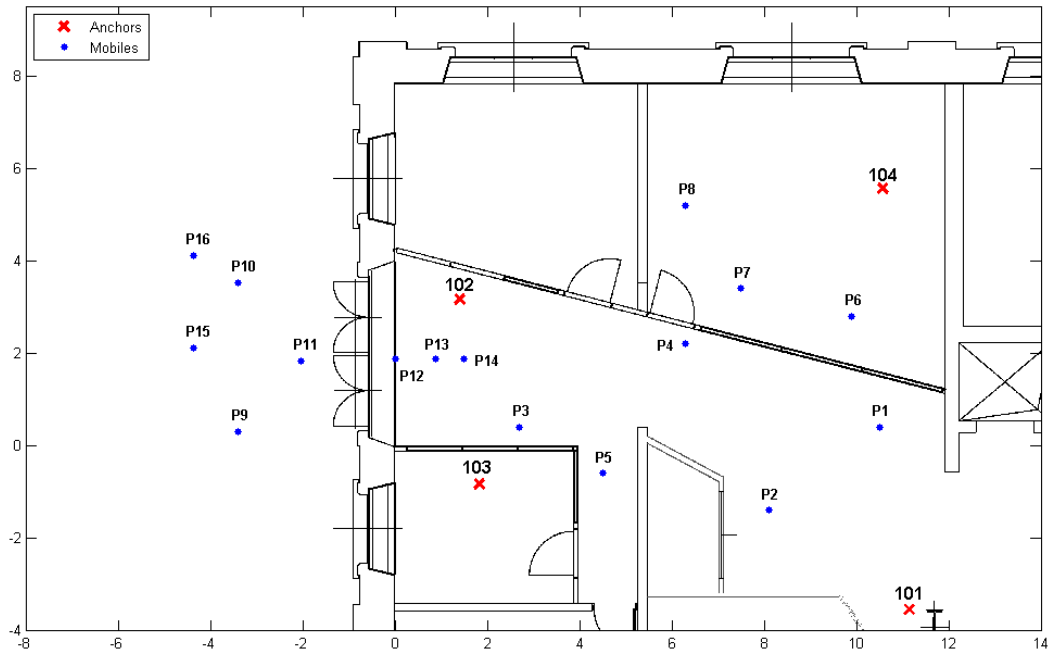

Figure 5.9: Node deployment of static positioning.

the configurations using UWB measurements have stable positioning performance as time passes by. Usually, the range measurement from a UWB sensor is much better than GPS pseudoranges. Sometimes there are some bad measurements from GPS receiver, so that the positioning errors diverge

from 70 to 90 seconds. The UWB measurements are neither adequate nor accurate in outdoors, causing the positioning estimates with errors up to 8.2 meters. However, the joint use of GPS and UWB can reduce the positioning errors to 4.5 meters.

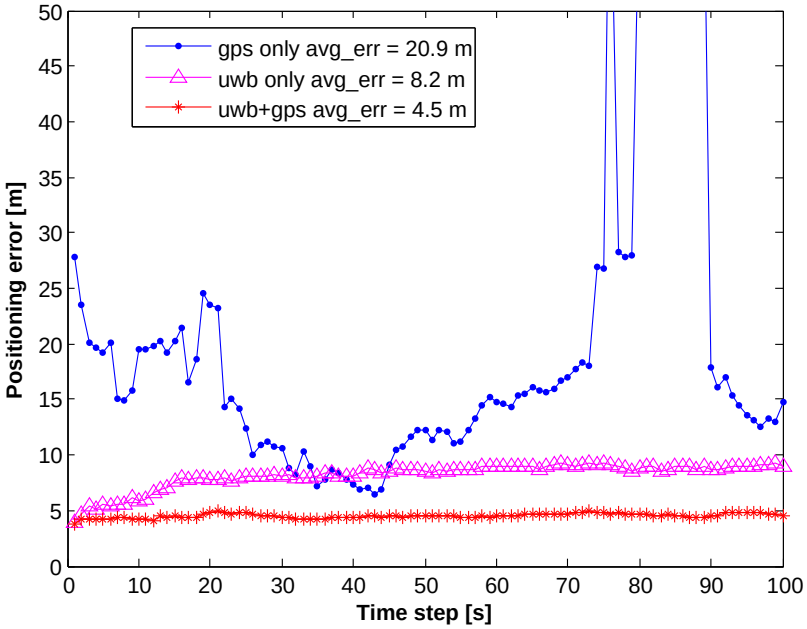

Figure 5.10: Outdoor positioning performance.

Fig. 5.11 presents the results of light indoors (point 12 in Fig. 5.9). The GPS only configuration diverge fast, due to the lack of visible satellites. The accurate UWB distance measurements dominate the positioning. With GPS measurements, the positioning performance is slightly better, because they can help the positioning algorithm with fast convergence.

Fig. 5.12 presents the results of light indoors (point 4 in Fig. 5.9). In this case, the GPS receiver cannot see any satellite, and only the UWB system can locate the mobile.

5.2.3 *Dynamic Tracking*

The dynamic scenario is shown in Fig. 5.13, where a trajectory containing 30 points was considered. The distance between two points (blue-dot points on mobile trajectory) is exactly one meter. The trajectory is composed of three segments: the first segment is in outdoor; the second segment connects the indoor and outdoor through the door; the third segment is in the corridor (deep indoor). The mobile cart moved along the trajectory and collected measurements for analysis.

We tried to move the cart with steady speed along the path and took both measurements from GPS and UWB every second. But it is impossible to manage the same speed and pass one blue point in one exact second. The measurements and mobile position need to be synchronized, Here we

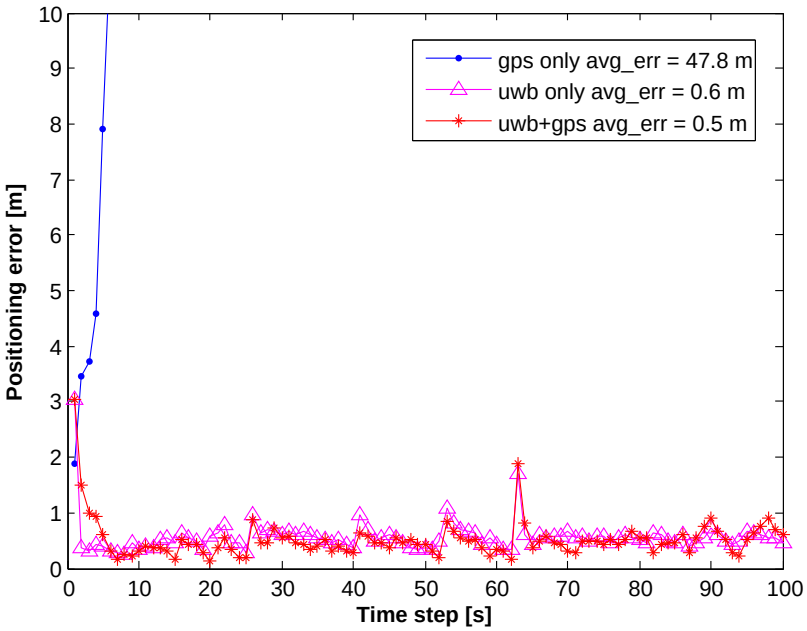

Figure 5.11: Light indoor positioning performance.

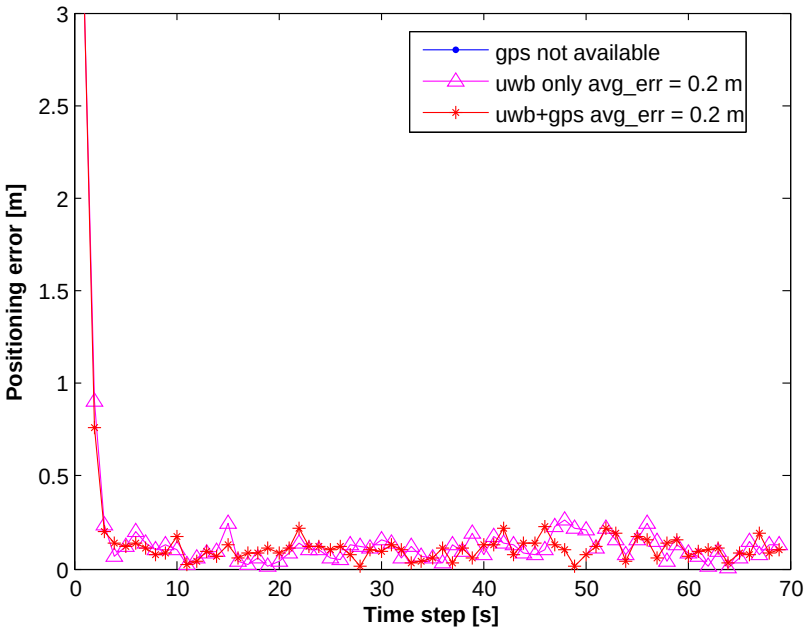

Figure 5.12: Deep indoor positioning performance.

supposed that the moving speed within two consecutive points was the same. We referred to the time stamp from the received GPS signal and took video of the movement, so as to calculate the precise passing time of each points. Based on the time difference between the passing time of each point and the GPS time, it is possible find out the exact mobile position, on which the hybrid measurements were taken. The red-star points in Fig. 5.13 represent the exact mobile positions per second. After synchronization with

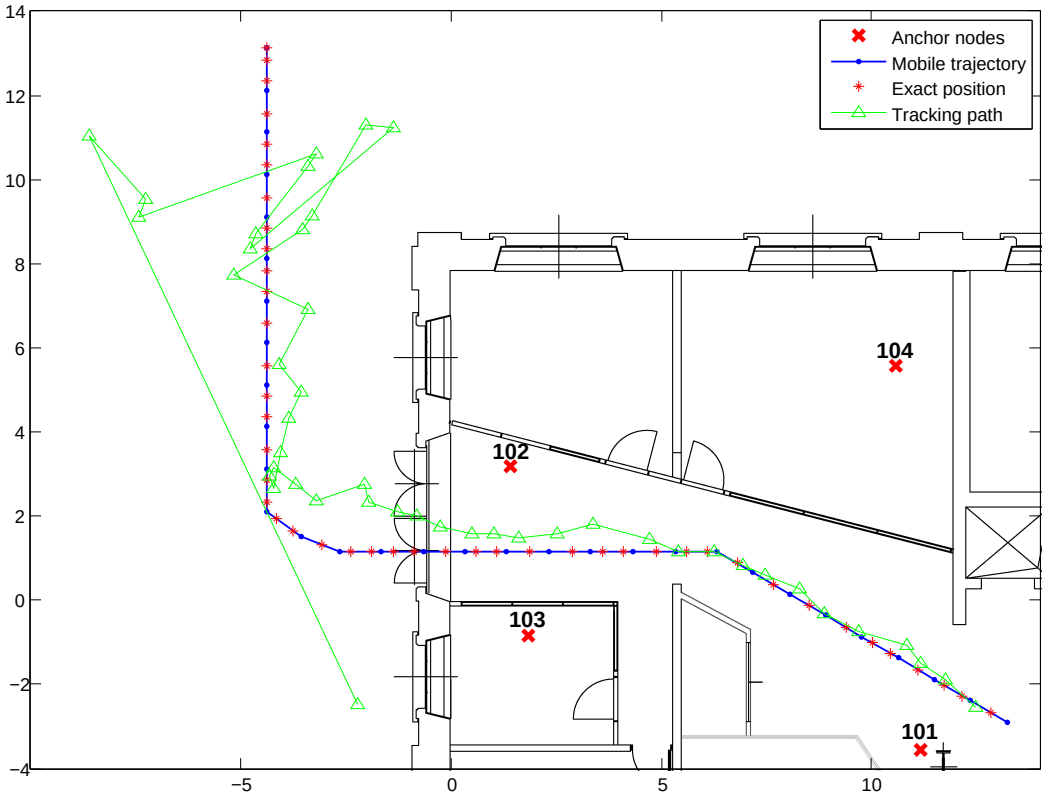

Figure 5.13: Trajectory of dynamic tracking.

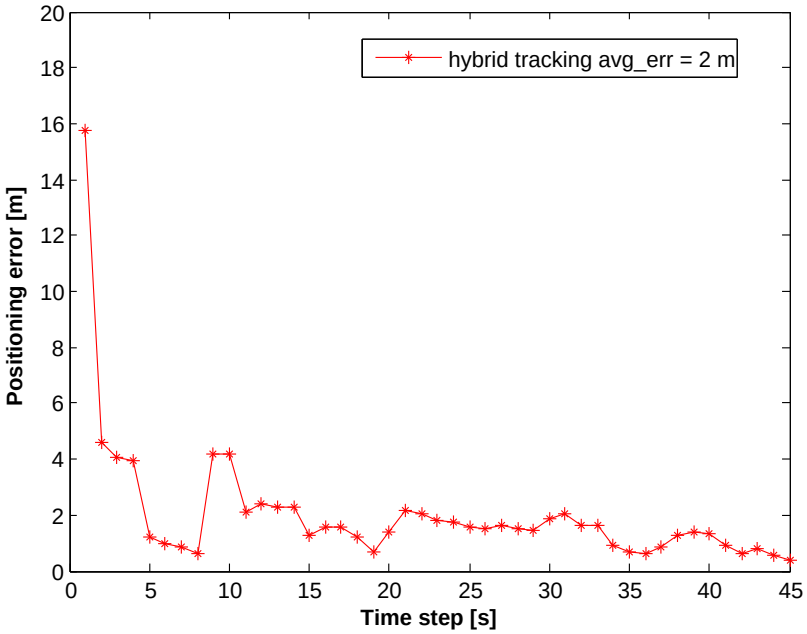

Figure 5.14: Deep indoor positioning performance.

exact positions, the obtained measurements are feed the hybrid positioning algorithm.

Fig. 5.13 also presents the tracked path as green triangle line. During the start, the tracked path is with large errors, which is caused by two reasons.

One is that the algorithm is initialized and needs some transient time to catch movement of the mobile. The other one is that the GPS pseudoranges are with large errors and can make the position estimate fluctuate. Due to the high accurate UWB measurements, the hybrid algorithm can catch the movement of the mobile after 10 seconds, as it can be seen from Fig. 5.14. By using the hybrid technologies, the final positioning performance is about two meters, realizing seamless navigation connecting outdoors and indoors.

5.3 SUMMARY

This chapter presented the hybrid and cooperative positioning algorithms to improve localization performance in urban canyons and indoor environments. First, it demonstrated that the hybrid cooperative positioning approach can track the movement of vehicles in urban canyons even without fixed terrestrial infrastructure. Then it showed that this approach also worked for seamless indoor and outdoor navigation.

Part III

ADVANCED POSITIONING ALGORITHMS FOR INDOOR APPLICATIONS

6

COGNITIVE AND COOPERATIVE TRACKING

This section presents a novel Cognitive and Cooperative Tracking (CCT) approach based on EKF to localize mobile nodes in wireless networks. The proposed algorithm shows three important features: energy efficient, cognitive and cooperative. More specifically, the tracking algorithm adaptively adjusts the transmission power to optimize the energy consumption while meeting the required localization accuracy P_a imposed by a generic application. Moreover, it adopts a self-learning scheme to track the time-variant environment's characteristics (e.g., range measurement noise) and use this knowledge to improve tracking performance. Finally, the algorithm exploits the cooperation among unknown nodes that leads to further improved performance and reduced power consumption. Simulation results show that the proposed CCT approach is able to improve positioning performance and meet the required accuracy P_a while energy consumption is optimized.

6.1 INTRODUCTION TO COGNITIVE TRACKING

Most of localization and tracking algorithms in the literature aim to increase positioning accuracy but ignore other important aspects, e.g., energy consumption. Since mobile devices are battery powered, designing an energy efficient algorithm is of primary importance [89]. Another aspect to be taken into account is how to deal with time-variant environments. In fact, the radio channel condition is not always constant but it changes along time, which affects the ranging accuracy in a negative way. Even if unknown nodes are static, the environment continuously changes as many obstacles (e.g., other users) move around and cause time-variant interference. This negative effect increases even more when unknown nodes are in movement because the environment is not uniform but the sizes of it change, materials are different as well as sources of interference.

This motivated us to design an innovative *cognitive tracking* approach that is able to react to the time-variant environment and to increase reliability and accuracy of the positioning service as well as to optimize energy consumption while meeting the accuracy requirement P_a that is predefined by the user, e.g., indoor tracking application may require positioning error within 1 meter. Cognitive positioning is an emerging technique that is aware of the users' needs and environment's characteristics and incorporates this knowledge into the location engine to improve the overall performance. On the other hand, cooperation among mobiles leads to manifold

benefits, e.g., for the purpose of settling geometrical ambiguities, enhancing positioning accuracy by measurements redundancy and spatial diversity, or simply improving coverage and availability of service [90]. By introducing cooperation, it enables to track the mobile node more accurately and alternatively to save more energy to reach a certain positioning accuracy.

Based on these concepts, this paper proposes a CCT algorithm able to react to the time-variant channel [91] and to optimize energy consumption. Different from common cognitive positioning approaches [92, 93], which adaptively adjust power allocation in different frequency bands, the CCT approach focuses on adjusting the transmitting power just in one frequency band.

6.2 FRAMEWORK OVERVIEW

The section overviews the related framework, the applied ranging model, the cooperative Cramér-Rao Lower Bound (CRLB) and the energy efficient tracking. The formulation of EKF is omitted, as it is introduced in Chapter 2.

6.2.1 *Ranging Model*

The theoretical ranging performance is investigated in [71], where the primary sources of error in ToA ranging, such as multipath, interference and clocks drift, are discussed. In this paper, we simply consider these effects as time-variant ranging noise:

$$\tilde{d} = d + v, \tag{6.1}$$

where d is the true distance between two nodes and v is the additive noise assumed to be Gaussian distributed with zero mean and a time-variant standard deviation, i.e., $v \sim \mathcal{N}\left(0, \sigma^2(t)\right)$. In particular, the standard deviation of the range measurement error is not constant but it change with time according to a specific model $\sigma(t)$.

Let $\mathcal{A}$ and $\mathcal{M}$ be the set of anchors and mobiles, respectively, in the whole network. Let $\boldsymbol{z}_m^{(k)}$ be the available range measurements performed by a generic mobile node m at a given time $t^{(k)}k$. The vector $\boldsymbol{z}_m^{(k)}$ can be divided into two subsets: range measurements from anchors and those from mobiles:

$$\boldsymbol{z}_m^{(k)} = \left\{ \left\{ \tilde{d}_{a\to m}^{(k)} \right\}_{a\in\mathcal{A}_m^{(k)}}, \left\{ \tilde{d}_{n\to m}^{(k)} \right\}_{n\in\mathcal{M}_m^{(k)}} \right\}, \tag{6.2}$$

where $\mathcal{A}_m^{(k)} \subseteq \mathcal{A}$ and $\mathcal{M}_m^{(k)} \subseteq \mathcal{M}$ are the subsets of anchors and mobiles connected to the mobile m, respectively, at time $t^{(k)}$. Positions of anchors $a \in \mathcal{A}$ and mobiles $m \in \mathcal{M}$ are denoted with $\boldsymbol{x}_a^{(k)}$ and $\boldsymbol{x}_m^{(k)}$, respectively, whose dimensions are equal to D.

The range measurement model from an anchor node can be written as:

$$\tilde{d}_{a\to m}^{(k)} = \left\| \boldsymbol{x}_m^{(k)} - \boldsymbol{x}_a^{(k)} \right\| + \upsilon_{a\to m}^{(k)}, \tag{6.3}$$

where $\upsilon_{a\to m}^{(k)}$ is the measurement noise that is assumed to be Gaussian with a time-variant standard deviation $\sigma_{a\to m}^{(k)}$. Analogously, the range measurement model from a mobile node can be written as:

$$\tilde{d}_{n\to m}^{(k)} = \left\| \boldsymbol{x}_m^{(k)} - \boldsymbol{x}_n^{(k)} \right\| + \upsilon_{n\to m}^{(k)}, \tag{6.4}$$

where $\upsilon_{n\to m}^{(k)}$ is the measurement noise that is also assumed to be Gaussian with a time-variant standard deviation $\sigma_{n\to m}^{(k)}$.

Assuming that all the range measurements are independent, then the measurement covariance matrix $\boldsymbol{R}^{(k)}$ can be written as:

$$\boldsymbol{R}_m^{(k)} = \operatorname{diag}(\underbrace{\ldots \sigma_{a\to m}^{(k)^2} \ldots}_{a\in\mathcal{A}_m^{(k)}} \underbrace{\ldots \sigma_{n\to m}^{(k)^2} \ldots}_{n\in\mathcal{M}_m^{(k)}}). \tag{6.5}$$

6.2.2 *Cramér-Rao Lower Bound*

This section presents the CRLB for cooperative positioning [94]. This study will be used later to support a procedure that selects the closest neighbors (comprising both anchors and mobiles) that meets the positioning accuracy requirements P_a. As a result, the energy consumption is optimized.

The CRLB provides a lower bound on the mean square error of any unbiased estimator. It is obtained by inverting the Fisher information matrix. Since the CCT algorithm is fully distributed, it is impossible to obtain the global Fisher information matrix as [94]. The mobile node m calculates locally Fisher information at each time step.

$$\boldsymbol{F}_m^{(k)} = \sum_{a\in\mathcal{A}_m^{(k)}} \frac{1}{\sigma_{a\to m}^{(k)^2}} \boldsymbol{u}_{am}^{(k)} \left(\boldsymbol{u}_{am}^{(k)}\right)^T + \sum_{n\in\mathcal{M}_m^{(k)}} \frac{1}{\sigma_{n\to m}^{(k)^2}} \boldsymbol{u}_{nm}^{(k)} \left(\boldsymbol{u}_{nm}^{(k)}\right)^T, \tag{6.6}$$

where $\boldsymbol{u}_{im}^{(k)} = \frac{\boldsymbol{x}_i^{(k)} - \boldsymbol{x}_m^{(k)}}{\left\| \boldsymbol{x}_i^{(k)} - \boldsymbol{x}_m^{(k)} \right\|}$ is the unitary column vector between two positions $\boldsymbol{x}_i^{(k)}$ and $\boldsymbol{x}_m^{(k)}$.

Then the CRLB is calculated as:

$$\Omega_m^{(k)} = \sqrt{\operatorname{tr}\left((\boldsymbol{F}_m^{(k)})^{-1} \right)}. \tag{6.7}$$

where $\operatorname{tr}(\cdot)$ is the trace of a square matrix.

This bound is compared with respect to the required positioning accuracy P_a. Based on this comparison, the proposed algorithm adaptively adjusts the communication range in order to properly select its neighbors for positioning. Since the true mobile's position is not known, in the implementation the *a priori* location estimation $\hat{\boldsymbol{x}}_m^{(k|k-1)}$ is used to calculate this bound.

6.2.3 *Energy Efficient Tracking Approach*

According to the *Log-normal shadowing path loss* model [67], the transmission loss is proportional to the distance between the transmitter and the receiver. In other words, the larger connectivity radius, the higher transmitted power.

Traditional tracking approaches use a fixed transmitted power, to which corresponds a fixed connectivity radius R_f [89]. In a mobile scenario, it might happen that in a certain point of the trajectory, many range measurements are available. If all of them are used, the tracking algorithm provides a positioning accuracy much higher than P_a, thus the transmitted power can be decreased to save energy. On the contrary, it might happen that only few range measurements are available and a larger transmitted power is needed to increase the number of neighbors such that the location accuracy achieves P_a. In conclusion, an adaptive connectivity radius R_a should be adopted to meet the required localization accuracy while at the same time to save energy consumption.

As reported in [89], the average transmission power reduction expressed in dBm can be expressed as:

$$\Delta\overline{P}_t = 10\alpha\log_{10}\left(R_f/\overline{R}_a\right). \tag{6.8}$$

where α is the path loss exponent and $\overline{R}_a$ is the average connectivity radio. Thus, for instance, if the fixed transmitted power is 0 dBm and $\Delta\overline{P}_t = 3$ dBm, then the average transmitted power corresponding to the adaptive approach is -3 dBm.

Fig. 6.1 shows an example of the connectivity information of R_a and R_f in a certain point of the environment. As it can be observed, there are fewer anchors within the adaptive range R_a than those within the fixed range R_f, but the localization errors could be in the same level.

The next section will present an approach that selects the closest neighbors to be used in the current position estimation step and on the basis of this it proposes the connectivity radio to be used in the next position estimation step.

6.3 COGNITIVE AND COOPERATIVE TRACKING ALGORITHM

The proposed CCT is composed of three main components, (*i*) neighbors selection scheme, (*ii*) environment awareness and (*iii*) cooperation, which are presented in the following subsections.

6.3.1 *Neighbors Selection Algorithm*

In [89], an *anchors selection scheme* is proposed to select the closest anchors for communication. Thanks to the cooperation among mobiles, it is extended to be the Neighbors Selection Algorithm (NSA), which selects the

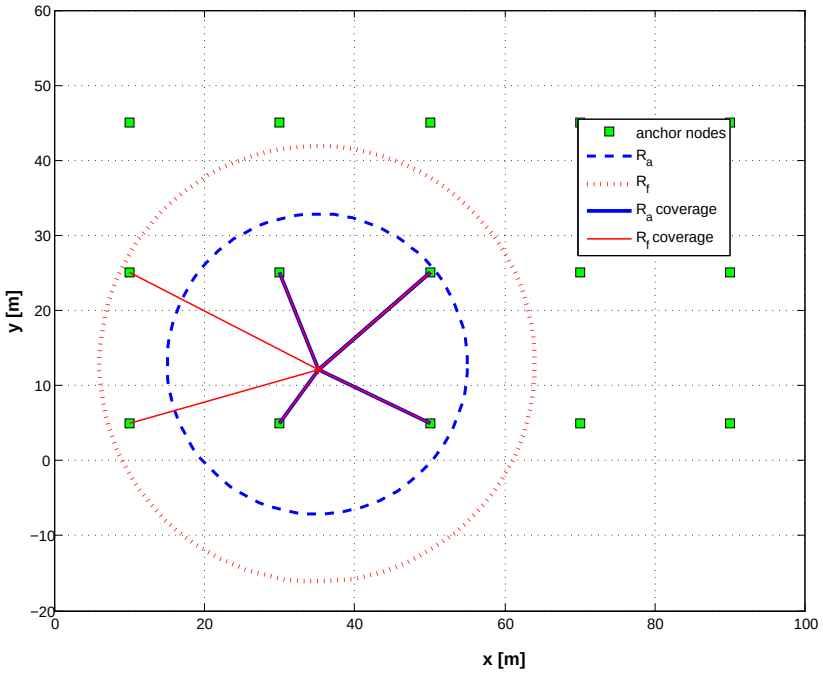

Figure 6.1: A example mobile radio connectivity.

closest neighbors, taking into consideration not only anchors but also mobiles. In fact, no larger connectivity radius is required to include farther anchors if closer mobiles are presented and the energy efficiency could be further improved.

Given a generic mobile m, the NSA takes as inputs: current measurement set $z_m^{(k)}$ (6.2), corresponding neighbor set $\mathcal{N}_m^{(k)}$, current *a priori* estimate $\hat{x}_m^{(k|k-1)}$, and current connectivity radio $R_m^{(k)}$. As outputs, it provides the selected measurement set $z_{m,s}^{(k)}$, the corresponding neighbor set $\mathcal{N}_{m,s}^{(k)}$, and the radio connectivity $R_m^{(k+1)}$ to be used in the next position estimation step. The whole algorithm is reported as pseudo code in Alg. 6.1.

Particularly, N_{min} denotes the minimum number of neighbors to be used for localization and it is set to 4 by default to satisfy the trade-off between energy consumption and position accuracy. If N_{min} is greater than or equal to 5, the accuracy is high but energy consumption for ranging is also high. On the other hand, if N_{min} is less than or equal to 3, energy consumption for ranging is low but positioning accuracy is also low.

As reported in row 3 of Alg. 6.1, if the cardinality C of the measurement set $z_m^{(k)}$, is greater than or equal to N_{min}, the algorithm selects the closest neighbor subset based on the calculated CRLB (6.7) and sets the radio connectivity radius $R_m^{(k+1)}$ for next position estimation step. Note that $R_m^{(k+1)}$ is set as the largest value between the selected range measurements $z_{m,s}^{(k)}$ and R_{min}, where R_{min} is the minimum radio connectivity range that guarantees enough links for communication. On the contrary, if C is less than N_{min}, there are not enough range measurements to locate the mobile node

Algorithm 6.1: Neighbors Selection Algorithm

input : $\boldsymbol{z}_m^{(k)}$, $\mathcal{N}_m^{(k)}$, $\hat{\boldsymbol{x}}_m^{(k|k-1)}$, $R_m^{(k)}$ $\forall m$
output: $\boldsymbol{z}_{m,s}^{(k)}$, $\mathcal{N}_{m,s}^{(k)}$, $R_m^{(k+1)}$ $\forall m$

Set $C = \left|\boldsymbol{z}_m^{(k)}\right|$
Set $N_{min} = 4$ {minimum number of neighbors}
Initialize: $\boldsymbol{z}_{m,s}^{(k)} = \boldsymbol{z}_m^{(k)}$, $\mathcal{N}_{m,s}^{(k)} = \mathcal{N}_m^{(k)}$, $R^{(k+1)} = R^{(k)}$
if $C \geqslant N_{min}$ **then**
    Sort $\boldsymbol{z}_m^{(k)}$ in ascending order
    Sort neighbors $\mathcal{N}_m^{(k)}$ according to $\boldsymbol{z}_m^{(k)}$
    for $i = N_{min}$ *to* C **do**
        Calculate CRLB $\Omega_m^{(k)}$ using $\hat{\boldsymbol{x}}_m^{(k|k-1)}$ and the first i elements of $\boldsymbol{z}_m^{(k)}$ and $\mathcal{N}_m^{(k)}$
        Set $\boldsymbol{z}_{m,s}^{(k)} = \boldsymbol{z}_m^{(k)}(1:i)$ {take first i elements}
        Set $\mathcal{N}_{m,s}^{(k)} = \mathcal{N}_m^{(k)}(1:i)$ {take first i elements}
    end
    Set $R_m^{(k+1)} = \max\left(\max\left(\boldsymbol{z}_{m,s}^{(k)}\right), R_{min}\right)$
else
    Set $R_m^{(k+1)} = R_m^{(k)} + \Delta R_c$
end

and the communication range is simply increased by ΔR_c, whose value is chosen according to the node density of the network.

6.3.2 *Environment Awareness*

Traditional tracking approaches assume that the range measurement noise statistics is always the same and perfectly known, which is not true. In practical, the localization environment is time variant even when the unknown mobile is static because there are some moving obstacles that make the environment changing.

In order to improve the tracking performance, it is necessary to adopt a cognitive approach that recognizes the environment parameter changing when collecting range measurements from neighbors. Consequently, a novel environment recognition strategy is proposed to continuously estimate the standard deviation of the range measurement noise. Assuming that at given time the values of range measurement standard deviation of mobile m w.r.t. to all its visible anchors are the same (i.e., $\sigma_{a_1 \to m}^{(k)} =$

$\sigma^{(k)}_{a_2\to m} = \ldots = \sigma^{(k)}_{m}$), then the standard deviation can be estimated as follows:

$$\hat{\sigma}^{(k)}_{m,\text{curr}} = \sqrt{\frac{1}{A^{(k)}_m - 1}\sum_{n=1}^{A^{(k)}_m}\left(\tilde{d}^{(k)}_{a\to m} - \hat{d}^{(k)}_{a\to m}\right)^2}, \tag{6.9}$$

where $\tilde{d}^{(k)}_{a\to m}$ is the measured distance between the node m and a-th anchor node at time t_k while $\hat{d}^{(k)}_{a\to m}$ is the estimated distance calculated by applying the Euclidean distance formula, given the estimated mobile's position and anchor's position. $\hat{\sigma}^{(k)}_{m,\text{curr}}$ is the current estimation of the measurement noise standard deviation; $A^{(k)}_m = \left|\mathcal{A}^{(k)}_m\right|$ denotes the number of anchors visible by the mobile m at time t_k.

In order to obtain a smooth standard deviation estimation, a sliding window with length L is applied:

$$\hat{\sigma}^{(k)}_{m} = \sqrt{\frac{1}{L}\sum_{l=k-L+1}^{l=k}\hat{\sigma}^{(l)^2}_{m,\text{curr}}}. \tag{6.10}$$

6.3.3 *Cooperation Scheme*

Applying the cooperation among unknown nodes leads to improved positioning performance in terms of both accuracy and robustness. The cooperation enables mobile nodes to share positioning data among them.

One of the most critical point of cooperative localization approaches has proven to be the quantification of the uncertainties related to the shared positioning data. The position estimation process could even diverge if those uncertainties are not properly evaluated [90].

The solution proposed in [62] considers the range measurement variance of a generic mobile m w.r.t. a generic neighboring mobiles n as the sum of the intrinsic range measurement variance $\sigma^{(k)^2}_{n\to m}$ and a contribution from the neighboring mobile position's uncertainty. This position uncertainty can be calculated as the trace of the position estimated covariance matrix $\boldsymbol{P}^{(k)}_n$:

$$\hat{\sigma}^{(k)^2}_{n\to m} = \sigma^{(k)^2}_{n\to m} + \text{tr}\left(\boldsymbol{P}^{(k)}_n\right). \tag{6.11}$$

The designed CCT algorithm, which is described in pseudo code form in Alg.6.2, uses both the estimated range noise standard deviation of mobiles with respect to anchors (6.10) and the new range uncertainties among mobiles (6.11). Note that in the initialization phase, the CCT uses a Linear Least Squares (LLS) algorithm to reduce the transient time as in [89].

Algorithm 6.2: Cognitive and Cooperative Tracking Algorithm

Set initial value for $R_m^{(0)}$ and $\hat{\sigma}_m^{(0)}$ $\forall m \in \mathcal{M}$
Perform distance measurements according to $R_m^{(0)}$, $\boldsymbol{z}_m^{(0)} = \left\{\tilde{r}_{a\to m}^{(0)}\right\}_{a\in\mathcal{A}_m^{(0)}}$ $\forall m \in \mathcal{M}$
Initialize $\hat{\boldsymbol{x}}_m^{(0)}$ by using LLS algorithm
for *timestep* $k = 1$ *to* K **do**
  for *nodes* $m \in \mathcal{M}$ ***in parallel*** **do**
    Predict the *a priori* state $\hat{\boldsymbol{x}}_m^{(k)^-}$
    Collect range measurements from neighbors $\boldsymbol{z}_m^{(k)} = \left\{\left\{\tilde{d}_{a\to m}^{(k)}\right\}_{a\in\mathcal{A}_m^{(k)}}, \left\{\tilde{d}_{n\to m}^{(k)}\right\}_{n\in\mathcal{M}_m^{(k)}}\right\}$
    Receive positioning data from neighbors: $\hat{\boldsymbol{x}}_n^{(k)}$ and $\mathrm{tr}\left(\boldsymbol{P}_n^{(k)}\right)$ $\forall n \in \mathcal{M}_m^{(k)}$
    Update neighbor set $\mathcal{N}_m^{(k)} = \left\{\mathcal{A}_m^{(k)}, \mathcal{M}_m^{(k)}\right\}$
    Estimate $\hat{\sigma}$ using (6.10) and (6.11)
    Apply neighbors selection as reported in Alg. 6.1 $\left[\boldsymbol{z}_{m,s}^{(k)}, \mathcal{N}_{m,s}^{(k)}, R_m^{(k+1)}\right] = \mathrm{NSA}\left(\boldsymbol{z}_m^{(k)}, \mathcal{N}_m^{(k)}, \hat{\boldsymbol{x}}_m^{(k|k-1)}, R_m^{(k)}\right)$
    Set $\boldsymbol{z}_m^{(k)} = \boldsymbol{z}_{m,s}^{(k)}$ and $\mathcal{N}_m^{(k)} = \mathcal{N}_{m,s}^{(k)}$
    Update covariance $\boldsymbol{R}_m^{(k)}$ according to (6.5)
    Update state $\hat{\boldsymbol{x}}_m^{(k)}$ and covariance matrix $\boldsymbol{P}_m^{(k)}$
    Calculate current $\hat{\sigma}_{m,\mathrm{curr}}^{(k)}$ using (6.9)
    Broadcast positioning data $\hat{\boldsymbol{x}}_m^{(k)}$ and $\mathrm{tr}\left(\boldsymbol{P}_m^{(k)}\right)$ to neighbors
  end
end

6.3.4 *Complexity Analysis*

As mentioned in Chapter 3.2.2, the complexity of EKF is mainly introduced by the matrix inversion and multiplication. Suppose that each mobile connects on average $\bar{N}$ neighbors and estimates its position in a D dimensional environment. For each state vector estimation, the asymptotic complexity of EKF is $\mathcal{O}(\bar{N}^3)$ (matrix inversion) or $\mathcal{O}(D^3)$ (matrix multiplication) [87]. Since the dimension of the state D is usually less than the average number of available measurements $\bar{N}$, the EKF has complexity $\mathcal{O}(\bar{N}^3)$.

The proposed CCT algorithm computes the CRLB (6.7), and the overall complexity is increased by $\mathcal{O}(D^3)$. Since $\mathcal{O}(D^3)$ is less than $\mathcal{O}(\bar{N}^3)$, the complexity of the CCT algorithm is still $\mathcal{O}(\bar{N}^3)$, which is similar to the standard EKF. In fact, CCT may use less range measurements to calculate matrix inversion, and the complexity would be reduced. Therefore, the proposed approach is in fact with low complexity and can be implemented in many cheap devices. However, the CCT algorithm requires more memory

to store the noise variance estimation and more network traffic to transmit positional information.

6.4 Simulation of Cognitive and Cooperative Tracking

Simulations have been carried out in a 2D environment of size 120 m × 70 m, where a cooperative network composed of 4 mobiles and 24 anchors is deployed (see Fig. 6.2). Four different trajectories are simulated, one for each mobile, and the position update rate is set to once per second. In particular, mobiles move along the x axis with constant speed equal to 1 m/s. By considering a connectivity radius of about 20 m, mobile M1 along its trajectory fully cooperates with M2 and M3, while partially cooperates with M4.

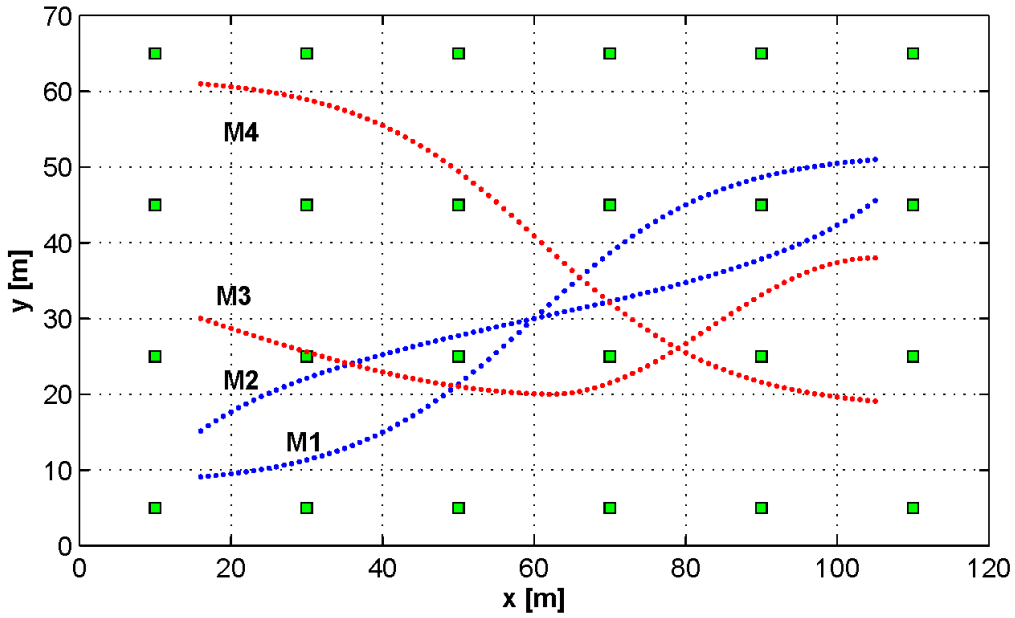

Figure 6.2: Simulated scenario of cognitive cooperative tracking.

The performance of the simulated algorithms are evaluated by means of MC simulations based on Matlab. In particular, the tracking performance is calculated as the positioning RMSE given in (3.17). In more details, there are 1000 MC trials, each of which consists of four paths with 90 positions to be estimated.

First of all, some simulation results have been carried out to test only the advantage of applying a cognitive tracking approach that tries to estimate the ranging error noise standard deviation by means of (6.10) and uses this knowledge into the EKF update equations. Note that for these preliminary simulations both cooperation among mobiles and connectivity radius adap-

tation scheme are not applied. In particular, Fig. 6.3 shows the performance of five tracking algorithms based onEKF as a function of the average value of a time-variant range noise standard deviation. Those results refer only to the tracking performance of mobile M1 which is localized without cooperation and without using any energy consumption approach. In fact, the connectivity radio is fixed for all of them to $R_f = 29$ m. The first algorithm is the *benchmark*, it is an EKF which perfectly knows the ranging noise standard deviation value along the time whose behavior is linear increasing as the one showed in showed in Fig. 6.4(a); the second one is the *proposed* cognitive approach that estimates the ranging noise standard deviation value and uses this estimation into the EKF update formulae; the remaining three algorithms are simple EKF that do not know the exact value of the range noise standard deviation and they use constant values equal to 1, 2 and 3 m, respectively, in the EKF update equations. As it can be observed from Fig. 6.3, the proposed cognitive approach is the only one whose performance gets closer to the benchmark one.

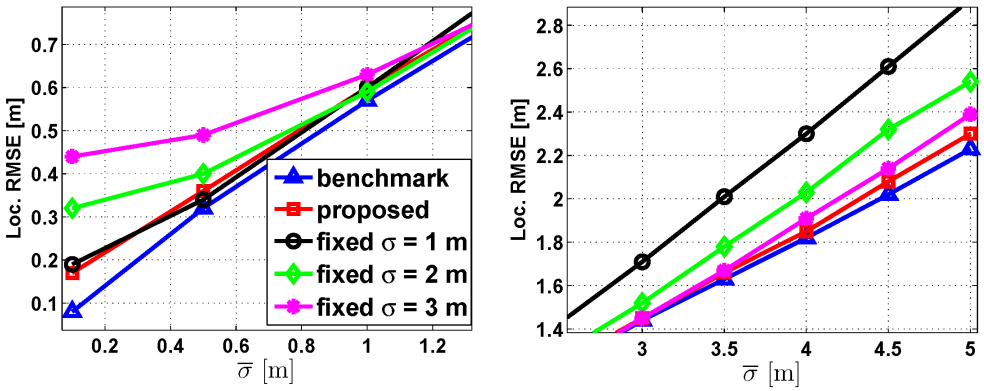

Figure 6.3: Comparison of cognitive approach with non cognitive ones.

Finally, in order to assess the performance of the complete CCT algorithm, four different tracking algorithms have been simulated for comparison purposes. The first one is a standard EKF that uses a fixed connectivity radius and a constant range noise standard deviation value in the update formulae (S-EKF); the second one is a cognitive tracking EKF that estimates the range noise standard deviation and uses the adaptive connectivity radius (CT); the third one is a cooperative EKF that uses a fixed connectivity radius and perfectly knows the range noise standard deviation (C-EKF); the last one is the proposed CCT algorithm, which includes adaptive connectivity radius scheme, range noise standard deviation estimation and mobile cooperation (CCT). Four different time-variant range noise standard deviation models are simulated, one for each mobile as showed in Fig. 6.4. The four standard deviation models are: linear for M1, segmented for M2, constant for M3 and sinusoidal for M4.

Based on this deployment, the minimum communication range R_{min} and range increment ΔR_c are set to 12 m and 2 m, respectively, for the CCT

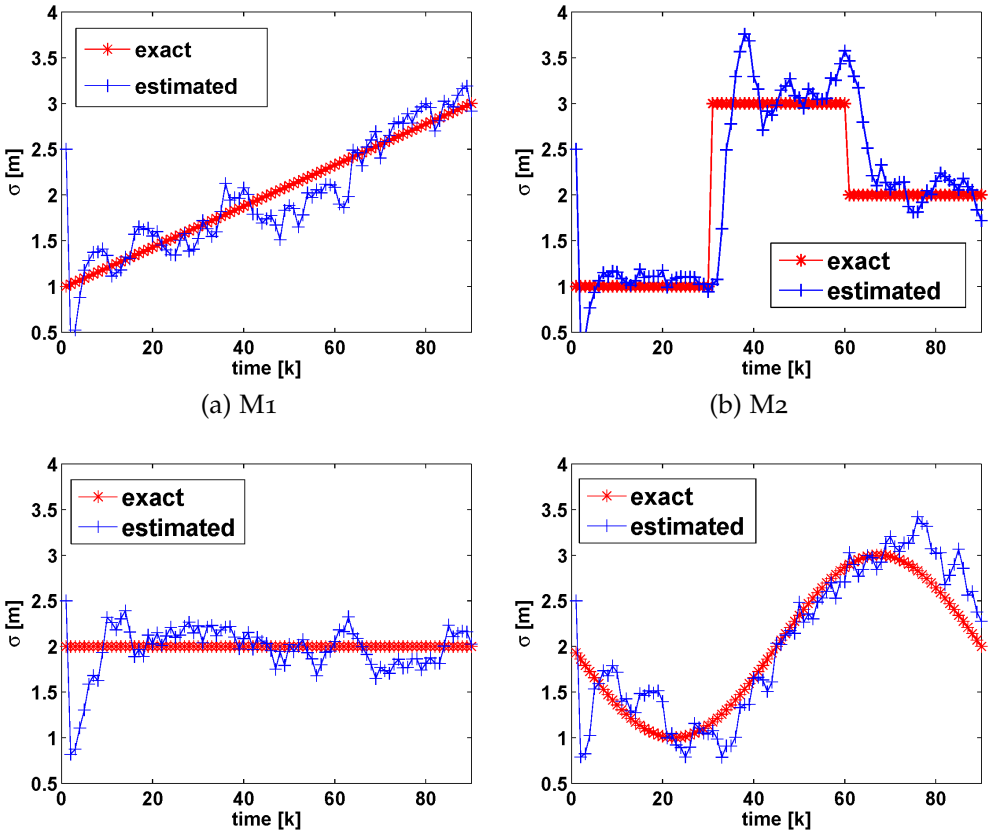

(a) M1 (b) M2

(c) M3 (d) M4

Figure 6.4: Range noise standard deviation estimation performed by each mobile in the CCT algorithm.

algorithm. The saved energy is calculated by using (6.8) with a path loss exponent equal to $\alpha = 2.5$. All the above mentioned algorithms have been tuned to achieve exactly the required positioning accuracy $P_a = 1$ m.

Tab. 6.1 shows the numerical performance in terms of transmission power reduction ($\Delta\overline{P}_t$) and Fig. 6.4 shows the range noise standard deviation tracking performed by the CCT algorithm. As it can be observed from Table 6.1, the proposed CCT algorithm uses the smallest connectivity radius. In fact, on average a mobile has 6.4 neighbors ($\overline{N}_{nei}$) during the localization process. As a result, the CCT saves more energy compared to other algorithms. Finally, from Fig. 6.4 it can be observed that every mobile is able to track the range noise standard deviation behavior along the time in the CCT algorithm. Therefore, the cognitive tracking is able to remarkably cut down transmission power and accurately perceive environment changing while keeping the same positioning performance.

6.5 SUMMARY

This section presented a novel cognitive and cooperative tracking algorithm based on EKF to track mobile nodes in wireless networks. The pro-

Table 6.1: Comparison of tracking algorithms in terms of energy consumption when the required accuracy P_a is 1 meter .

EKF	$\overline{R}$ [m]	$\overline{N}_{nei}$	$\overline{\sigma}_{err}$	$\Delta\overline{P}_t$ [dBm]
S-EKF	32.0	7.3	–	–
CT	24.9	5.2	0.22	2.7
C-EKF	24.0	5.7	–	3.1
CCT	21.7	6.4	0.22	4.2

posed algorithm selects the closest neighbors to save transmitting power, estimates measurement noise standard deviation to recognize environment and adopts cooperation among unknown mobile nodes to improve tracking accuracy. Though three more features are enabled, the CCT approach is a low-complexity tracking algorithm. Simulation results demonstrated that the proposed algorithm was able to meet the required accuracy P_a while optimizing the energy consumption.

7

POSITIONING WITH NLOS DETECTION

NLoS propagation of RF signal has proven to be challenging for the localization of unknown nodes in wireless networks. In particular, the NLoS range measurements can greatly affect the accuracy of mobile node's position and in turn may cause the position estimation error diverging. This section analyzes the CRLB of cooperative localization in presence of NLoS measurements and proposes a cooperative NLoS identification scheme as well as a cooperative positioning algorithm based on BP. The proposed algorithm is fully distributed and does not require prior NLoS state of range measurements. Simulation results show that the proposed algorithm is able to detect the state of each range measurement (NLoS or LoS) and improve positioning accuracy in several NLoS conditions

7.1 LOCALIZATION IN NLOS ENVIRONMENT

Localization based applications often require very accurate position estimation even in challenging environments (e.g., in indoor and industrial environments). One aspect that affects the accuracy of radio-based localization systems is NLoS propagation that makes range observations to be positively biased. In the literature, lots of approaches have been proposed to mitigate large errors caused by the NLoS links.In [95, 96, 97] , some algorithms have been adopted to identify whether a range measurement is in NLoS or LoS status based on channel statistics. In [98] and [99] the authors have proposed some NLoS mitigation algorithms in vehicular applications, but they did not take into account cooperation among unknown mobile nodes. In [100] and [101], cooperation among unknown nodes is exploited, but they required to know the exact status of NLoS links, which might be unrealistic.

Since the number of wireless devices is constantly increasing, cooperative localization can improve both positioning accuracy and availability are improved. One important aspect of cooperative localization is how to appropriately take into account the uncertainty of unknown nodes' positions. This task has been already investigated mostly in LoS condition [60], where ranging errors are relatively small and corresponding uncertainty can be well modeled. However, in NLoS conditions, ranging errors are much larger and more irregular, thus cooperative localization processes may diverge if the NLoS state associated to range measurements are not identified.

This paper focuses on cooperative localization in NLoS scenarios and it adopts a cooperative approach based on a modified version of the BP al-

gorithm [60, 100]. The proposed algorithm estimates mobile positions and the status of range measurements in parallel. Moreover, it analyzes the positioning bounds in NLoS environment and uses it to check the result of position estimates and NLoS identification. Furthermore, the knowledge of the observation state, which indicates if a range measurement is performed in NLoS or LoS condition, can be also used to properly select neighboring nodes and optimize the energy consumption as in [89].

7.2 MEASUREMENTS MODELS

Concerning range measurement models, in this work the models presented in [100] have been adopted as they are extracted from experimental measurements by using UWB modules [97].

7.2.1 *LoS Measurement Model*

Range measurements in LoS condition are assumed as Gaussian distributed:

$$\tilde{d} = d + \upsilon_{los}, \tag{7.1}$$

where d is the exact distance between the two nodes involved in the measurement, and υ_{los} is a Gaussian distributed noise, $\upsilon_{los} \sim \mathcal{N}(0, \sigma^2)$, with zero mean and standard deviation $\sigma = 0.25$ m.

7.2.2 *NLoS Measurement Model*

Range measurements in NLoS condition are supposed as the exact distance plus an additional exponential noise (7.2). It is widely used to model the range measure in NLoS condition and the always positive noise models the effect of obstacle penetration.

$$\tilde{d} = d + \upsilon_{nlos}, \tag{7.2}$$

where υ_{nlos} is the measurement noise supposed to be exponentially distributed, $p_{\upsilon_{nlos}}(x) = \lambda \exp(-\lambda x)$ when $x \geqslant 0$, with rate parameter $\lambda = 0.38$ m^{-1}.

7.2.3 *State Definition*

A generic range measurement can be performed either in LoS condition with probability $P(0)$ or in NLoS condition with probability $P(1)$ such that $P(0) + P(1) = 1$ (Only two states of measurements are considered in this paper but it can be extended to many states).

Let $s_{n\to m}$ be the state associated to the range measurement $\tilde{d}_{n\to m}$ from neighbor n to mobile m. The state $s_{n\to m}$ can be assumed as either 0 if the

corresponding range measurement is performed in LoS condition or 1 in NLoS condition. As a consequence, $P(s_{n\to m}=0)+P(s_{n\to m}=1)=1$.

Based on the above definitions and assuming that the states associated to range measurements are not previously known, the likelihood function of the range measurement could be simply expressed as the weighted sum on the state:

$$p(\tilde{d}_{n\to m}|\boldsymbol{x}_m,\boldsymbol{x}_n)=\sum_{i=0}^{1}P(s_{n\to m}=i)\,p(\tilde{d}_{n\to m}|\boldsymbol{x}_m,\boldsymbol{x}_n,s_{n\to m}), \tag{7.3}$$

where $\boldsymbol{x}_m=[x_m,y_m]$ is the position of the mobile m and $\boldsymbol{x}_n=[x_n,y_n]$ the position of the neighbor n. Note that the likelihood function could be either a normal distribution or an exponential one depending on the link condition:

$$p(\tilde{d}_{n\to m}|\boldsymbol{x}_m,\boldsymbol{x}_n,s_{n\to m})=\begin{cases}\frac{1}{\sqrt{2\pi\sigma^2}}\exp\left(-\frac{(\tilde{d}_{n\to m}-\|\boldsymbol{x}_n-\boldsymbol{x}_m\|)^2}{2\sigma^2}\right), & s_{n\to m}=0\\ \lambda\exp\left(-\lambda\left(\tilde{d}_{n\to m}-\|\boldsymbol{x}_n-\boldsymbol{x}_m\|\right)\right), & s_{n\to m}=1\end{cases}. \tag{7.4}$$

where $\|\cdot\|$ denotes the Euclidean distance.

Suppose there are N range measurements available for node m, the possible permutations could be 2^N, which could be so large when mobile m hears from many neighbors that it is not able to implement the exhaustive approach for real time positioning.

Some NLoS identification techniques presented in literature are based on the processing of the received signal [96, 97], but they are too complex and not feasible to be implemented on cheap devices. Since range measurements are correlated with the position of the mobile m, it would be efficient to proceed in parallel both mobile position estimate and NLoS identification for all the involved range measurements as presented in sec. 7.4.

7.3 CRLB FOR COOPERATIVE POSITIONING WITH NLOS MEASURES

The CRLB expresses a lower bound on the variance of any unbiased estimator. In localization, this information can be used to know which is the maximum achievable positioning accuracy in a given scenario. Also it can be used during on-line estimation process to select the closest set of neighbors that are able to meet the required positioning accuracy while energy for ranging is minimized [89]. In fact, following this approach, the transmission power is adaptively adjusted to reach the selected neighbors.

In cooperative localization, the available set of range measurements can be written as:

$$\boldsymbol{Z}=\left\{\left\{\left\{\tilde{d}_{a\to m}\right\}_{a\in\mathcal{A}_m},\left\{\tilde{d}_{n\to m}\right\}_{n\in\mathcal{M}_m}\right\}_{m\in\mathcal{M}}\right\}. \tag{7.5}$$

Let $\mathcal{A}$ and $\mathcal{M}$ denote the full set of anchors and mobiles, respectively, in the network. In (6.2), $\mathcal{A}_m \subseteq \mathcal{A}$ and $\mathcal{M}_m \subset \mathcal{M}$ are the set of anchors and mobiles, respectively, connected to m. The corresponding log-likelihood function is given by:

$$\begin{aligned}\log\left(p\left(\boldsymbol{Z}|\boldsymbol{X}\right)\right) \;=\; & \sum_{m\in\mathcal{M}}\sum_{a\in\mathcal{A}_m} \log\, p(\tilde{d}_{a\to m}|\boldsymbol{x}_m,\boldsymbol{x}_a) + \\ & \sum_{m\in\mathcal{M}}\sum_{n\in\mathcal{M}_m} \log\, p(\tilde{d}_{n\to m}|\boldsymbol{x}_m,\boldsymbol{x}_n),\end{aligned} \tag{7.6}$$

where $\boldsymbol{X}$ is the set of mobiles' positions, that is, $\boldsymbol{X} = [\boldsymbol{x}_1, \boldsymbol{x}_2, \ldots, \boldsymbol{x}_M]$, where M is the cardinality of $\mathcal{M}$.

The CRLB is obtained by inverting the Fisher Information Matrix (FIM) that is given by the negative expectation of the second-order derivatives of the log-likelihood function:

$$\boldsymbol{F} = -\mathbb{E}\left[\frac{\partial^2}{\partial \boldsymbol{X}^2}\log\, p(\boldsymbol{Z}|\boldsymbol{X})\right]. \tag{7.7}$$

From (7.6) and (7.7), the global FIM can be decomposed as the sum of two matrices: the first one takes into account links between mobiles and anchors while the second one considers links among mobiles (see [94] for more details)

$$\boldsymbol{F} = \boldsymbol{F}^{\text{anch}} + \boldsymbol{F}^{\text{mob}}. \tag{7.8}$$

In particular, $\boldsymbol{F}^{\text{anch}}$ is a block diagonal matrix whose corresponding values depend on the anchor measurements, (7.9). On the contrary, $\boldsymbol{F}^{\text{mob}}$ is not a block diagonal matrix as it depends on the partial derivatives among mobiles, (7.10).

$$\boldsymbol{F}^{\text{anch}} = \begin{bmatrix} \boldsymbol{F}_1^{\text{anch}} & & & \\ & \boldsymbol{F}_2^{\text{anch}} & & \\ & & \ddots & \\ & & & \boldsymbol{F}_M^{\text{anch}} \end{bmatrix}, \tag{7.9}$$

$$\boldsymbol{F}^{\text{mob}} = \begin{bmatrix} \boldsymbol{F}_1^{\text{mob}} & \boldsymbol{K}_{12} & \ldots & \boldsymbol{K}_{1M} \\ \boldsymbol{K}_{21} & \boldsymbol{F}_2^{\text{mob}} & \ldots & \boldsymbol{K}_{2M} \\ \vdots & \vdots & \ddots & \vdots \\ \boldsymbol{K}_{M1} & \boldsymbol{K}_{M2} & \ldots & \boldsymbol{F}_M^{\text{mob}} \end{bmatrix}, \tag{7.10}$$

where $\boldsymbol{K}_{mn}$ is a zero matrix if there is no measurement between n and m.

Considering the fact the a generic range measurement from mobile m to an anchor a can be performed either in LoS or NLoS condition, the set of anchors connected to the mobile m, $\mathcal{A}_m$, can be subdivided into two

subsets: LoS subset denoted with $\mathcal{A}_m^{los}$ and NLoS subset denoted with $\mathcal{A}_m^{nlos}$. Therefore, the matrix $\boldsymbol{F}_m^{anch}$ can be expressed as the sum of two matrices that take into account to the above defined subsets:

$$\boldsymbol{F}_m^{anch} = \boldsymbol{F}_m^{anch\_los} + \boldsymbol{F}_m^{anch\_nlos}, \tag{7.11}$$

where $\boldsymbol{F}_m^{anch\_los}$ and $\boldsymbol{F}_m^{anch\_los}$ are given by:

$$\boldsymbol{F}_m^{anch\_los} = \sum_{a \in \mathcal{A}_m^{los}} \frac{1}{\sigma^2 d_{am}^2} \begin{bmatrix} \Delta x_{am}^2 & \Delta x_{am}\Delta y_{am} \\ \Delta y_{am}\Delta x_{am} & \Delta y_{am}^2 \end{bmatrix}, \tag{7.12}$$

$$\boldsymbol{F}_m^{anch\_nlos} = \sum_{a \in \mathcal{A}_m^{nlos}} \frac{\lambda}{d_{am}^3} \begin{bmatrix} -\Delta y_{am}^2 & \Delta x_{am}\Delta y_{am} \\ \Delta y_{am}\Delta x_{am} & -\Delta x_{am}^2 \end{bmatrix}, \tag{7.13}$$

where Δx_{am} and Δy_{am} are the differences of x and y components, respectively, between nodes a and m, i.e., $\Delta x_{am} = x_a - x_m$, $\Delta y_{am} = y_a - y_m$, while d_{am} is the Euclidean distance defined as before.

Note that (7.12) is obtained by second-order differentiating of Gaussian distribution and σ is the noise standard deviation. (7.13) is the second-order derivative of exponential distribution and λ is the rate parameter. In (7.13) there is negative sign for the diagonal elements, which means that NLoS measurements decrease the Fisher information and have negative effects on the positioning performance.

Following the same approach, the matrix $\boldsymbol{F}_m^{mob}$ that takes into account the connection among mobiles is given by:

$$\boldsymbol{F}_m^{mob} = \boldsymbol{F}_m^{mob\_los} + \boldsymbol{F}_m^{mob\_nlos}, \tag{7.14}$$

$$\boldsymbol{F}_m^{mob\_los} = \sum_{n \in \mathcal{M}_m^{los}} \frac{1}{\sigma^2 d_{nm}^2} \begin{bmatrix} \Delta x_{nm}^2 & \Delta x_{nm}\Delta y_{nm} \\ \Delta y_{nm}\Delta x_{nm} & \Delta y_{nm}^2 \end{bmatrix}, \tag{7.15}$$

$$\boldsymbol{F}_m^{mob\_nlos} = \sum_{n \in \mathcal{M}_m^{nlos}} \frac{\lambda}{d_{nm}^3} \begin{bmatrix} -\Delta y_{nm}^2 & \Delta x_{nm}\Delta y_{nm} \\ \Delta y_{nm}\Delta x_{nm} & -\Delta x_{nm}^2 \end{bmatrix}. \tag{7.16}$$

Concerning the correlation block $\boldsymbol{K}_{mn}$, if there is measurement from node n and m, it could be calculated as:

$$\boldsymbol{K}_{mn} = -\frac{1}{\sigma^2 d_{nm}^2} \begin{bmatrix} \Delta x_{nm}^2 & \Delta x_{nm}\Delta y_{nm} \\ \Delta y_{nm}\Delta x_{nm} & \Delta y_{nm}^2 \end{bmatrix}, s_{n\to m} = 0$$

$$\boldsymbol{K}_{mn} = -\frac{\lambda}{d_{nm}^3} \begin{bmatrix} -\Delta y_{nm}^2 & \Delta x_{nm}\Delta y_{nm} \\ \Delta y_{nm}\Delta x_{nm} & -\Delta x_{nm}^2 \end{bmatrix}, s_{n\to m} = 1$$

Let $\boldsymbol{J}$ be the inverse matrix of FIM and $\boldsymbol{J}_m$ be the 2×2 block related to the mobile m, then the CRLB for mobile m can be calculated as:

$$\Omega_m \triangleq \sqrt{\boldsymbol{J}_m(1,1) + \boldsymbol{J}_m(2,2)}. \tag{7.17}$$

As it can be observed from (7.13) and (7.16), the presence of NLoS measurements makes the Fisher information decreasing, as a consequence the variance on the position error increases. In fact, the more severe the NLoS condition the larger localization error. This effect can be shown in the simulation results.

7.4 MESSAGE PASSING ALGORITHM

Since there is no prior information about the state of each range measurement, the basic idea would be to use range measurements to infer first the mobile's position, then the state of range measurements. Alternatively, in order to improve positioning accuracy, both mobile's positions and links' states can be estimated in parallel through some iterations of the BP algorithm. However, this approach has some drawbacks. One is the network traffic generated by the cooperation packets (note that the size of messages depends on the number of particles used to approximate the distributions). Another drawback is the computational effort required to calculate the integral of neighbor's belief. The proposed algorithm assumes that the belief of mobile's position is Gaussian distributed, thus the mobile just needs to send to its neighbors the estimated position and the corresponding uncertainty. This approach known as Expectation Propagation (EP) is an approximation of the BP algorithm [102]. Based on this assumption, we propose a NLoS identification and positioning algorithm, namely cooperative NLoS identification and positioning (C-NLoS-IP) algorithm. In the following sections, the message passing for a generic mobile m are introduced.

7.4.1 *Incoming Messages*

The localization approach is realized by factor graph as Fig. 7.1. In particular, the joint posteriori distribution can be factorized by messages from anchor nodes and mobile neighbors as follows.

7.4.1.1 *Message from Anchors*

The incoming message from an anchor $a \in \mathcal{A}_m$ is proportional to the integral of the multiplication between the likelihood function and the belief of the anchor that is a Dirac delta function centered on $\boldsymbol{x}_a$, i.e., $b(\boldsymbol{x}_a) = \delta(\boldsymbol{x} - \boldsymbol{x}_a)$:

$$\begin{aligned} \mu_{a\to m} &\propto \int p(\tilde{d}_{a\to m}|\boldsymbol{x}_m, \boldsymbol{x}_a) b(\boldsymbol{x}_a) d\boldsymbol{x}_a \\ &= p(\tilde{d}_{a\to m}|\boldsymbol{x}_m, \boldsymbol{x}_a). \end{aligned} \tag{7.18}$$

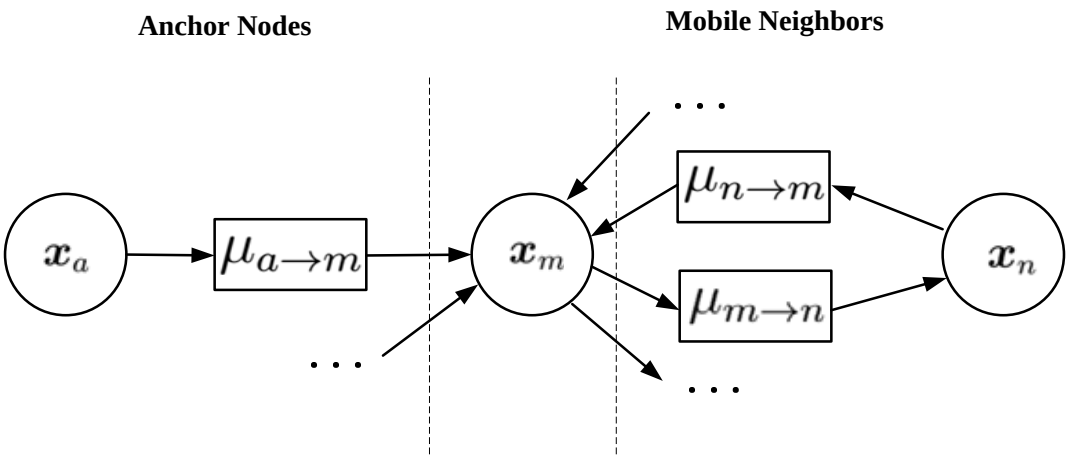

Figure 7.1: Factor graph for cooperative positioning.

When referring to more than one state, the likelihood function can be calculated by using (7.3), thus $p(\tilde{d}_a|\boldsymbol{x}_m, \boldsymbol{x}_a)$ becomes:

$$p(\tilde{d}_{a\to m}|\boldsymbol{x}_m, \boldsymbol{x}_a) = \sum_{i=0}^{1} P\left(s_{a\to m} = i\right) p(\tilde{d}_{a\to m}|\boldsymbol{x}_m, \boldsymbol{x}_a, s_{a\to m}), \tag{7.19}$$

where $P_a\left(s_j\right)$ and $p(\tilde{r}_{a\to m}|\boldsymbol{x}_m, \boldsymbol{x}_a, s_j)$ denote the probability and the likelihood of the observation model, respectively. Same as before, s_0 means LoS model and s_1 means NLoS model. And the likelihood functions are defined in (7.4).

7.4.1.2 *Message from Mobile Neighbor*

Similarly, the incoming message from a mobile neighbor can be expressed as:

$$\mu_{n\to m} \propto \int p(\tilde{d}_{n\to m}|\boldsymbol{x}_m, \boldsymbol{x}_n) b(\boldsymbol{x}_n) d\boldsymbol{x}_n. \tag{7.20}$$

Since the mobile neighbor's position x_n has a certain uncertainty, the belief $b(\boldsymbol{x}_n)$ is not a Dirac delta function. In principle, it can be represented by the distribution of the samples. Thus, the calculation in (7.20) is too complex to be performed. In order to simplify that calculation, some approaches, presented in [100], assume that $b(\boldsymbol{x}_n)$ is a Gaussian function. In this paper, to further reduce the complexity, the belief of the mobile neighbor n is approximated as a Dirac delta function (i.e., as if it is an anchor, $b(\boldsymbol{x}_n) \approx \delta(\boldsymbol{x} - \hat{\boldsymbol{x}}_n)$). To compensate this important approximation, the position uncertainty associated to neighbor n is considered as an additional noise for the range measurement $\tilde{d}_{n\to m}$. More specifically, the variance associated to ranging (given by σ^2 for LoS measurements and $1/\lambda^2$ for NLoS measurements) are increased by the position uncertainty of the mobile's neighbor. For simplicity, this uncertainty is calculated as the trace of the

estimated covariance matrix [62], i.e., $\mathrm{tr}(\boldsymbol{P}_n)$. As a consequence, the new parameters σ_{nm} and λ_{nm} to be used in the likelihood function are given by (7.21) and (7.22), respectively.

$$\sigma_{nm} = \sqrt{\sigma^2 + \mathrm{trace}(\boldsymbol{P}_n)}, \tag{7.21}$$

$$\lambda_{nm} = \frac{\lambda}{\sqrt{1 + \lambda^2 \mathrm{trace}(\boldsymbol{P}_n)}}. \tag{7.22}$$

In conclusion, by using the above approximation, the incoming message is given by:

$$\mu_{n\to m} \propto p(\tilde{d}_{n\to m} | \boldsymbol{x}_m, \hat{\boldsymbol{x}}_n), \tag{7.23}$$

where $p(\tilde{d}_{n\to m} | \boldsymbol{x}_m, \hat{\boldsymbol{x}}_n)$ is the likelihood function evaluated by using the new modified parameters σ_{nm} and λ_{nm} that take into account the uncertainty of mobile neighbor n.

7.4.2 *Position Estimate*

When all the messages from the anchors and mobile's neighbors are available, the mobile node can calculate its belief $b(\boldsymbol{x}_m)$ that is proportional to the factorization all the incoming messages and the *a priori* pdf $p(\boldsymbol{x}_m)$:

$$b(\boldsymbol{x}_m) \propto p(\boldsymbol{x}_m) \prod_{a \in \mathcal{A}_m} \mu_{a\to m}(\boldsymbol{x}_m) \times \prod_{n \in \mathcal{M}_m} \mu_{n\to m}(\boldsymbol{x}_m), \tag{7.24}$$

where $\mu_{a\to m}(\boldsymbol{x}_m)$ and $\mu_{n\to m}(\boldsymbol{x}_m)$ are calculated by using (7.18) and (7.20), respectively. After that, the estimated position is calculated as the average value of the belief distribution while the estimated covariance matrix $\boldsymbol{P}_m$ calculated by using the set of particles as reported in [62]. Therefore, the belief is approximated with a Gaussian distribution and the related parameters, i.e., the mean value and the trace of $\boldsymbol{P}_m$, are broadcast to its neighbors.

7.4.3 *Outgoing Messages*

The outgoing message is simply proportional to the belief dividing the incoming message from a specific factor node.

7.4.3.1 *Messages to Anchor*

The message from mobile to an anchor node is

$$\mu_{m\to a}(\boldsymbol{x}_m) \propto \frac{b(\boldsymbol{x}_m)}{\mu_{a\to m}(\boldsymbol{x}_m)}. \tag{7.25}$$

The state probability is defined as the integration of multiplication of likelihood and message from the mobile:

$$P(s_{a\to m}) = \int p\left(\tilde{d}_{a\to m} | \boldsymbol{x}_m, \boldsymbol{x}_a, s_{a\to m}\right) \mu_{m\to a}(\boldsymbol{x}_m)\, d\boldsymbol{x}_m. \tag{7.26}$$

By applying the assumption that $b(\boldsymbol{x}_m)$ is a delta function, the previous equation can be simplified as:

$$P(s_{a\to m}) \approx \frac{p\left(\tilde{d}_{a\to m}|\hat{\boldsymbol{x}}_m, \boldsymbol{x}_a, s_{a\to m}\right)}{\mu_{a\to m}(\hat{\boldsymbol{x}}_m)}. \tag{7.27}$$

Since the probability of one range measurement should be normalized, the LoS or NLoS probability can be furthermore simplified as

$$\begin{aligned} P(s_{a\to m}) &= \frac{P(s_{a\to m})}{\sum_{i=0}^{1} P(s_{a\to m}=i)} \\ &= \frac{p\left(\tilde{d}_{a\to m}|\hat{\boldsymbol{x}}_m, \boldsymbol{x}_a, s_{a\to m}\right)}{\sum_{i=0}^{1} p\left(\tilde{d}_{a\to m}|\hat{\boldsymbol{x}}_m, \boldsymbol{x}_a, s_{a\to m}=i\right)}. \end{aligned} \tag{7.28}$$

Based on previous assumption, the message coming from mobile is not necessary to decide the range measurement state. In fact, only the estimated position and the corresponding trace are necessary to compute the probability of NLoS.

7.4.3.2 *Messages to Mobile*

The outgoing message to mobile $\mu_{m\to n}$ is the similar to the one to anchor, but it can be canceled out when calculating the NLoS state. Therefore, it is not calculated in the implementation of the algorithm. Similarly, the LoS or NLoS probability is given by

$$P(s_{n\to m}) = \frac{p\left(\tilde{d}_{n\to m}|\hat{\boldsymbol{x}}_m, \hat{\boldsymbol{x}}_n, s_{n\to m}\right)}{\sum_{i=0}^{1} p\left(\tilde{d}_{n\to m}|\hat{\boldsymbol{x}}_m, \hat{\boldsymbol{x}}_n, s_{n\to m}=i\right)}. \tag{7.29}$$

Finally, hard decision is made when the algorithm converges. For a given range measurement, if $P(s_{n\to m})$ is larger than 0.5, it is assumed in NLoS state, otherwise it is in LoS state. The designed C-NLoS-IP algorithm is shown as pseudo-code in Alg. 7.1

The fact that the belief of mobile's position is approximated with a Dirac delta function may result in inaccurate position estimate in NLoS state condition. However, the computational complexity and network traffic can be greatly reduced, making the proposed algorithm suitable for distributed localization and feasible to be implemented in mobile devices with low computational capability.

7.5 Simulation of NLoS Detection Algorithm

The performance of the proposed C-NLoS-IP algorithm has been tested by MC simulations. The simulated scenario is typical office environment with size 20×20 meters and the wireless network is a small-scale network composed of 15 nodes (see Fig. 7.2). Blue squares are anchor nodes and are fixed. Red dots are unknown nodes and are randomly generated for each

Algorithm 7.1: Cooperative NLoS Identification and Positioning

input : Measurement vector $\boldsymbol{Z}$ (7.5)
output: Position estimate $\hat{\boldsymbol{x}}_m$, measurement state LoS or NLoS $\forall m$

repeat
  for *node* $m \in \mathcal{M}$ ***in parallel*** **do**
    Receive position estimate $\hat{\boldsymbol{x}}_n$ and $\mathrm{tr}(\boldsymbol{P}_n)$ from all neighbors $n \in \mathcal{M}_m^{(k)}$
    Compute messages from anchors $\mu_{a\to m}$ as (7.18) $\forall a \in \mathcal{A}_m$
    Compute messages from mobile neighbors $\mu_{n\to m}$ as (7.20) $\forall n \in \mathcal{M}_m$
    Estimate mobile positions $\hat{\boldsymbol{x}}_m$ and covariance $\boldsymbol{P}_m$
    Communicate $\hat{\boldsymbol{x}}_m$ and $\mathrm{tr}(\boldsymbol{P}_m)$ to neighbors
    Calculate measurement state probability of anchors (7.28) $\forall a \in \mathcal{A}_m$
    Calculate measurement state probability of mobiles (7.29) $\forall n \in \mathcal{M}_m$
  end
until *converge*
for *node* $m \in \mathcal{M}$ ***hard decision*** **do**
  for $a \in \mathcal{A}_m$ **do**
    if $P(s_{a\to m} = 1) > 0.5$ **then**
      $\tilde{d}_{a\to m}$ is in NLoS state
    else
      $\tilde{d}_{a\to m}$ is in LoS state
    end
  end
  for $n \in \mathcal{M}_m$ **do**
    if $P(s_{n\to m} = 1) > 0.5$ **then**
      $\tilde{d}_{n\to m}$ is in NLoS state
    else
      $\tilde{d}_{n\to m}$ is in LoS state
    end
  end
end

run. Five of them are anchors deployed at the four corners and in the center of environment in order to provide a good geometry for localization . The remaining ten nodes are static unknown nodes whose positions are randomly selected in each run of the simulation. The radio connectivity is chosen as 20 meters. Since NLoS condition is generated by obstacles, symmetric links are considered between unknown nodes, e.g., if $\tilde{r}_{n\to m}$ is in NLoS state then $\tilde{d}_{m\to n}$ is also in NLoS state, but the two range measurements are not the same due to the different measurement errors.

Three positioning algorithms have been tested and then compared. The first one is sum-product algorithm over a wireless network (SPAWN) proposed in [60], and it is a generic belief propagation algorithm for localization. It is supposed to have no knowledge of NLoS states, denoted as

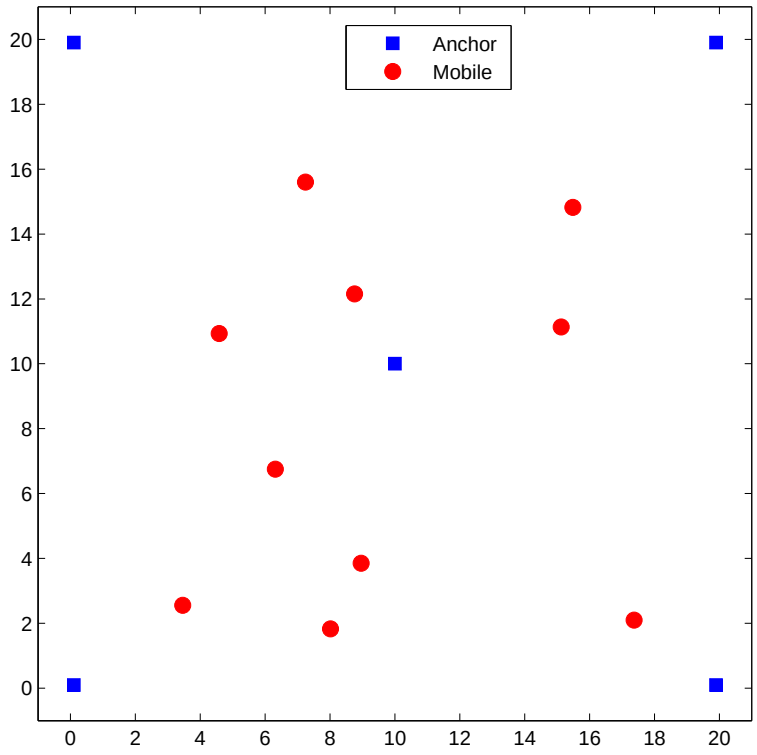

Figure 7.2: Simulation environment for NLoS positioning.

SPAWN-NLoS-U. The second one is SPAWN proposed in [100], which supposed to perfectly know the NLoS states, denoted as SPAWN-NLoS-K. The last one is the proposed C-NLoS-IP algorithm. 1000 MC runs have been performed for a chosen NLoS probability, and the RMSE have been calculated for performance comparison.

Fig. 7.3 shows the positioning performance of the above mentioned algorithms and the corresponding CRLB. As it can be observed, the presence of NLoS conditions greatly degrade the positioning performance, increasing the positioning errors. If this is not well aware of, the standard belief propagation algorithm could diverge. The proposed C-NLoS-IP algorithm is about 0.5 meter worse than SPAWN-NLoS-K, but it does not require to know whether a range measurement is in LoS or NLoS condition. Furthermore, the estimated CRLB, which uses the estimated positions and estimated NLoS status, can bound the positioning errors well. Hence this bound can be used to provide some insights to positioning accuracy and can be used in the energy-efficient positioning algorithm as [89].

The performance of NLoS identification is presented in Fig. 7.4 and Fig. 7.5. In particular, Fig. 7.4 shows the detection error rate for each range measurement and Fig. 7.5 shows the estimated NLoS probability of all the measurements. The identification performance of measurements from anchors and mobile neighbors shows similar behavior. The error rate is high-

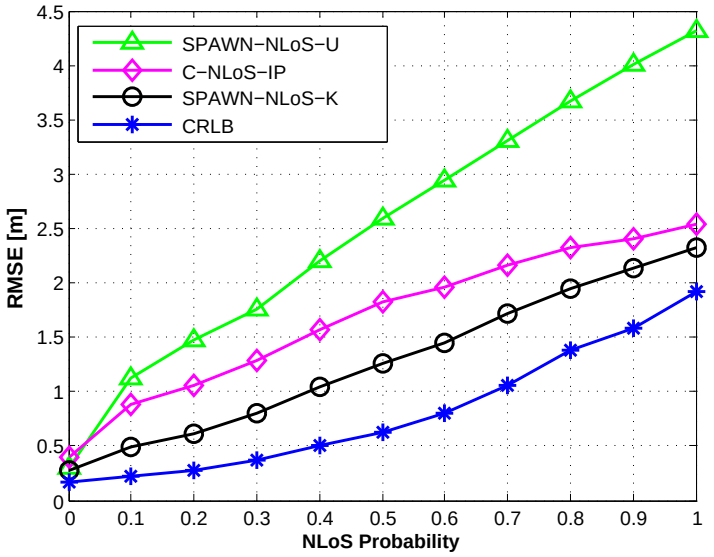

Figure 7.3: Positioning performance.

est when NLoS probability is around 0.6, which indicates that the proposed algorithm has high miss detection rate when NLoS and LoS is equally distributed. At low NLoS probability, the detection performance of mobile measurements is slightly better than that of anchor measurements, due to the simulation condition of symmetric links. At high NLoS probability, the detection performance of anchor measurements is better, because of the increased uncertainty of neighbors' positions caused by the bad NLoS range measurements.

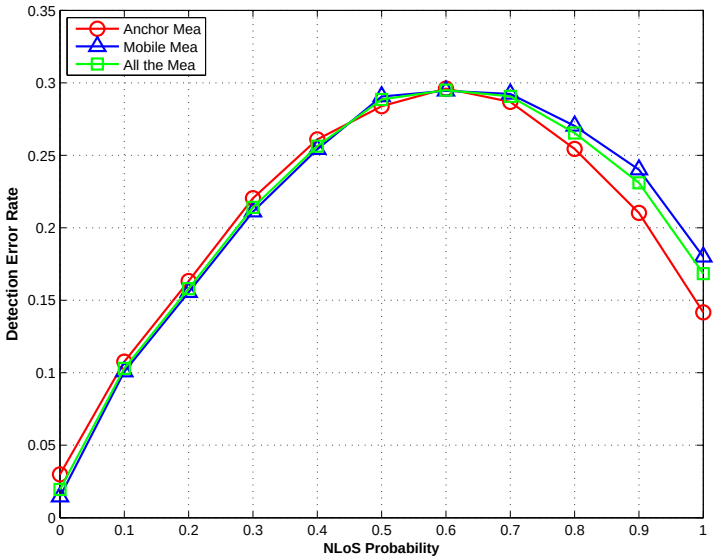

Figure 7.4: State detection error rate.

As it can be observed from Fig. 7.5, the estimated NLoS probability is close to real probability. When NLoS probability is smaller than 0.6, the proposed algorithm overestimates the NLoS probability; while the probability

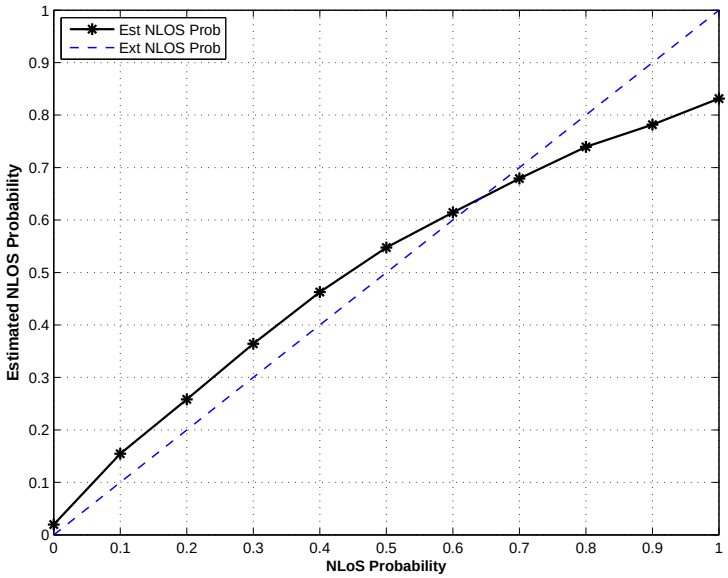

Figure 7.5: NLoS probability estimate.

is larger than 0.6, the algorithm underestimate the NLoS probability. That is because the detection is based on position estimates. If there are enough LoS range measurements, the range measurements with large errors will be identified as NLoS; but if there are not enough LoS range measurements, the range measurements with small errors will be identified as LoS. When NLoS probability goes up to 0.8, the detection errors become larger, which means the LoS range measurements are not enough to localize the nodes. In full NLoS conditions, the error on probability detection is around 0.17. The reason is that the range error may not be large even in NLoS condition, e.g., the probability of NLoS ranging error less than 0.5 meter is about 0.17, which coincides estimated probability error in full NLoS condition.

7.6 SUMMARY

This section analyzed the CRLB of cooperative localization in presence of NLoS range measurements and proposed a cooperative NLoS identification and positioning algorithm. The proposed algorithm was fully distributed with low complexity and low network traffic and did not require prior information of NLoS state. Simulation results showed that the proposed algorithm was able to detect NLoS range measurements and to improve positioning accuracy in the NLoS conditions.

Part IV

FINAL REMARKS

8

CONCLUSIONS AND FUTURE WORK

In this thesis, some hybrid and cooperative solutions have been proposed to locate the users in wireless networks. The proposed solutions adopt SoO approach, and fuse information from nearby anchors and mobiles, which may use different RF technologies. In particular, RFID technology is employed to enhance the WSN-based positioning system for indoor environments. Terrestrial ranging techniques (e.g., UWB) are used to assist the GNSS localization in challenging environments like urban canyon and indoors. The obtained results give some insights into the potential of implementing hybrid and cooperative methodology to provide LBS in GNSS-challenged environments. The problem of hybridization of different RF technologies for network localization has been addressed by using conventional Bayesian positioning approaches, like EKF and PF.

More specifically, a novel mathematical model was developed to model RFID proximity as distance measurement, and integrated with RSSI measurements from WSN anchors and mobile neighbors. A novel scheme was designed to model the uncertainties of RSSI measurements form mobile neighbors, causing by the uncertainties of mobiles' positions. The resulting positioning algorithms combines RSSI from WSNneighbors and proximity information from RFID readers, and provides the *a posteriori* estimate of mobile nodes' position in a wireless network. The designed hybrid algorithms were verified by computer simulation and a prototype of hybrid WSN-RFID positioning system. These results demonstrated that the joint use of both WSN and RFID could overcome the drawback of RSSI ranging and enhance the WSN-based localization system.

Moreover, some recent hybrid cooperative GNSS-terrestrial positioning algorithms were analyzed and adopted for urban navigation. The simulation results showed that the hybrid cooperative positioning approach can track the movement of vehicles in urban canyons even without fixed terrestrial infrastructure. A hybrid GPS-UWB measurement campaign was carried out to test the real performance of the hybrid positioning algorithms. The derived results showed that the hybrid usage of GPS and UWB could provide seamless indoor and outdoor navigation.

Besides, some advanced positioning algorithms were studied for the indoor applications. A CCT approach was proposed to provide the desirable positioning accuracy and reduce the energy consumption for positioning. This approach adaptively adjusts the transmission power, adopts self learning to recognize the environment changes and exploits cooperation among

unknown nodes to further improve the positioning power consumption. Then the CRLB of cooperative localization in presence of NLoS measurements was analyzed and a cooperative NLoS detection and positioning algorithm was proposed based on the well-known BP.

Since indoor environments are extremely harsh for RF signal propagation, further realistic simulations could be included to test and possibly improve the proposed algorithms. When the more devices become available, a large wireless network could be set up to verify the simulated performance and move the proposed solutions to real implementation. In addition, an energy-efficient positioning algorithm in NLoS environment would be necessary for indoor applications, which could be developed based on the derived CRLB formulae in Chapter 7 as [89].

BIBLIOGRAPHY

[1] Z. Xiong, Z. Song, A. Scalera, E. Ferrera, F. Sottile, P. Brizzi, R. Tomasi, and M.A. Spirito "Hybrid WSN and RFID indoor positioning and tracking system," in *EURASIP Journal on Embedded Systems*, 2013:6

[2] F. Sottile, Z. Xiong, C. Pastrone "Analysis of Real-Time Hybrid-Cooperative GNSS-Terrestrial Positioning Algorithms," to appear in *Advancing Embedded Systems and Real-Time Communications with Emerging Technologies*, IGI Global, 2014.

[3] Z. Xiong, M. Dai, F. Sottile, M.A. Spirito and R. Garello, "A Cognitive and Cooperative Tracking Approach in Wireless Networks," in *Proceedings of IEEE International Conference on Communications (ICC)*, Budapest, Hungary, June 9–13, 2013, pp. 1310–1314.

[4] Z. Xiong, F. Sottile, M.A. Spirito and R. Garello, "Analysis of Hybrid and Cooperative Positioning Algorithms in Urban Canyon Scenarios," in *Proceedings of International Conference on Localization and GNSS (ICL-GNSS)*, Turin, Italy, June 25–27, 2013, pp. 1–6.

[5] Z. Xiong, Z. Song, A. Scalera, E. Ferrera, F. Sottile, P. Brizzi, R. Tomasi, and M.A. Spirito, "Enhancing WSN-based Indoor Positioning and Tracking through RFID Technology," in *Proceedings of fourth International EURASIP Workshop on RFID Technology*, Turin, Italy, September 27–28, 2012, pp. 107–114.

[6] Z. Xiong, F. Sottile, M.A. CACERES, M.A. Spirito and R. Garello, "Hybrid WSN-RFID Cooperative Positioning Based on Extended Kalman Filter," in *Proceedings of IEEE Topical Conference on Antennas and Propagation in Wireless Communications*, Turin, Italy, September 12–17, 2011, pp. 990–993.

[7] Z. Xiong, F. Sottile, M.A. Spirito and R. Garello, "Hybrid Indoor Positioning Approaches Based on WSN and RFID," in *Proceedings of 4th IFIP International Conference on New Technologies, Mobility and Security (NTMS)*, Paris, France, February 7–10, 2011, pp. 1–5.

[8] J. Hightower and G. Borriello, "A survey and taxonomy of location systems for ubiquitous computing," Tech. Rep. University of Washington UW-CSE 01-08-03, Computer Science and Engineering, 2001.

[9] J. Hightower and G. Borriello, "Location systems for ubiquitous computing," *Computer*, vol.34, no.8, pp. 57–66, Aug. 2001.

[10] Introduction to Global Positioning System. [Online]. Available: http://www.geoplane.com/gpsbasics.pdf.

[11] H. Liu, H. Darabi, P. Banerjee, and J. Liu, "Survey of Wireless Indoor Positioning Techniques and Systems," *IEEE Transactions on Systems, Man, and Cybernetics, Part C: Applications and Reviews*, vol.37, no.6, pp. 1067–1080, Nov. 2007.

[12] T. Yan, T. He, and J. Stankovic, "Differentiated surveillance for sensor networks," in *Proceedings of the 1st Internal Conference on Embedded Networked Sensor Systems*, pp. 51–62, 2003.

[13] T. Budinger, "Biomonitoring with wireless communications," *Annu. Rev. Biomed. Eng.*, vol.5, pp. 383-412, 2003.

[14] J. Caffery and G. Stuber, "Radio location in urban CDMA microcells,", in *Proceedings of the 6th IEEE International Symposium on Personal, Indoor and Mobile Radio Communications. Wireless: Merging onto the Information Superhighway*, 1995, pp. 858-862.

[15] K. Curran, E. Furey, T. Lunney, J. Santos, D. Woods and A. M. Caughey, "An Evaluation of Indoor Location Determination Technologies," *Journal of Location Based Services*, vol. 5, no. 2, pp. 61-78, June 2011.

[16] R. E. Kalman, "A new approach to linear filtering and prediction problems," *Journal of Basic Engineering*, vol. 82, pp. 35–45, 1960.

[17] N. J. Gordon, D. J. Salmond, and A. F. M. Smith, "Novel approach to nonlinear/non-Gaussian Bayesian state estimation," *IEE Proceedings F Radar and Signal Processing*, vol.140, no.2, pp. 107–113, Apr. 1993.

[18] F. R. Kschischang, B. J. Frey, and H.-A. Loeliger, "Factor graphs and the sum-product algorithm," *IEEE Transactions on Information Theory*, vol.47, no.2, pp. 498–519, Feb. 2001.

[19] R. Prasad and M. Ruggieri, "Applied satellite navigation using GPS, GALI-LEO, and augmentation systems," Artech House, 2005.

[20] L. Monteiro, T. Moore, and C. Hill, "What is the Accuracy of DGPS?" *The Journal of Navigation*, vol. 58, pp. 207–225, 2005.

[21] F. van Diggelen, "A-GPS: Assisted GPS, GNSS, and SBAS." New York: Artech House, 2009.

[22] N. Deblauwe and P. Ruppel, "Combining GPS and GSM Cell-ID positioning for Proactive Location-based Services," in *Fourth Annual International Conference on Mobile and Ubiquitous Systems: Networking & Services*, 2007., pp. 1–7.

[23] P. Paimblanc, W. Chauvet, D. Bonacci, T. Sadiki, and F. Castanié, "Improved positioning using GSM and GNSS tight hybridization," in *Proceedings of the European Navigation Conference on Global Navigation Satellite Systems*, 2008.

[24] G. Heinrichs, P. Mulassano, and F. Dovis, "Hybrid Positioning Algorithm for Cellular Radio Networks by Using a Common Rake Receiver Architecture," in *Proceedings of the 15th IEEE International Symposium Personal, Indoor and Mobile Radio Communications*, vol. 4, 2004, pp. 2347–2351.

[25] Z. Deng, D. Zou, J. Huang, X. Chen, and Y. pei Yu, "The assisted gnss boomed up location based services," in *Wireless Communications, Networking and Mobile Computing, 2009. WiCom '09. 5th International Conference on*, 2009, pp. 1–4.

[26] C. Mensing, S. Sand, and A. Dammann, "Gnss positioning in critical scenarios: Hybrid data fusion with communications signals," in *Communications Workshops, 2009. ICC Workshops 2009. IEEE International Conference on*, 2009, pp. 1–6.

[27] G. De Angelis, G. Baruffa, and S. Cacopardi, "GNSS/Cellular Hybrid Positioning System for Mobile Users in Urban Scenarios," *IEEE Transactions on Intelligent Transportation Systems*, vol. 14, no. 1, pp. 313–321, 2013.

[28] S. Soliman, P. Agashe, I. Fernandez, A. Vayanos, P. Gaal, and M. Oljaca, "gpsOneTM: A Hybrid Position Location System," in *Proceedings of the IEEE Sixth International Symposium on Spread Spectrum Techniques and Applications*, vol. 1, 2000, pp. 330–335.

[29] P. Kovar and F. Vejrazka, "Multi system navigation receiver," in *Proceedings of the IEEE/ION Position, Location and Navigation Symposium*, 2008, pp. 860–864.

[30] J. Huang and L. Lo Presti, "Using two GNSS satellites and few DVB-T signals for positioning in dynamic scenarios," in *6th ESA Workshop on Satellite Navigation Technologies and European Workshop on GNSS Signals and Signal Processing* 2012, pp. 1–6.

[31] J. Huang, L. Lo Presti, and R. Garello, "Digital Video Broadcast-Terrestrial (DVB-T) Single Frequency Networks Positioning in Dynamic Scenarios," *Sensors 2013*, vol. 13, pp. 10191–10218, 2013.

[32] R. Want, A. Hopper, V. Falcão, and J. Gibbons, "The active badge location system," *ACM Transactions on Information Systems*, vol. 10, no. 1, pp. 91–102, 1992.

[33] P. Bahl and V. N. Padmanabhan, "Radar: an in-building RF-based user location and tracking system," in *Proceedings of INFOCOM 2000*, vol. 2, 2000, pp. 775 –784.

[34] L. M. Ni, Y. Liu, Y. C. Lau, and A. p. Patil, "LANDMARC: indoor location sensing using active RFID,", in *Proceedings of the First IEEE International Conference on Pervasive Computing and Communications*, 2003, pp.407–415.

[35] R. Battiti, N. T. Le, and A. Villani, "Location-aware Computing: A Neural Network Model for Determining Location in Wireless LANs," University of Trento, Tech. Rep., February 2002.

[36] B. Eissfeller, D. G. änsch, S. M. üller, and A. Teuber, "Indoor positioning using wireless LAN radio signals, " in *Proceedings of the 17th International Technical Meeting of the Satellite Division of The Institute of Navigation*, 2004, pp. 21–24.

[37] K. Lorincz and M. Welsh, "MoteTrack : A robust, decentralized approach to RF-based location tracking," *Location-and Context-Awareness*, pp. 63–82, 2005.

[38] W. Tranter, K. Shanmugan, T. Rappaport, and K. Kosbar, "Principles of Communication Systems Simulation with Wireless Applications," Prentice Hall Press, Upper Saddle River, 2003.

[39] J. Yin; G. Holland, T. ElBatt, F. Bai, and H. Krishnan,"DSRC Channel Fading Analysis from Empirical Measurement," in *First International Conference on Communications and Networking in China*, 2006, pp. 1–5.

[40] J. Kwon, B. Dundar, and P. Varaiya, "Hybrid algorithm for indoor positioning using wireless LAN," in *IEEE 60th Vehicular Technology Conference*, vol.7, 2004, pp.4625–4629.

[41] R. Singh, M. Guainazzo, and C. Regazzoni, "Location Determination Using WLAN in Conjunction with GPS Network (Global Positioning System)," in *IEEE 59th Vehicular Technology Conference*, 2004, pp. 2695–2699.

[42] S.-c. Yeh, W.-h. Hsu, M.-y. Su, C.-h. Chen, and K.-h. Liu, "A Study on Outdoor Positioning Technology using GPS and WiFi Networks," in 2009 International Conference on Networking, Sensing and Control, 2009, pp. 597–601.

[43] G. MacGougan, K. O'Keefe, and R. Klukas, "Ultra-wideband ranging precision and accuracy," *Measurement Science and Technology*, vol. 20, no. 9, 2009.

[44] K. M. Tan and C. L. Law, "GPS and UWB Integration for Indoor Positioning," in *6th International Conference on Information, Communications & Signal Processing*, 2007, pp. 1–5.

[45] G. MacGougan, K. O'Keefe, and D. S. Chiu, "Multiple UWB Range Assisted GPS RTK in Hostile Environments," in *Proceedings of the ION GNSS*, 2008.

[46] G. D. MacGougan and R. Klukas"Method and apparatus for high precision GNSS/UWB surveying," in *Proceedings of the ION GNSS*, 2009.

[47] G. Macgougan, K. O'Keefe, and R. Klukas, "Tightly-coupled GPS/UWB Integration," *The Journal of Navigation*, vol. 63, no. 1, pp. 1–22, Jan. 2010.

[48] I. F. Akyildiz, W. Su, Y. Sankarasubramaniam, and E. Cayirci, "Wireless sensor networks: a survey," *Computer Networks*, vol. 38, no. 4, pp. 393–422, 2002.

[49] J. A. Costa, N. Patwari, and A. O. Hero III, "Distributed multidimensional scaling with adaptive weighting for node localization in sensor networks," *ACM Journal Name*, vol. V, no. N, pp. 1–23, June 2004.

[50] D. Moore, J. Leonard, D. Rus, and S. Teller, "Robust distributed network localization with noisy range measurements," in *Proc. 2nd ACM SenSys. Baltimore*, MD: ACM Press, Nov. 2004, pp. 50–61.

[51] C. Meesookho, U. Mitra, and S. Narayanan, "On energy-based acoustic source localization for sensor networks," *IEEE Transactions on Signal Processing*, vol. 56, no. 1, pp. 365–377, Jan. 2008.

[52] L. Xu, Z. Deng, W. Ren, and H. Wang, "Location Algorithm Integrating GPS and WSN in Pervasive Computing," in *third International Conference on Pervasive Computing and Applications*, 2008, op. 461–466.

[53] W. Ren, "A Rapid Acquisition Algorithm of WSN-aided GPS Location," in *Proceedings of the Second International Symposium Intelligent Information Technology and Security Informatics*, 2009, pp. 42-46.

[54] D. Hahnel, W. Burgard, D. Fox, K. Fishkin, and M. Philipose, "Mapping and localization with RFID technology," in *IEEE International Conference on Robotics and Automation*, vol. 1, New Orleans, LA, Apr. 2004, pp. 1015–1020.

[55] M. Bouet and A. L.dos Santos, "RFID tags: positioning principles and localization techniques," in *Wireless Days, 2008. WD '08. 1st IFIP*, 2008, pp. 1–5.

[56] J. S. Choi, H. Lee, R. Elmasri, and D. W. Engels, "Localization systems using passive UHF RFID," in *Fifth International Joint Conference on INC, IMS and IDC*, Seoul, Aug. 2009, pp. 1727–1732.

[57] G. Retscher and Q. Fu, "Integration of RFID, GNSS and DR for Ubiquitous Positioning in Pedestrian Navigation," *Journal of Global Positioning Systems*, vol. 6, pp. 56–64, 2007.

[58] N. Patwari, J. N. Ash, S. Kyperountas, A. O. Hero, R. L. Moses, and N. S. Correal, "Locating the Nodes: Cooperative localization in wireless sensor networks," *IEEE Signal Processing Magazine*, vol. 22, no. 4, pp. 54–69, July 2005.

[59] F. Chiti, R. Fantacci, S. Menci, and A. Zappoli, "Cooperative Localization Protocols for Wireless Sensor Networks," in *2007 IEEE Global Telecommunications Conference*, 2007, pp. 1048–1052.

[60] H. Wymeersch, J. Lien, and M. Win, "Cooperative Localization in Wireless Networks," *Proceedings of the IEEE*, vol. 97, no. 2, pp. 427–450, Feb. 2009.

[61] M. A. Caceres, F. Sottile, R. Garello, and M. A. Spirito, "Hybrid GNSS-ToA Localization and Tracking via Cooperative Unscented Kalman filter," in Proceedings of the IEEE 21st International Conference on Personal, Indoor and Mobile Radio Communications Workshops, 2010, pp. 272–276.

[62] F. Sottile, H. Wymeersch, M. Caceres, and M. Spirito, "Hybrid GNSS-Terrestrial Cooperative Positioning based on Particle Filter," in *2011 IEEE Global Telecommunications Conference*, 2011, pp. 1–5.

[63] M. A. Caceres, F. Penna, H. Wymeersch, and R. Garello, "Hybrid Cooperative Positioning Based on Distributed Belief Propagation," *IEEE Journal on Selected Areas in Communications*, vol. 29, no. 10, pp. 1948–1958, Dec. 2011.

[64] R. Garello, L. Lo Presti, G. E. Corazza, and J. Samson, "Peer-to-Peer Cooperative Positioning Part I: GNSS Aided Acquisition," *Inside GNSS*, March/April 2012, pp. 55–63.

[65] R. Garello, J. Samson, M. A. Spirito, and H. Wymeersch, "Peer-to-Peer Cooperative Positioning Part II: Hybrid Devices with GNSS & Terrestrial Ranging Capability," *Inside GNSS*, July/August 2012, pp. 20–29.

[66] W. G. Figel, N. H. Shepherd, and W. F. Trammel, "Vehicle location by a signal attenuation method," *IEEE Transactions on Vehicular Technology*, vol. 18, no. 3, pp. 105–109, Nov. 1969.

[67] S. Rao, "Estimating the ZigBee transmission-range ISM band," *EDN*, vol. 52, no. 11, pp. 67–74, 2007.

[68] H. Hashemi, "The indoor radio propagation channel," *Proceedings of the IEEE*, vol. 81, no. 7, pp. 943-968, July 1993.

[69] N. Patwari, A. O. Hero, M. Perkins, N. S. Correal, and R. J. O'Dea, "Relative location estimation in wireless sensor networks," *IEEE Transactions on Signal Processing*, vol. 51, no. 8, pp. 2137–2148, July 2003.

[70] Y. Qi and H. Kobayashi, "On Relation Among Time Delay and Signal Strength based Geolocation Methods," in *Proceedings of the IEEE Global Telecommunications Conference*, Dec. 2003, pp. 4079-4083.

[71] D. Dardari and F. Sottile, "WPR.B database: Annex of progress report II on advanced localization and positioning techniques: Data fusion and applications," Tech. Rep. Deliverable DB.3 Annex, 216715 Newcom++ NoE, WPR.B, Dec. 2009.

[72] C. E. Cook and M. Bernfeld, "Radar Signals: An Introduction to Theory and Applications," New York: Academic, 1970.

[73] H. V. Poor, "An Introduction to Signal Detection and Estimation," 2nd ed. New York: Springer-Verlag, 1994.

[74] J. A. Stankovic, "Wireless sensor networks," University of Virginia, Tech. Rep. Charlottesville, Virginia 22904, 2006.

[75] Wireless sensor network. [Online]. Available: http://en.wikipedia.org/wiki/Wireless_sensor_network.

[76] TelosB. [Online]. Available: http://www.xbow.jp/TelosbCatalog.pdf.

[77] Ultra-wideband Wikipedia. [Online]. Available: http://en.wikipedia.org/wiki/Ultra-wideband.

[78] P400 UWB module. [Online]. Available: http://www.timedomain.com/p400.php.

[79] N. Patwari, and A. O. Hero, "Using proximity and quantized RSS for sensor localization in wireless networks," in *WSNA '03 Proceedings of the 2nd ACM international conference on Wireless sensor networks and applications*, Sep. 2003, pp. 20-29.

[80] G. Welch and G. Bishop, "An Introduction to the Kalman Filter," University of North Carolina at Chapel Hill, Tech. Rep. Chapel Hill, NC 27599-3175, 2006.

[81] M. S. Arulampalam, S. Maskell, N. Gordon, T. Clapp, "A tutorial on particle filters for online nonlinear/non-Gaussian Bayesian tracking," *IEEE Transactions on Signal Processing*, vol. 50, no. 2, pp. 174–188, Feb. 2002.

[82] A. Doucet, S. Godsill and C. Andrieu, "On sequential Monte Carlo sampling methods for Bayesian filtering," University of Cambridge, *Statistics and Computing*, vo1.10, pp.197-2008, 2000.

[83] F. Gustafsson, F. Gunnarsson, N. Bergman, U. Forssell, J. Jansson, R. Karlsson, and P.-J. Nordlund, "Particle filters for positioning, navigation and tracking," *IEEE Transactions on Signal Processing*, vol. 50, no. 2, pp. 425–437, Feb. 2002.

[84] S. A. Mitilineos, D. M. Kyriazanos, O. E. Segou J. N. Goufas and S. C. A. Thomopoulos, "Indoor Localization with Wireless Sensor Networks," *Progress In Electromagnetics Research*, vol. 109, pp. 441–474, 2010.

[85] Y.-T. Chan, W.-Y. Tsui, H.-C. So, P.-C. Ching, "Time-of-Arrival Based Localization Under NLOS Conditions," *IEEE Transactions on Vehicular Technology*, vol. 55, no. 1, pp. 17–24, Jan. 2006.

[86] Z. Yifeng and S. Ali, "Comparisons of three Kalman filter tracking algorithms in sensor network," in *International Workshop on Networking, Architecture, and Storages, 2006. IWNAS '06*.

[87] Computational complexity of mathematical operations on Wikipedia. [Online]. Available: http://en.wikipedia.org/wiki/Computational_complexity_of_mathematical_operations.

[88] F. Sottile, M. A. Caceres, and M. A. Spirito, "A simulation tool for hybrid-cooperative positioning,", in *2011 International Conference on Localization and GNSS*, 2011, pp. 64-70.

[89] M. Dai, F. Sottile, M. A. Spirito, and R. Garello, "An energy efficient tracking algorithm in uwb-based sensor networks," in *IEEE 8th International Conference on Wireless and Mobile Computing, Networking and Communications (WiMob)*, Oct. 2012, pp. 173–178.

[90] B. Denis, M. Maman, and L. Ouvry, "On the scheduling of ranging and distributed positioning updates in cooperative ir-uwb networks," in *2009 IEEE International Conference on Ultra-Wideband*, Sept. 2009, pp. 370–375.

[91] A. Khitwongwattana and T. Maneewarn, "Extended kalman filter with adaptive measurement noise characteristics for position estimation of an autonomous vehicle," in *2008 IEEE/ASME International Conference on Mechtronic and Embedded Systems and Applications*, Oct. 2008, pp. 505–509.

[92] H. Celebi and H. Arslan, "Cognitive positioning systems," *IEEE Transactions on Wireless Communications*, vol. 6, no. 12, pp. 4475–4483, Dec. 2007.

[93] R. R. Thomas and B. T. Maharaj, "Towards a bandwidth efficient cognitive positioning system," *Electronics Letters*, vol. 48, no. 12, pp. 736–737, June 2011.

[94] F. Penna, M. A. Caceres, and H. Wymeersch, "Cramér-Rao Bound for Hybrid GNSS-Terrestrial Cooperative Positioning," *IEEE Communications Letters*, vol. 14, no. 11, pp. 1005–1007, Nov. 2010.

[95] S. Gezici, H. Kobayashi, and H. V. Poor, "Nonparametric nonline-of-sight identification," in *Vehicular Technology Conference, 2003. VTC 2003-Fall*, vol. 4, Oct. 2003, pp. 2544–2548.

[96] I. Guvenc, C.-C. Chong, F. Watanabe, and H. Inamura, "NLOS Identification and Weighted Least-Squares Localization for UWB Systems Using Multipath Channel Statistics," *EURASIP Journal on Advances in Signal Processing*, no. 1, 2008.

[97] H. Wymeersch, S. Marano, W. M. Gifford, and M. Z. Win, "A Machine Learning Approach to Ranging Error Mitigation for UWB Localization," *IEEE Transactions on Communications*, vol. 60, no. 6, pp. 1719–1128, June 2012.

[98] K. Yu and Y. J. Guo, "Improved Positioning Algorithms for Nonline-of-Sight Environments," *IEEE Transactions on Vehicular Technology*, vol. 57, no. 4, pp. 2342–2353, July 2008.

[99] H. Liu, F. Chan, and H. C. So, "Non-Line-of-Sight Mobile Positioning Using Factor Graphs," *IEEE Transactions on Vehicular Technology*, vol. 58, no. 9, pp. 5279–5283, Mov. 2009.

[100] S. Van de Velde, H. Wymeersch, and H. Steendam, "Comparison of message passing algorithms for cooperative localization under nlos conditions," in *9th Workshop on Positioning Navigation and Communication*, Mar. 2012, pp. 1–6.

[101] R. M. Vaghefi and R. M. Buehrer, "Cooperative sensor localization with nlos mitigation using semidefinite programming," in *9th Workshop on Positioning Navigation and Communication*, Mar. 2012, pp. 13–18.

[102] T. Minka, "Expectation propagation for approximate bayesian inference," in *17th Conference in Uncertainty in Artificial Intelligence*, Aug. 2001, pp. 362–369.